Improved Electric Vehicle Powertrain Incorporating a Lithium-Ion Battery and a Range Extender Zinc-Air Battery, plus Associated Health and Economic Benefits

by

Steven Sherman

A thesis

presented to the University of Waterloo

in fulfillment of the

thesis requirement for the degree of

Masters of Applied Science

in

Chemical Engineering

Waterloo. Ontario, Canada, 2019

Author’s Declaration

I hereby declare that I am the sole author of this thesis. This is a true copy of the thesis, including any required final revisions, as accepted by my examiners.

I understand that my thesis may be made electronically available to the public

Abstract

As the world confronts the serious challenge posed by anthropogenic climate change, electric vehicles have emerged as a serious candidate to displace gasoline-burning vehicles. In spite of the environmental and operational advantages of electric vehicles, however, and in spite of billions in investment, electric vehicles have not attained meaningful market share in the main national vehicle markets. This is a serious problem not only for climate change mitigation but also for air pollution mitigation, given the substantial air pollution generated by vehicles. The inability of electric vehicles to attain market share may be due to the inadequacies of the lithium-ion batteries which power electric vehicles, and which are heavy and expensive.

In this work an electric vehicle with a novel powertrain is designed, optimized and modelled. The novel powertrain uses a lithium-ion battery as the primary energy storage system and a lighter and cheaper zinc-air battery as a range extender. The first objective of this work is to compare this novel powertrain to a conventional electric vehicle powertrain and quantify the benefits. The optimized two-battery electric vehicle achieves 400 km of range, over 12 years of zinc-air battery life and an MSRP of $26,300 – over $5000 lower than that of the conventional electric vehicle. As part of this work, it is necessary to create a zinc-air cell model based on academic literature, since there are no commercially available rechargeable zinc-air cells that are suitable for use in vehicles. The cell model achieved 10% greater specific energy to the lithium-ion cell at a much lower price. An improved cell model achieved even greater specific energy – 65% greater than the lithium-ion cell.

The second objective of this work is to analyze the air pollution impacts of electric vehicles in a local context. Specifically, the air pollution impact of increasing levels of electric vehicles on Highway 401 is simulated. Using Ontario Ministry of Transportation data for traffic flows on Highway 401, pollution modelling software and Transport Canada guidance it is estimated that pollution from Highway 401 costs $18.5M per year, and that replacing all the light passenger vehicles with electric vehicles could reduce these costs by 45.6%. The modelling demonstrates that NO_x and $PM_{2.5}$ are the costliest pollutants, and that $PM_{2.5}$ experiences the least relative reduction in emissions with increased electric vehicle penetration.

Acknowledgements

First and foremost, I would like to thank my family, especially my mother and father. They made me who I am and supported me through the most challenging period of my life. I would not have succeeded without their patience and love.

I would like to also thank Dr. Fowler for his role in my studies. Dr. Fowler's guidance and insight were key to the completion of this work and to my academic growth. I am forever grateful for his support in this foundational stage of my career.

Third, I would like to thank Zachary Cano and Ehsan Samadani, whose insight has made this work immeasurably better and from whom I have learned a great deal. Zachary answered all my battery questions patiently and clearly, and deepened my understanding of how batteries in general and zinc-air batteries in particular work. Ehsan reviewed and edited my thesis more than once, and his insights helped me improve the quality of my work.

A special thanks for Mohammad Munshed, Dr. Jesse Thé and Lakes Environmental for providing the air pollution modelling software TRAQS. Without their software, and without Mohammad's patient explanations of how TRAQS works and frequent help solving problems it would have been impossible to incorporate air pollution modelling into this work. A special thanks also to Christopher Bee at the Ontario Ministry of Transportation, who provided traffic data for Highway 401 that made it possible to perform the air pollution analysis for this thesis.

I would also like to thank Ramin Shaikhi and Paul McInnis for their assistance in troubleshooting the vehicle model. Ramin is a member of UWAFT and provided non-proprietary motor data for use in the vehicle model. Paul provided frequent clarifications on his vehicle model, which was the precursor to the vehicle model used in this work.

I would like to thank Judy Caron, who looks after all the students here so well. I am so grateful for her clear and insightful guidance on any and all challenges I faced.

I would be remis if I did not thank the many colleagues not yet mentioned who helped me in ways large and small. There are too many to name, but they include John, Mehran, Manoj, Manan, Megan, Matthew, Mohammad, Xiaolei, Yinning, Salah and Bert.

Dedication

To Mom, Dad, Laura and Michael

who helped me believe in myself again.

Table of Contents

List of Figures

List of Tables

Nomenclature

2BEV	Two-battery electric vehicle; the given name for the vehicle model of study in this work
AADT	Annual average daily traffic; used in equation 8
ADT_i	Average daily traffic for period *I*; used in equation 8
AERMOD	American Meteorological Society/Environmental Protection Agency Regulatory Model; an air pollution modelling software
B	Buffer; used in equations 10 and 11
BEV	Battery electric vehicle
BTS	Bureau of Transportation Statistics
C or C/X	C-rate; a measure of current which is relative to the capacity of the battery. X refers to the number of hours it would take to fully exhaust the battery's capacity.
cBEV	Control battery electric vehicle; the given name for the vehicle model with one battery which serves as a point of comparison for the 2BEV
CAD	Canadian dollars
CC	Combined costs; used in equation 12
C_{CO2}	Concentration of CO_2; used in equation 10
CMA	Cellulose membrane assembly
cmd	Command; refers to the pedal input in the vehicle models; used in equation 5
DEC	Diethyl carbonate
DMC	Dimethyl carbonate
DOE	Department of energy
e^-	Electron; used in equations 1-4
EMC	Ethylene carbonate
EMC	Ethyl methyl carbonate
EPA	Environmental Protection Agency
ESS	Energy storage system
EV	Electric vehicle
f_i	Conversion factor; used in equation 8
FC	Fuel costs; used in equation 12
FE_{final}	Final fuel economy; used in equation 9
$FE_{initial}$	Initial fuel economy; used in equation 9
GDL	Gas diffusion layer
HEV	Hybrid electric vehicle
HI	Heat index; used in equation 5
HST	Harmonised Sales Tax; used in equation 12
HWFET	Highway Fuel Economy Test
ICE	Internal combustion engine
ICEV	Internal combustion engine vehicle
K_{100}	Adsorption capacity of absorbent; used in equation 10
LCO	Lithium cobalt oxide
LFP	Lithium iron phosphate
LiX-ZnY	Shorthand for the battery configuration of the 2BEV; X represents the number of lithium-ion battery arrays, and Y represents the number of zinc-air battery arrays
LMO	Lithium manganese oxide

m_{ads}	Mass of adsorbent; used in equation 10
m_{H2O}	Mass of water; used in equation 11
m_{Zn}	Mass of zinc; used in equations 10 and 11
mm_{CO2}	Molar mass of CO_2; used in equation 10
mm_{H2O}	Molar mass of water; used in equation 11
mm_{Zn}	Molar mass of zinc; used in equations 10 and 11
MATLAB	Matrix Laboratory; software used to model vehicle
MOVES	Motor Vehicle Emissions Simulator; an air pollution modelling software
MSRP	Manufacturer's Suggested Retail Price; used in equation 12
MTO	Ontario Ministry of Transportation
N	Number of zinc-air battery cycles per year; used in equations 10 and 11
n_{air}	Moles of air; used in equation 10
n_{O2}	Moles of oxygen; used in equations 10 and 11
n_{Zn}	Moles of zinc; used in equations 10 and 11
NCA	Nickel cobalt aluminum
NMC	Nickel manganese cobalt
NO_x	Nitrous oxides
OER	Oxygen evolution reaction
ORR	Oxygen reduction reaction
P_{atm}	Atmospheric pressure
P_{vap}	Vapour pressure
PHEV	Plug-in hybrid electric vehicle
PM	Particulate matter
$PM_{2.5}$	Particulate matter with a diameter of less than 2.5 μm
PM_{10}	Particulate matter with a diameter of less than 10 μm
SOC	State of charge
SOC_{max}	Maximum allowed state of charge
SOC_{min}	Minimum allowed state of charge
T	Motor torque; used in equation 5
T_{cont}	Continuous torque; used in equation 5
T_{max}	Maximum torque; used in equation 5
T_{peak}	Peak torque; used in equation 5
TRAQS	Transportation Air Quality System; the air pollution modelling software used in this work
UDDS	Urban Dynamometer Driving Schedule
UF	Utilization factor
UWAFT	University of Waterloo Alternative Fuels Team
VOC	Volatile organic compounds
ZEV	Zero emissions vehicle
τ	Time constant; used in equation 5

1. Introduction

Anthropogenic climate change is a major threat to humanity and to life on earth, according to a recent Intergovernmental Panel on Climate Change (IPCC) report (IPCC, 2018). The impacts of climate change include, with varying degrees of confidence, increases in mean temperature in most regions, increases in extreme high temperatures, increases in heavy precipitation in some regions, increases in the probability of drought in some regions and increases in sea level. The indirect risks to humans from climate change include negative impact to human health, livelihoods, food security, water supply, human security and economic growth. The impact of these climactic changes on species at risk and ecosystems around the world is to reduce their climatically determined geographic range by over half in some cases and to negatively impact their viability (IPCC, 2018). Anthropogenic climate change is caused by ever increasing greenhouse gas emissions such as carbon dioxide (CO_2). In order to reduce the degree of climate change, CO_2 emissions have to be drastically reduced and, in some sectors, eliminated.

One large and growing source of carbon dioxide emissions is the transportation sector, responsible for 14% of global CO_2 emissions (IPCC, 2014). The transportation sector is dominated by vehicles which use internal combustion engines (ICEs) to capture heat energy from the combustion of oil products and propel themselves. Not only does this combustion process release large amounts of carbon dioxide, it also results in the emission of other gases which are hazardous to human health, including carbon monoxide, nitrous oxides, sulphur dioxide and volatile organic compounds. Vehicles can also emit particulate matter, which are not gases but small solid particles that can penetrate deep into the lungs and cause health problems. Exposure to air pollutants from vehicles increases the risk of asthma, diabetes, dementia and premature death, among other health problems (Requia, Mohamed, Higgins, Arain, & Ferguson, 2018).

One promising solution to transportation-sector emissions is electric vehicle (EV) technology. An EV is powered by electricity instead of oil, and uses a motor instead of an engine to turn that electricity into motion. Most EVs today use lithium-ion batteries to store their electricity, although fuel cells or other battery chemistries are also possible. EVs have much lower health and environmental impacts compared to ICE-powered vehicles (ICEVs) because they do not emit pollutants directly, and because electricity production is on average much cleaner than oil

consumption. This is particularly true in areas where nuclear and renewable energy play a large role in electricity generation (Nealer, Reichmuth, & Anair, 2015).

In spite of the benefits of EVs they face some major barriers to widespread adoption. The high upfront cost of EVs, which are generally several thousand dollars more expensive than comparable ICEVs, is a major deterrent. The limited range of all but the most expensive EVs is another major barrier (Haustein & Jensen, 2018). Both the high cost and limited range of the vehicle derive from the lithium-ion batteries which power the vehicles. Lithium-ion batteries are expensive, and EV batteries can comprise a large portion of the cost of the vehicle (Bullard, 2019). Although they are more energy dense than lead-acid or nickel-metal hydride batteries, lithium-ion batteries are still much less energy dense than gasoline. Improvements to lithium-ion batteries, or the development of an alternate battery chemistry, are therefore critical to the promotion of EVs. EVs face other barriers as well, such as the lack of fast-charging infrastructure, but the battery technology is a more central challenge (Berkeley, Jarvis, & Jones, 2018).

Because the shortcomings of lithium-ion batteries are the main barriers to EV adoption, researchers have investigated other energy storage technologies to supplant lithium-ion batteries as the EV energy source. One highly touted alternative is zinc-air batteries, which are actually a hybrid between a battery and a fuel cell. The anode is composed of solid zinc, as in a battery, but the cathode is an inert mesh where oxygen reacts as in a fuel cell. Zinc-air batteries are lighter, cheaper and more energy dense than lithium-ion batteries but are not yet ready for commercial use. Their main disadvantages are their low cycle life which limits their longevity, and their low power density which has made them impractical for use in vehicles (Fu, Cano, et al., 2017).

In this thesis a vehicle with a novel powertrain, incorporating a lithium-ion battery as the primary energy storage system (ESS) and a zinc-air battery as the range extender, is modelled. The powertrain is optimized so as to maximize the value of each battery and minimize their individual disadvantages. A similar vehicle with a more traditional EV powertrain is also modelled. This vehicle has no zinc-air battery, only one large lithium-ion battery. The two vehicle models are compared in order to demonstrate the advantages of the novel powertrain. Most of the vehicle components – including the motor, the vehicle body and the lithium-ion batteries – are based on data from commercial components; the exception is the zinc-air battery model. Zinc-air batteries are not yet commercialized, so the model was instead created by combining the results from several

published papers. The resulting model is subject to a sensitivity analysis in order to show which aspects of the model are most important in driving cell performance. The benefits of EVs are further explored by examining their potential effect on pollution levels in the vicinity of North America's busiest highway, Highway 401 in Toronto. Toronto's worst air pollution is concentrated along the 401 (Toronto Public Health, 2014) due to the emissions from the nearly hundreds of thousands of vehicles that use the 401 every day. The pollution along the 401 will be modelled and the effect of increasing levels of zero emission vehicles (ZEVs) will be explored.

The rest of this work is organized as follows. Section 2 provides background information on the areas of study relevant to this work: vehicle powertrains, lithium-ion batteries, zinc-air batteries and air pollution. This includes for each topic an overview of the important aspects and a review of the relevant literature. Section 3 describes in detail the models and methodology used in this work, including an overview of the relevant software, model specifications and data sources, and a description of some analysis done externally to the main models. In section 4 the results are presented with more analysis and discussion. This includes results from the vehicle model and the air pollution model. Section 5 concludes this work, highlighting the main results and offering recommendations for future work.

2. Background

2.1. Powertrain review

The Canadian automotive sector is a $86B/year industry, with annual sales of passenger cars, minivans, sport utility vehicles, light and heavy trucks, vans and buses totalling 2 million per year (Statistics Canada, 2018a); the number of cars and light trucks in operation in Canada is estimated to be 23.1 million (Statistics Canada, 2018b). The emissions from passenger cars and passenger light trucks was 85.1 Mt in 2017, equivalent to 12% of Canada's total emissions that year (Environment and Climate Change Canada, 2019). Health Canada estimates that in 2015 gasoline emissions (Charman et al., 2017) and diesel emissions (Brewer et al., 2016) were respectively responsible for 940 and 710 premature deaths, with a societal economic cost of $7.3B and $5.1B ($7.9B and $5.5B respectively, in 2019 CAD).

Over the course of the 20th century the public became aware of several negative societal consequences of substantial oil consumption. Scientific research found significant health impacts from the uncontrolled tailpipe exhaust and lead to tailpipe emissions standards, the elimination of leaded gasoline as a fuel and a reduction in carbon monoxide and sulphur emissions from vehicles (EPA, n.d.-b). Also, the oil crisis of the 1970s revealed the degree to which oil-dependent economies depended on Middle East oil production and the consequent national security concerns. More recently, growing awareness of anthropogenic climate change and its consequences has focused public attention on the negative impacts of carbon dioxide emissions from vehicles. Together these issues created a public appetite for an alternative to oil-powered vehicles.

The first major innovation in response to these concerns was the introduction of hybrid powertrains. Vehicles with hybrid powertrains are powered by internal combustion engines as in conventional vehicles but also have small batteries – typically nickel-metal hydride batteries – to assist with vehicle propulsion and auxiliary power usage. The battery powers the vehicle when pulling off from a stop or driving at low speeds, which is when the engine is least efficient. The battery is charged by the engine, but because the engine has to do less work at its least efficient operating region there is a net reduction in fuel consumption (Husain, 2011). The battery can also be charged via regenerative braking – instead of using only the brake pads to stop the car, the

motor is allowed to run in reverse. This slows the car and also generates electricity, which is stored in the battery.

Hybrid vehicles (HEVs) were commercially successful but had a limited impact on the overall vehicle market. HEVs comprised 2-3% of the new vehicle market in the United States, the world's second-largest vehicle market, from 2007 to 2017, with a peak market share of 3.8% in 2010 (EPA, 2019). The only market in which they had a sizable impact was the Japanese market, where hybrids reached 19% of all passenger vehicles in service (Jiji, 2018). The limited popularity of HEVs can be attributed to their higher upfront cost and their limited benefit. HEVs are ultimately powered by gasoline the same as conventional vehicles; they just use somewhat less. Because of this HEVs do not substantially mitigate the social problems posed by gasoline consumption.

As Toyota was pioneering the Prius HEV, General Motors was experimenting with their own response to public concerns about gasoline consumption. Starting in 1996 GM produced the EV1, an electric car propelled with a large lead-acid battery (Edwards, 2006). The vehicle was soon cancelled due to a lack of demand, but a few years later automakers began production of electric cars with large lithium-ion batteries, a more advanced battery compared to lead-acid batteries. Battery electric vehicles (BEVs) don't have internal combustion engines; instead they have large batteries, usually lithium-ion batteries, which powers a motor.

BEVs have significant health and environmental advantages over ICEVs and HEVs. BEVs have no tailpipe emissions, so they emit no greenhouse gas emissions and almost no air pollutants directly (vehicles also cause particulate emissions by kicking up road dust, so direct air pollution is not entirely eliminated). EVs may still cause pollution indirectly if their electricity is made from burning fossil fuels in a power plant, but the overall environmental and health impact of EVs is usually still positive (Nealer et al., 2015). This is because EVs are dramatically more efficient than conventional vehicles, so unless the power plant is very inefficient there will be a net reduction of greenhouse gas emissions. Also, because the power plant emissions are generally located some distance away from major population centres, the impact of their air pollution in cities is less compared to the same pollution emitted from city streets (Ji et al., 2015). Indirect EV emissions may be eliminated entirely if the vehicles are charged with renewable energy or nuclear power, which emit no greenhouse gas emissions and no air pollutants.

Although BEVs have major potential environmental and health benefits, they have not yet had a major impact on the vehicle market. One major barrier is the range anxiety many potential BEV owners experience. Lithium-ion batteries, though more efficient than engines, contain far less energy per unit weight and volume than oil. Consequentially BEVs usually drive significantly shorter distances on a single charge than a comparable gasoline car. Furthermore, fast-charging stations are currently far less common than gas stations, which are ubiquitous. Together this makes prospective BEV owners concerned they will find themselves stranded on the side of the road (Haustein & Jensen, 2018). Another major barrier is the cost of BEVs. Lithium-ion batteries are expensive and make up a significant portion of the cost of a vehicle. Prices are coming down as manufacturing techniques improve and economies of scale are achieved, but presently the cost of batteries creates a significant price gap between BEVs and comparable gasoline-powered vehicles (Bullard, 2019). These and other challenges must be overcome if lithium-ion battery-powered BEVs are to gain significant market share, and some challenges – such as the fire risk posed by lithium-ion batteries as well as battery charging speed – are likely to remain a barrier far into the future unless new EV technology is developed.

In order to overcome the challenges of cost and range, a new hybrid vehicle architecture was introduced. A plug-in hybrid electric vehicle (PHEV) has a battery and an engine, as in an HEV, but with a very different powertrain design and operation. A PHEV has a small-to-medium sized lithium-ion battery which powers a motor which propels the car. There is also an engine, and in the most common PHEV configuration (a series configuration) the engine powers a generator which charges the battery (Husain, 2011). The series configuration of the PHEV differs from the typical HEV powertrain configuration, which is series-parallel split. Unlike in HEVs, a PHEV battery is large enough and powerful enough to power the vehicle independently of the engine for short-to-medium distances at high speeds. Also unlike in HEVs, the PHEV battery can be charged externally (i.e. directly from the electrical grid) and so can run off a fuel apart from oil. When the vehicle runs low on charge, the engine turns on and powers the vehicle through the battery, effectively charging the battery as the battery powers the vehicle (Husain, 2011). Because most people don't drive very far each day, a moderately-sized battery is still sufficiently large to power the vehicle most of the time, and while the battery is running off electricity from the grid the same environmental benefit can be derived as from a BEV. But since the batteries are much smaller

PHEVs are much cheaper than BEVs; additionally, since PHEVs have an engine and a gas tank, drivers do not need to fear running out of charge.

There are several hybrid powertrain configurations, but the main variations are series, parallel and series-parallel split. In a series powertrain the engine is not connected mechanically to the wheels at all; instead it powers a generator, which charges the battery, which in turn powers a motor which turns the wheels (Figure 1). The power delivered to the wheels is determined entirely by the battery and motor, not the engine – though the engine can recharge the battery as the battery powers the wheels. Series powertrains are common in PHEVs since the battery is easily operated independently of the engine, resulting in the greatest reduction in gasoline consumption. The engine can be smaller and more efficient than in a comparable ICE vehicle since it has lower power requirements, and can generally be operated more efficiently since its power output does not have to closely match demand (Husain, 2011).

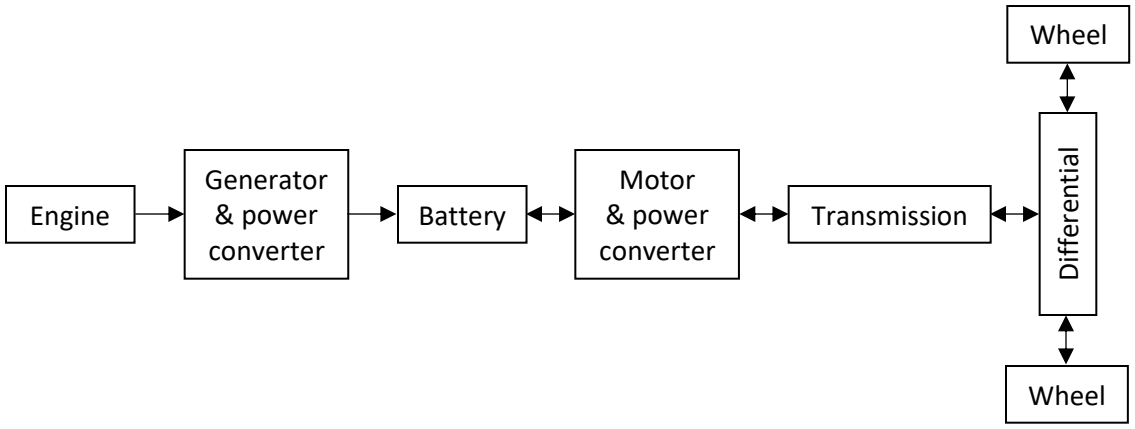

Figure 1: Schematic depiction of a series powertrain (Husain, 2011).

HEVs rarely utilize a series configuration since the battery has to be large enough and powerful enough to power the vehicle independently of the engine. HEVs more commonly employ a parallel hybrid powertrain, in which an engine and an electric motor are each connected mechanically to the wheels and simultaneously provide power to the wheels (Figure 2). In this configuration the battery and engine can power the vehicle independently or together – although in HEVs the batteries only do this in low-power situations – and the battery can be recharged via regenerative braking or via the engine (Husain, 2011). Because the engine is usually responsible for powering the car in high-energy situations it has to be almost as large and powerful as in a comparable ICE

vehicle, but having the battery increases the operating efficiency of the engine. This powertrain is more complicated to control than a series powertrain, but eliminates the need for a separate generator to charge the battery. In addition, because the engine is connected directly to the wheels there is improved efficiency at highway speeds because the energy from the engine does not have to be transformed from mechanical energy to electrical energy and then back to mechanical energy (Union of Concerned Scientists, n.d.-b)

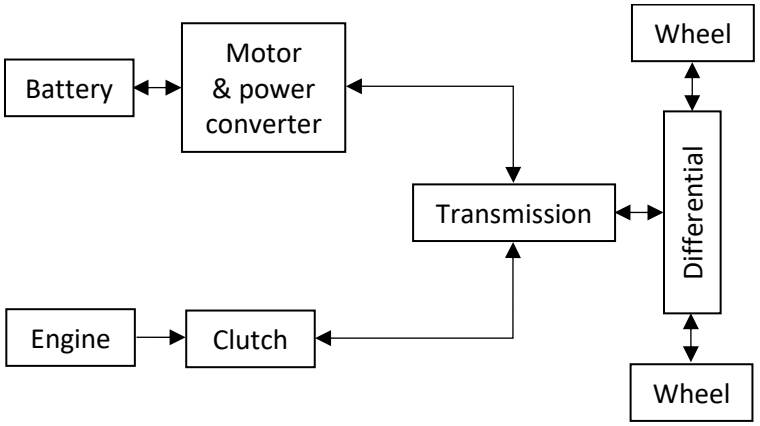

Figure 2: Schematic depiction of a parallel hybrid powertrain (Husain, 2011).

Another common HEV powertrain configuration is the series-parallel split powertrain. In a series-parallel split powertrain the motor and engine are both connected to the wheels as in a parallel powertrain, but the engine is also connected to the battery through a generator (Figure 3). A vehicle with a series-parallel powertrain can have a smaller and more efficient engine as in a series powertrain and operate it efficiently as in a series powertrain but also have it power the wheels directly as in a parallel powertrain (Union of Concerned Scientists, n.d.-b). However, the powertrain is the most complicated both in design and to operate, and requires a separate generator as in a series powertrain (Husain, 2011). A summary of the advantages and disadvantages of each powertrain can be found in Table 1.

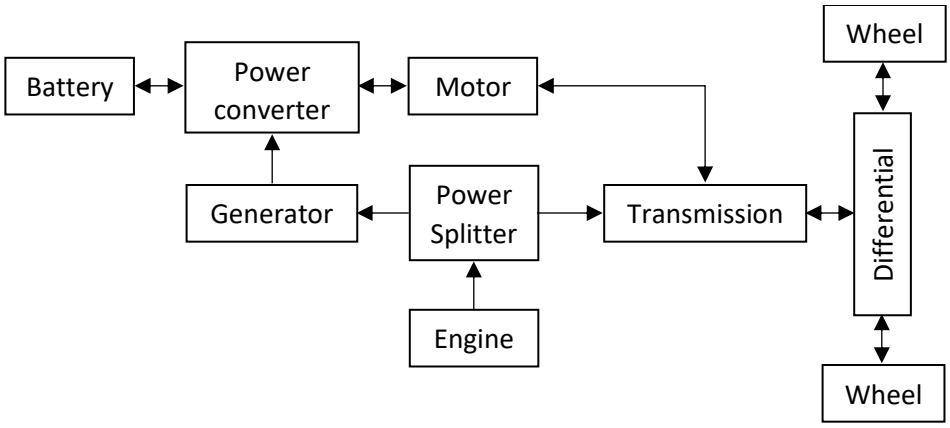

Figure 3: Schematic depiction of a series-parallel split hybrid powertrain (Husain, 2011).

Table 1: Hybrid powertrain comparison.

	Advantages	Disadvantages
Series	• Simple architecture and control • Smaller, more efficient engine • Simple power control • Efficient city driving due to high regen • Efficient engine operation	• Needs powerful battery • Highway inefficiency due to multiple energy conversions • Needs extra generator
Parallel	• Can be powered by battery and/or engine • Better highway efficiency due to direct engine connection • No extra generator	• Needs a powerful, less efficient engine • More complex to control
Series-Parallel Split	• Smaller, more efficient engine • Efficient city driving due to high regen • Efficient highway driving due to mechanical engine connection • More efficient engine operation • Can be powered by battery and/or engine	• Most complex to control • Most complex architecture • Needs extra generator

(Husain, 2011; Union of Concerned Scientists, n.d.-b)

PHEVs were explicitly conceived to address the main problems with BEVs, and they have largely succeeded, but they still have not had a major impact on the vehicle market. One reason for this might be that PHEVs, though cheaper than BEVs, are still more expensive than comparable ICE-powered vehicles. Another might be that even though the PHEV offers substantial environmental benefit, the fact that they still sometimes use gasoline creates confusion for potential buyers or reduces their attractiveness as an environmental solution (Haustein & Jensen, 2018).

In recent years, researchers have examined the idea of modifying the PHEV concept to have an alternative battery or fuel cell as the secondary power source instead of an internal combustion engine. Some have sought to pair fuel cells with batteries purely to improve the power response of the system, rather than to enable significant battery-only range. For example, Ahmadi and coworkers designed a powertrain with a fuel cell, battery and ultracapacitor and implemented a fuzzy logic control technique to optimize power output (Ahmadi, Bathaee, & Hosseinpour, 2018). However, Fernandez and coworkers looked specifically at the advantages of pairing a sizable lithium-ion battery with a fuel cell for range extension. The vehicle they designed travelled 105 km on a 16 kWh battery and an additional 525 km on a 32 kW fuel cell stack. In contrast, most long-range BEVs have batteries with 60 kWh of storage or greater, and most fuel cell vehicles (FCVs) have 80-100 kW fuel cell stacks (Fernández, Cilleruelo, & Martínez, 2016). The vehicle can be charged at home and refuelled in under ten minutes, although an improved hydrogen refuelling network would still be needed. Fernandez and coworkers did a basic power-sharing optimization in order to maximize range and reduce hydrogen consumption, but Martel and coworkers specifically focused on optimizing power-sharing for operating cost reduction and battery and fuel cell longevity (Martel, Dubé, Kelouwani, Jaguemont, & Agbossou, 2016). They managed to improve battery longevity by 18% versus the next best power control strategy or by 41% versus the worst power control strategy. Economic gains through reduced operating costs improved by 3-6%.

Others have investigated the benefits of using a battery as a secondary power source. Bockstette and coworkers showed, using a Ragone plot, that while individual batteries have trade-offs between energy density and power density, a two-battery energy storage system can improve on each characteristic (Bockstette, Habermann, Ogrzewalla, Pischinger, & Seibert, 2013). Using a hand-built test system they demonstrated considerable improvement on conventional batteries, reducing weight by 22% and costs by 12%. They also note that each battery has different cycle life requirements, with the power battery needing to survive over 300,000 short cycles (i.e. covering a small capacity range) while the energy battery needs to survive fewer (less than 5000) deep discharge cycles. Although they do not specify, it is understood that Bockstette and coworkers use different lithium-ion battery chemistries for both their power pack and energy pack (Bockstette et al., 2013). In contrast, Riczu and coworkers used a lithium-ion chemistry for their primary power source and a lithium-silicon chemistry, with a 16% mass reduction compared to lithium-ion, for

their range extender (Riczu, Habibi, & Bauman, 2018). For a set vehicle range they optimized the size of the lithium-ion and lithium-silicon battery packs for vehicle efficiency and battery pack cost, under three different scenarios for lithium-silicon cell cost. Although they noted lithium-silicon's poor cycle life and poor power response as a reason why lithium-silicon cannot be a primary power source, they did not examine these limitations in detail. Yamauchi and coworkers did analyze battery life improvements in their combined battery system. They presented a two-battery powertrain with the two batteries in parallel, rather than in series as in conventional PHEVs and with no current controller as in previously described studies (Yamauchi, Inoue, Chandra, Makino, & Komatsu, 2018). Both the energy and power packs are in operation at all times, with the power pack designed to respond to match rapid changes in power demand. Yamauchi and coworkers characterized the current distribution in the energy pack and power pack and then analyzed battery life improvements in the energy pack based on temperature changes in the pack and the resultant battery degradation. With a configuration in which the power pack is only 5% of the capacity of the energy pack they managed to reduce the temperature rise in the energy pack by 4°C, resulting in a doubling in the life of the energy pack (Yamauchi et al., 2018).

A few researchers have demonstrated range extender concepts specifically with zinc-air batteries as the secondary power source. Eckl and coworkers designed and characterized a set of zinc-air cells based on commercial zinc-air cell components (Eckl, Burda, Foerg, Finke, & Lienkamp, 2013). They recharged the cells mechanically, but postulated that in the future range extending zinc-air batteries could be recharged mechanically or electrically. Based on a vehicle model featuring a 4-kWh zinc-air range extender, they managed to extend the vehicle range by 45-77 km. Catton and coworkers modelled and compared a number of alternative powertrains, including a zinc-air extended range powertrain (Catton, Wang, Sherman, Fowler, & Fraser, 2017). Using a sophisticated vehicle model, they optimized each powertrain for certain performance metrics – range, cost, acceleration, etc. They used a decision matrix to demonstrate that the zinc-air range extender vehicle was superior to the other vehicles, followed closely by the fuel cell vehicle. Sherman and coworkers did extensive analysis of a zinc-air extended range vehicle (S. B. Sherman, Cano, Fowler, & Chen, 2018). They created a zinc-air battery model based on results reported in the literature, modelled the battery within a vehicle model also containing a lithium-ion battery, and optimized the powertrain for vehicle range, battery longevity and overall costs. By analyzing the daily driving patterns of typical American drivers, they were able to design the

powertrain to minimize use of the zinc-air battery and so extend its limited cycle life to over 15 years (neglecting the impact of temperature) while keeping costs down and vehicle range high.

2.2. Lithium-ion battery review

Since lithium-ion batteries were first put into production by Sony in 1991, they have exploded in popularity to become a $36B ($49B in 2019 CAD) global market ("Lithium Ion Battery Market To Reach USD 109.72 Billion By 2026," 2019) with production of 109 GWh of production in 2017 (Deign, 2019). They have become the dominant power source for consumer electronics and EVs. Their popularity is due to their longevity and high cycle life, relatively high specific energy and energy density and their declining costs. Modern lithium-ion batteries have graphite anodes, metal oxide or metal phosphate cathodes and organic salt electrolytes. When discharging, the lithium travels through the graphite structure and electrolyte to the cathode, where it reacts with the cathode material and is incorporated into the cathode structure. During charging, the lithium-ions travel the other way and are absorbed into the graphite structure. Because the lithium is incorporated physically into the electrode structures without significantly altering that structure, lithium-ion batteries are referred to as intercalation batteries.

The cathode material of a lithium-ion battery is an important determinant of electrochemical performance and a key product differentiator relative to the anode and electrolyte, which are fairly similar across commercial products. Lithium-ion cathodes are mostly transition metal oxides or polyanion compounds and mostly have a layered, spinel or olivine crystal structure (Nitta, Wu, Lee, & Yushin, 2015). The lithium-ion batteries first produced by Sony used a layered lithium cobalt oxide (LCO) material, a material which is still commonly used today. LCO batteries were successful and are still successful today because of their high specific energy, high energy density and long cycle life (Du Pasquier, Plitz, Menocal, & Amatucci, 2003), but LCO has significant drawbacks as well. LCO's poor thermal stability makes it a fire/explosion risk (Dahn, Fuller, Obrovac, & von Sacken, 1994), they lose significant capacity when discharged at high currents or to deep discharge levels (Reimers & Dahn, 1992), and are expensive due to the large amount of cobalt used. Other cathode materials were developed to address these shortcomings without compromising LCO's good qualities or introducing new problems.

Nickel cobalt aluminum (NCA) cathodes were developed to reduce the cost of the cathode and improve the thermal stability. Substituting nickel for cobalt maintains the cathode structure while reducing the material cost (Nitta et al., 2015), and adding a small amount of aluminum improves the thermal stability of the cathode and the capacity retention with deep discharging (Chen et al., 2004). NCA manages to maintain a high specific capacity, a high cycle life and a high calendar life (Nitta et al., 2015), but still suffers from capacity fade at higher temperatures (Itou & Ukyo, 2005). NCA cathodes have become one of the two main cathode chemistries for EV batteries, the other being nickel manganese cobalt (NMC). NMC retains the layered structure of LCO and its high specific capacity while reducing the material cost, improving the cycle life and achieving greater thermal stability (Nitta et al., 2015).

Other notable cathode materials include lithium manganese oxide (LMO) and lithium iron phosphate (LFP). LMO can have either a layered or spinel structure, and is of research interest primarily because manganese is much cheaper than cobalt or even nickel. However, LMO has significant cycling stability issues. Layered LMO tends to convert to spinel LMO with cycling, and both layered and spinel LMO suffer from manganese leaching into the electrolyte, side reactions, and other chemical stability issues (Nitta et al., 2015). LFP has an olivine structure and is notable for its high thermal stability (Doughty & Roth, 2012), cycle life and power density, and has attracted commercial interest for EV batteries. But LFP's low average voltage results in a low specific energy relative to other cathodes, and its low electrical and ionic conductivity are problems as well (Nitta et al., 2015).

The anode and electrolyte of lithium-ion batteries are equally important to performance, but there is substantially less differentiation across the commercial market. 98% of the lithium-ion battery market in 2010 used graphite anodes, either modified natural graphite, artificial graphite or mesophase graphite. Modified natural graphite has become the most popular of these three forms of graphite due to its lower processing cost compared to artificial graphite (M. Li, Lu, Chen, & Amine, 2018). Electrolytes are organic solvents with lithium salts – most commonly ethylene carbonate (EC), dimethyl carbonate (DMC), diethyl carbonate (DEC), ethyl methyl carbonate (EMC) or some combination thereof, with lithium hexafluorophosphate ($LiPF_6$) salt (Schmuch, Wagner, Hörpel, Placke, & Winter, 2018). The right combination of solvents helps preserve the stability of the anode and facilitates higher voltages without risking a fire, while proprietary

additives provide further stability and longevity to the battery and prevent side reactions from taking place. The salt makes the electrolyte conductive and facilitates ion transfer.

Commercial lithium-ion batteries have experienced manufacturing improvements as well as chemical improvements over the past decades, and one manifestation of this is optimized cell formats. Lithium-ion batteries today are manufactured mainly in three formats: cylindrical, pouch and prismatic (see Figure 4). In cylindrical cells the anode, cathode, separator and current collectors are rolled to fit into a cylindrical metal canister. Historically the dominant format was the 18650 cell (for 18 mm in diameter, 65 mm tall) but the newer 2170 format (21 mm in diameter, 70 mm tall) resulted in a 35% increase in energy density as well as a reduction in manufacturing costs (Jain, 2017). Cylindrical cells have the highest energy density of all cell formats (M. Li et al., 2018), but they are in some respects more difficult to manufacture than the other formats (Schröder, Aydemir, & Seliger, 2017), and their shape makes them less space efficient. Consequentially some of that energy density advantage is lost at the pack level. Pouch cells use flat, flexible packaging to enclose several layers of anode/separator/cathode. Pouch cells are less energy dense than cylindrical cells but much more space efficient, and easier to handle and assemble due to their flat nature. Their flexible packaging reduces the weight of the cell and simplifies some aspects of the manufacturing, but in other respects makes manufacturing more complex (Schröder et al., 2017). Prismatic cells are rectangular in format, but use a metal container like the cylindrical cells and unlike the pouch cells. Consequentially some aspects of manufacturing are easier than pouch cells, but packaging is more difficult (Schröder et al., 2017). Although all three formats have been used in EVs, prismatic cells are less common than cylindrical and pouch cells (M. Li et al., 2018).

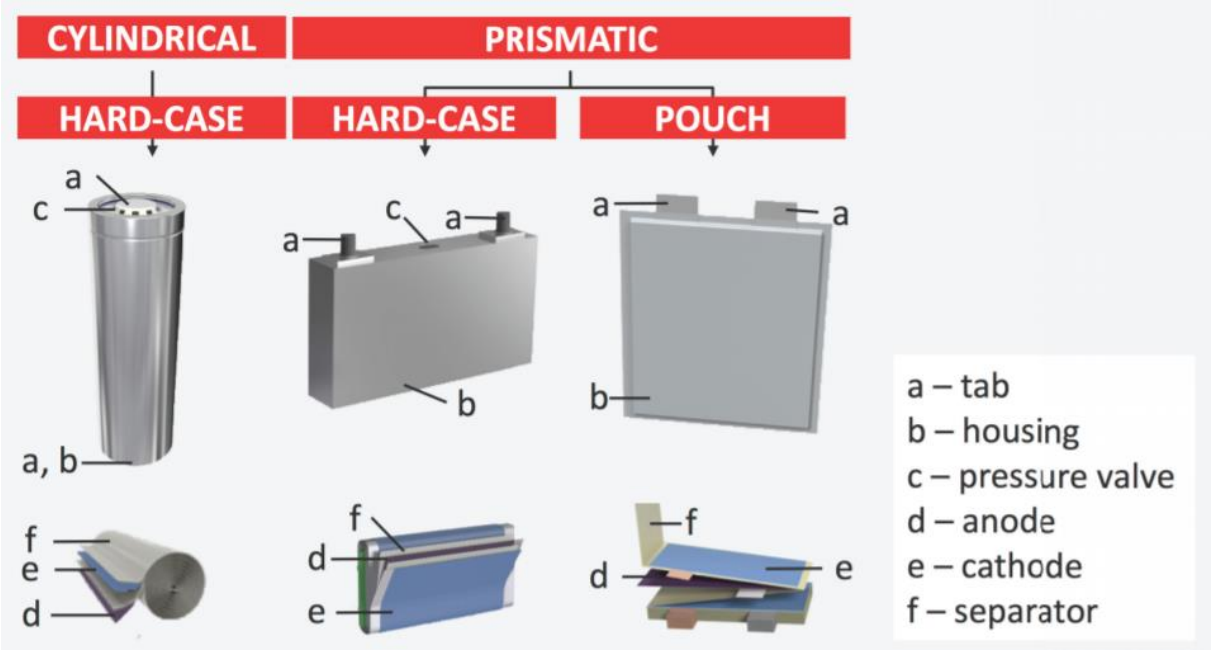

Figure 4: The three main lithium-ion cell shapes (reproduced with permission from (Schröder et al., 2017)).

The manufacturing and chemical improvements in lithium-ion battery technology, as well as improving economies of scale, has led to substantial cost declines. Battery prices have declined 14% annually between 2007 and 2014, according to Nykvist and Nilsson (2015). This implies a 14% cost reduction per doubling of cumulative production, or 8% if the analysis is restricted to the market leaders. They estimate the 2014 price of lithium-ion batteries to be \$300 kWh^{-1} (\$399 kWh^{-1} CAD). Nevertheless, lithium-ion batteries are expected to remain expensive for several years, making EVs uncompetitive with conventional vehicles for that time span.

Lithium-ion batteries represent a drastic improvement on older battery technologies, but their shortcomings may yet limit EV proliferation. Most importantly, their specific energy is still too low and their cost still too high to enable widespread EV use, although both are improving. The specific energy of a lithium-ion battery is only one fiftieth of that of gasoline, and the battery accounts for up to a third of the total cost of a vehicle (Bullard, 2019). Battery safety is also a significant concern. Lithium-ion batteries employ organic electrolytes such as ethylene carbonate, dimethyl carbonate and diethyl carbonate, because aqueous electrolytes would cause the lithium to react violently and destructively. However, these organic electrolytes are themselves flammable. EVs need advanced cooling systems to prevent their batteries from overheating, not only to ensure

optimal performance but to prevent damage to the battery and to the vehicle occupants. Finally, the practicalities of charging an EV leave much to be desired. Apart from the paucity of available fast-charging stations (which may improve over time) the actual rate of charging is much slower than the process of filling up a tank with gasoline. The limitation is due in part to the need to keep the battery temperature low so as to prevent overheating, which fast charging can easily cause. The capacity of the charging station and the stability of the electrical grid can also limit the charging speed.

2.3. Zinc-air battery review

Metal-air batteries have attracted significant interest for EV applications due to their high energy density and specific energy and lower expected cost (Fu, Cano, et al., 2017). Of the available anode materials, lithium, aluminum and zinc have attracted the most interest. Lithium-air batteries have the highest energy density of all the metal-air batteries but face significant hurdles to commercialization. They are inefficient, sensitive to moisture, have poor rate capability and experience irreversible side reactions, resulting in low cycle life and serious safety risk (C. Wang, Xie, & Zhou, 2019). Aluminum-air batteries have the highest energy density of all the metal-air batteries which have aqueous electrolytes, which are significantly safer than organic electrolytes (Fu, Cano, et al., 2017). The Israeli company Phinergy attempted to commercialize an aluminum-air battery for EVs and even attracted interest from global automaker Nissan ("Electric car with massive range in demo by Phinergy, Alcoa," 2014). However, aluminum-air batteries are not electrically rechargeable – they must be recycled after each use (Mokhtar et al., 2015). Consequentially, a battery swapping scheme such as the one proposed by Nixon would be needed to support the proliferation of this technology (United States Patent No. US 5542488, 1994).

Zinc-air batteries are not as energy dense as lithium-air or aluminum-air batteries, but have in light of the shortcomings of those chemistries attracted significant commercial and research attention. Zinc-air batteries have a much higher theoretical specific energy and energy density compared to lithium-ion batteries. They are made from much less expensive raw materials than lithium-ion batteries, which require large amounts of lithium, nickel and cobalt. Primary zinc-air batteries are already used in hearing aids and some specialized commercial applications, but rechargeable zinc-air batteries have not yet achieved significant commercial success (Fu, Cano, et al., 2017). In research settings, zinc-air batteries have been shown to be electrically rechargeable

to a limited number of cycles, and their aqueous electrolytes make them much safer and much less prone to side reactions than lithium-air batteries. Together this suggests zinc-air batteries may be feasible for EV applications.

Zinc-air batteries consist of a zinc anode, an inert cathode where oxygen reduction and evolution take place, a separator and an electrolyte. During discharge, the zinc undergoes a two-step reaction (equations 1a and 1b) to form zinc oxide as oxygen is reduced at the cathode (equation 2); equation 3 shows the overall reaction. Hydrogen evolution also occurs as a parasitic reaction at the anode (equation 4) (Fu, Cano, et al., 2017):

Negative electrode:	$Zn + 4OH^- \rightarrow Zn(OH)_4^{2-} + 2e^-$	(1a)
	$Zn(OH)_4^{2-} \rightarrow H_2O + 2OH^- + ZnO$	(1b)
Positive electrode:	$\frac{1}{2}O_2 + H_2O + 2e^- \rightarrow 2OH^-$	(2)
Overall reaction:	$2Zn + O_2 \rightarrow 2ZnO$	(3)
Parasitic reaction:	$Zn + 2H_2O \rightarrow Zn(OH)_2 + H_2$	(4)

The biggest limitation of zinc-air batteries is their poor cycle life, for which the anode bears most of the responsibility. Zinc anodes suffer from shape change, dendrite formation and passivation with repeated cycling, and can experience hydrogen evolution during charging. Dendrites are sharp protrusions of zinc which form due to preferential zinc deposition in areas of high $Zn(OH)_4^{2-}$ concentration; these then break off, resulting in a loss of capacity, or else puncture the separator and cause a short circuit. Shape change also results from non-uniform zinc deposition and over time reduces anode capacity. Passivation occurs when ZnO precipitates on the anode due to high $Zn(OH)_4^{2-}$ concentrations and clogs anode pores (Fu, Cano, et al., 2017). Researchers have experimented with several strategies to prevent or reduce dendrite formation, shape change, passivation and hydrogen evolution and improve the cycle life of the anode. Several have trialed foam or sponge shaped anodes with some success. Yan and coworkers electroplated zinc onto a copper foam current collector and achieved 9000 cycles at 100 mA cm^{-2} and a 754 mAh g^{-1} specific capacity (Yan, Wang, Jiang, & Sun, 2015). However, the physical characteristics of the anode were such that its capacity density was extremely low, at 39 Ah L^{-1}. Chamoun and coworkers attempted something similar with a nickel mesh and successfully cycled the anode 100 times at C/5 and 719 mAh g^{-1} specific capacity, but only to 40% depth of discharge (Chamoun et al., 2015). Parker and coworkers cast a zinc sponge anode with small quantities of indium and bismuth to

alleviate hydrogen evolution, and achieved a high specific energy (728 mAh g^{-1}) and capacity density (928 Ah L^{-1}) but only achieved 45 charge discharge cycles to 23% depth of discharge (Parker, Chervin, Nelson, Rolison, & Long, 2014). Apart from the practical shortcomings of the described anodes, their increased surface area increases the rate of hydrogen evolution (Parker and coworkers attempt to counter this with indium and bismuth additives). One way to reduce dendrite growth, shape change and passivation without increasing hydrogen evolution is to use calcium, as Wang and coworkers did, to prevent the movement of $Zn(OH)_4^{2-}$. The calcium bonds to the $Zn(OH)_4^{2-}$, causing it to precipitate out of solution; because its potential for migration is reduced the $Zn(OH)_4^{2-}$ does not move much and the zinc plates uniformly. Wang and coworkers achieved 250 cycles at a 2C rate and 100% depth of discharge, but the specific capacity and capacity density of the anode suffered due to the large amount of calcium required (R. Wang, Yang, Yang, Fan, & Wang, 2014). Huang and coworkers used a novel zinc-aluminum layered double-oxide powder, which has a high surface area and allows for efficient OH^- transfer into the solution (Huang et al., 2015). The anode achieved 1000 charge-discharge cycles at a rate of 1C, and though the specific capacity suffered (469 mAh g^{-1}) this is an improvement on Wang and coworkers. Li and coworkers (J. Li et al., 2017) have demonstrated an alternate solution in which zinc oxide microspheres are doped and coated with carbon. This makes them more conductive and inhibits passivation and shape change. The anode achieved 500 mAh g^{-1} and 200 charge-discharge cycles at 1C. The doped and coated carbon successfully supressed dendrite formation and reduced hydrogen generation (J. Li et al., 2017).

The air electrode presents its own set of limitations and challenges which manifest as short cycle life, low specific power and low roundtrip energy efficiency. Oxygen reduction is facilitated with a triple phase boundary, in which the electrode is in contact with both the gas phase and the electrolyte. The low specific power of zinc-air batteries is due to the difficulty in maintaining the triple phase boundary and consequent low current operation (Fu, Cano, et al., 2017). Within this triple phase boundary catalysts are used to enable oxygen reduction and evolution, and researchers have investigated many catalysts as alternatives to expensive precious-metal catalysts. Researchers have focused on bifunctional catalysts, as unifunctional catalysts would necessitate separate electrodes for charging and discharging and negate the energy density advantage of zinc-air batteries over lithium-ion batteries. D. Lee and coworkers used Co_3O_4 nanowires as their catalyst, which they grew directly onto the steel mesh that served as their gas diffusion layer (GDL). A

zinc-air cell using their cathode attained a discharge voltage of 0.9 V at 17.6 mA cm^{-2} (with a voltage polarization of 0.82 V) and had consistent performance through 1500 pulse cycles of five minutes each. However, the power density was quite low, at 40 mW cm^{-2} (Lee, Choi, Feng, Park, & Chen, 2014). B. Li and coworkers used Co_3O_4 nanoparticles along with carbon nanofibers on a stainless steel GDL. They achieved a much higher power density of 167 mW cm^{-2}, with 0.72 V voltage polarization at 25 mA cm^{-2} (B. Li et al., 2015). Another group used sulphur-deficient cobalt oxysulphide on nitrogen-doped graphene nanomeshes ($CoO_{0.87}S_{0.13}$/GN) as their catalyst. A cathode using this catalyst maintained a discharge voltage of 1.1 V at 20 mA cm^{-2} and a charge-discharge voltage gap of 0.77 V even after 320 cycles of one hour each (Fu, Hassan, et al., 2017).

Low cycle life and low power density are the main development challenges of zinc-air batteries, but there are others. Good air management is important to zinc-air battery longevity, both because the introduction of CO_2 can change the pH of the electrolyte and affect electrolyte conductivity and because the cell can dry out or flood if the incoming air removes or deposits too much water (Fu, Cano, et al., 2017). This is manageable with a good air control system and a CO_2 filter. Alternatively, some have elected to use neutral electrolytes that do not carbonize. Goh and coworkers demonstrated adequate performance of a zinc-air cell with a nearly neutral electrolyte, achieving 1000 hours and hundreds of charge-discharge cycles without forming carbonate (Thomas Goh et al., 2014). Eos Energy Storage uses a neutral electrolyte in their commercial zinc-air flow battery (US20150244031A1, 2013). Mohamad tested a gel electrolyte to alleviate water loss and found that a 6M KOH gel electrolyte improved specific capacity compared to a 2.8 M KOH gel electrolyte (Mohamad, 2006). Another important issue for zinc-air batteries is zinc corrosion leading to hydrogen evolution in the cell. Researchers have attempted several strategies – alloying the zinc with other metals (especially bismuth and indium), coating the surface of the electrode with aluminum oxide or lithium boron oxide, and using chemical additives – to reduce zinc corrosion (Fu, Cano, et al., 2017).

2.4. Air pollution from transportation review

In addition to greenhouse gas emission reduction, air pollution mitigation is a major societal impetus for the promotion of EVs. Health Canada estimates that anthropogenic North American pollution is responsible for 14,4000 deaths per year in Canada (2017). These mortalities are attributed entirely to fine particulate matter ($PM_{2.5}$), nitrogen dioxide (NO_2) and ozone (O_3) – other

chemicals contribute to air pollution but their impact was not analyzed due to there being less available data in Canada regarding those pollutants. In another study, the economic cost of $PM_{2.5}$ and O_3 is calculated to be $39 billion dollars ($42B in 2019 CAD) per year (Smith & McDougal, 2017). Health costs born by individuals – illness and premature deaths caused by these air pollutants – make up most of these costs at $36 billion dollars per year, while the costs imposed on the health care system (i.e. hospitals, health care workers, etc.) amount to $2 billion per year and the cost of lost working hours amounts to $800 million per year ($39B, $2B and $861M respectively in 2019 CAD). Another study looking at the impact of transportation specifically found that transportation-related emissions of $PM_{2.5}$, sulphur dioxide (SO_2) nitrous oxides (NO_x) and volatile organic compounds (VOCs) exacted a cost on the Canadian economy of $5.5 billion dollars in the year 2000 (Sawyer, Seton, & Welburn, 2007), which is equivalent to $7.9 billion in 2019. Pollution from light passenger vehicles alone cost $1.4 billion ($2B in 2019 CAD), although this estimate excludes pollution from road dust, as the study was not able to determine how much each mode of transportation contributed to road dust pollution. The study found that NO_x emissions accounted for 52% of overall emissions; that mortality from acute exposure accounted for 70% of the entire economic cost, while chronic exposure mortality accounted for another 26%; and that Toronto specifically had an air pollution cost of $614 million ($878B in 2019 CAD). A more recent study examined the impact of air pollution in Toronto specifically. The study found that air pollution led to 1,300 premature deaths and 3,550 hospitalizations annually in Toronto (Toronto Public Health, 2014). Over half of the city's air pollution was emitted from within the city's borders, and the largest portion of that comes from local traffic. Specifically, air pollution from Toronto traffic accounted for 280 deaths per year and 1090 hospitalizations per year, with larger implied instances of less severe health impacts such as acute bronchitis in children and acute respiratory symptom days.

The main direct air pollutants from ICEVs include NO_x and SO_x emissions, VOCs, carbon monoxide (CO) and particulate matter ($PM_{2.5}$ and PM_{10}). O_3 is an important pollutant which is not emitted directly from vehicles; rather, it is formed when NO_x and VOCs react in still air and sunlight (Union of Concerned Scientists, n.d.-a). EVs do not emit any of these pollutants at the street level, apart from the road dust (particulate matter) they kick up – as do all on-road vehicles. EVs therefore have significant potential to reduce air pollution, especially in major cities where traffic is a dominant contributor to air pollution. However, when accounting for the impact of EVs

on air pollution it is important to account for the emissions generated producing the electricity to charge the EVs.

The research shows that EVs can reduce certain types of air pollution but not others, and whether or not they do depends on the electricity generation profile (Requia et al., 2018). EVs have consistently been shown to reduce emissions of NO_x, VOCs and CO, while the impacts on SO_2, O_3 and PM are less clear and may even be negative. For example, one study found that replacing 100% of light-duty gasoline cars and trucks in Denver, Colorado with PHEVs would reduce NO_x and VOC emissions by 14% and 24% respectively, including the impact of increased emissions from power plants (a mix of coal and gas fired power plants) (Brinkman, Denholm, Hannigan, & Milford, 2010). Another study (N. Li et al., 2016) found that replacing all light vehicles in Taiwan with EVs would decrease levels of most air pollutants. The study found that NO_x, CO, VOCs and $PM_{2.5}$ emissions would be reduced by 7-21%, 45-65%, 20-21% and 4-8%, respectively, with greater reductions in emissions occurring in urban areas than in rural areas. The study also found an increase in SO_2 emissions (2-5%) when the electricity was generated from coal, and increased O_3 concentrations in urban areas. A different study found markedly different results: EVs were found to decrease CO_2 emissions but increase SO_2 emissions in each of China, Russia, India, Brazil, Germany, France, the U.S. and Japan, while NO_x emissions and PM_{10} emissions increased in all of those countries except France, where both decreased, and Brazil, where NO_x emissions decreased (Wu & Zhang, 2017). In contrast to the Taiwan study, SO_2 emissions increased substantially with increased EV penetration.

Particle matter emissions ($PM_{2.5}$ and PM_{10}) are an interesting case because some studies have found that EVs would not reduce these emissions even without accounting for increased emissions from power plants. PM emissions can be generated by internal combustion engines, but one study has estimated that 90% of PM_{10} emissions and 85% of $PM_{2.5}$ emissions generated due to traffic are non-exhaust emissions (Timmers & Achten, 2016). Non-exhaust vehicle emissions are generated from tire wear, brake wear, road surface wear and resuspension of road dust by the wake of the vehicle, all of which are dependent on vehicle weight. Since EVs are 24% heavier than comparable ICE vehicles (Timmers & Achten, 2016) it stands to reason that there would be an increase in the amount of particulate emissions generated from these non-exhaust sources. Timmers and Achten (2016) find that accounting for this increase in emissions from road dust there is no net reduction

in PM_{10} emissions and only a 1-3% reduction in $PM_{2.5}$ emissions, not accounting for any additional emissions from power plants to generate the necessary electricity. A Texas study (which did not account for increased road dust) showed that air pollution impacts (mainly from PM) increase by 350% with EVs powered by coal replacing ICE vehicles, while air pollution impacts (mainly from PM) decreased by 50% and 70% when charged with electricity generated from natural gas or renewable energy, respectively (Tessum, Hill, & Marshall, 2014).

3. Models and Methodology

3.1. Vehicle Model

3.1.1. Modelling software and model overview

In order to evaluate the potential of zinc-air battery technology to serve as a range extender in electric vehicles, two vehicle models are created. The main model is a two-battery electric vehicle (2BEV), in which a small lithium-ion battery and a large zinc-air battery power the vehicle in tandem. The second model is of a traditional BEV with a large lithium-ion battery; this model acts as a point of comparison to the 2BEV, and hence is named the cBEV, for control BEV. The vehicles are shown schematically in Figures 5 and 6 below:

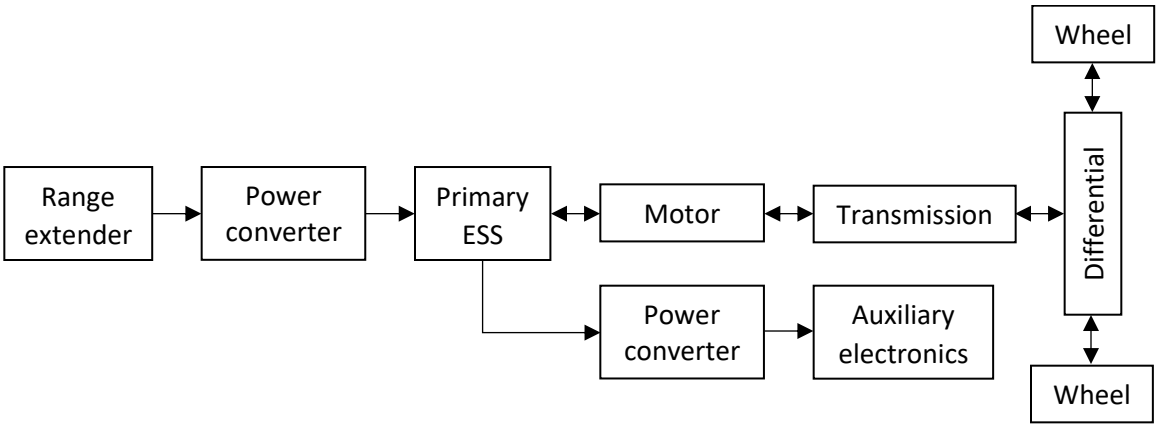

Figure 5: Schematic depiction of the 2BEV model.

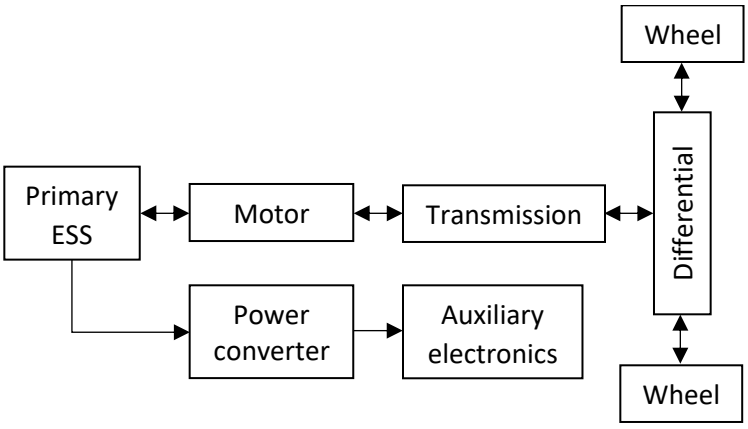

Figure 6: Schematic depiction of the cBEV model.

Both vehicle models were created in Simulink. Simulink is a graphical programming environment based on MATLAB, a programming language and numerical computing environment. MATLAB and Simulink are capable of handling large simulations and heavy numerical computation, making them well suited to vehicle modelling. By using the basic blocks available in Simulink as well as some special blocks available with the Simulink Powertrains Blockset, vehicle component models can be built, which in turn can be combined into a larger vehicle model.

Although the 2BEV model has been tailored to the work of this thesis, it was not built from scratch for this analysis. The original model was built by the University of Waterloo Alternative Fuels Team (UWAFT) for the EcoCAR 3 vehicle competition, in which they modified a 2016 Camaro to be a plug-in hybrid vehicle. The original model was a Simulink model created in Autonomie – a vehicle modelling environment created by Argonne National Laboratory. Subsequently the model was modified in order to replace the engine and related components with a zinc-air battery (S. B. Sherman et al., 2018). Then the model was exported to Simulink (so that using Autonomie was no longer necessary) and modified to include Simscape components for the drivetrain (McInnis, 2017). The vehicle specifications remained unchanged, only how they were modelled. This model was then tailored to suit this work. It should be mentioned that the focus of the work is not to develop a high-fidelity model of a full vehicle, but to model a zinc-air battery and use an accurate vehicle model to evaluate that battery model. The model used by McInnis (2017) was deemed a good platform for the zinc-air battery model.

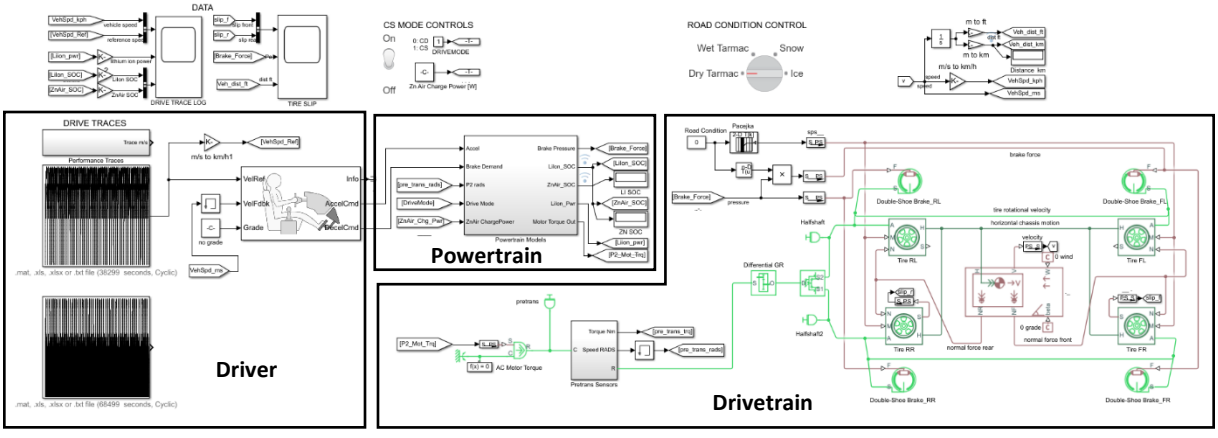

Figure 7: The Simulink model of the 2BEV.

The 2BEV model (Figure 7) is based on several sections, which in turn represent collections of individual components. These components themselves require their own models in order to represent their behaviour accurately. However, the overall vehicle model can be subdivided into three main sections: the powertrain, the drivetrain and the driver. The powertrain includes the batteries, motor, power converters and auxiliary power demand from the electronics. The drivetrain includes the transmission, differential, wheels, brakes and body. The drivetrain is mostly modelled using Simscape, which is like Simulink, except it treats the components as physical systems rather than a series of blocks to simulate sequentially. The driver controls the vehicle speed, and includes the drive cycle (i.e. the target speed, which changes continuously) and a controller which simulates the driver's response to the target vehicle speed.

The vehicle drivetrain includes the differential, the gear ratio, the half shafts, the wheels, the brakes and the body. Most of these values were unchanged from the model used by McInnis, but the vehicle weight and air resistance were changed to reflect a different vehicle. This is because the 2016 Camaro – the vehicle the original model was based on – is a relatively large and heavy vehicle and the vehicle's performance would have suffered relative to modern commercial EVs. Although a detailed comparison to commercial vehicles is inappropriate due to the inevitable discrepancies between simulated performance and real-world performance, the vehicle should achieve broadly similar performance to modern EVs accounting for differences in battery size and other technical details. Instead of the Camaro, the mass of a 2012 Nissan Leaf, less the mass of the battery and motor, was used. For consistency the air resistance coefficient and frontal area of the vehicle was also changed (D. Sherman, 2014). Some key parameters are shown in Table 2.

Table 2: Key drivetrain parameters.

Component	Parameter	Unit	Value
Body	Vehicle weight*	kg	1363
Body	Air resistance coefficient		0.32
Body	Frontal area	m^2	2.276
Tires	Rolling radius	in	12.5
Differential	Gear ratio		3.78

*including the weight of all components except the batteries

The vehicle powertrain includes the vehicle batteries, the motor, the power converters and the auxiliary electronics; also, although it is not a component per se, the decision logic as to when the zinc-air battery is or is not to be run is also housed in this subsection. Certain inputs to the brakes

are calculated here as well. The brake inputs, power converters and auxiliary electronics are unchanged from the model used by McInnis (2017); Table 3 shows some of the key parameters. The lithium-ion batteries are also unchanged, and the zinc-air battery decision logic is unchanged, although different setpoints are used to determine when the zinc-air battery activates and deactivates. The structure of the motor model is unchanged, but a different motor is used to avoid infringing on non-disclosure agreements made by UWAFT. The zinc-air battery model is completely novel.

Table 3: Key powertrain parameters excluding the motor and batteries.

Component	Parameter	Unit	Value
DC to DC Power Converter 1	Efficiency		0.92
DC to DC Power Converter 2	Efficiency		0.95
Auxiliary Electronics	Power consumption	W	200
Brakes	Pressure scaling		2250

3.1.2. The motor model

Although the motor is not a focus of this work, the characteristics of the motor significantly impact vehicle performance; therefore, descriptions of the motor model and the motor characteristics are included. The motor is an AF-130-5 GKN electric motor rated at 64 kW nominal output. The motor efficiency curves, continuous torque and peak torque are shown in Figure 8.

The peak torque is the maximum torque the motor can produce at a given speed; peak torque output can only be maintained for a short period of time – in the case of this particular motor, 20 seconds. Continuous torque is the torque (at a given speed) the motor can maintain for long periods of time. The coloured curves show the efficiency of the motor at the specified speed and torque.

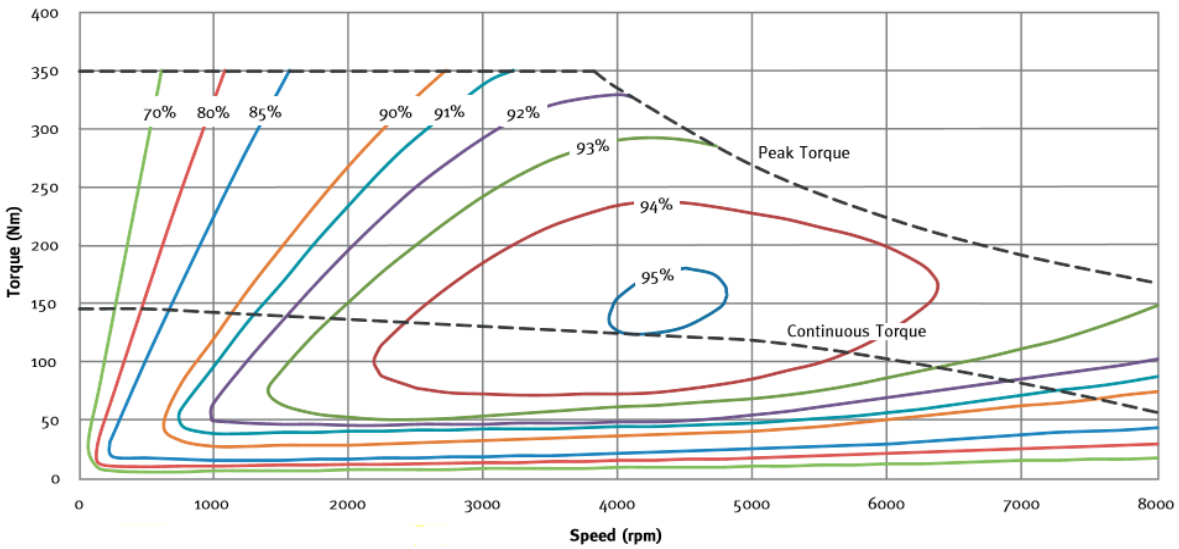

Figure 8: Torque and efficiency curves for the AF-130-5 GKN electric motor (GKN Land Systems, n.d.).

The motor model uses a formula to determine what the maximum torque (T_{max}) is at any given time given recent motor operation and then uses the pedal demand signals to determine how much torque to actually deliver. First, the model determines the continuous torque (T_{cont}) and peak torque (T_{peak}) at the given motor speed. Then a heat index (HI) is calculated, representing how hot the motor is. The hotter the motor is the lower the maximum torque. So, a HI value of 1 indicates that the maximum torque is equal to the continuous torque, while a HI value of 0 indicates that the maximum torque is equal to the peak torque. The HI is used to interpolate between the continuous torque and the peak torque to determine the maximum torque according to Equation 5:

$$T_{max} = T_{cont} \times HI + T_{peak} \times (1 - HI) \quad (5)$$

Then the actual torque (T) supplied by the motor is calculated by multiplying the pedal position (represented by a number from -1 to 1 (cmd)) with the maximum torque as in Equation 6:

$$T = cmd \times T_{max} \quad (6)$$

The HI is calculated according to the formula (Equation 7) developed by Argonne National Laboratory for their motor models (τ is a time constant):

$$HI = -0.3 + \int \frac{0.3}{\tau} \times \left(\frac{T}{T_{cont}} - 1\right) dt \quad (7)$$

Once the torque is calculated, the torque and speed are fed to a lookup table which determines the motor power output. The table is calculated factoring in the motor efficiency. The motor is capable of outputting negative power during regenerative braking. This negative power charges the lithium-ion battery.

3.1.3. Lithium-ion battery model

20 Ah prismatic cells manufactured by A123 serve as the basis for the lithium-ion cell characteristics. A123 cells have graphite anodes and LFP cathodes, making them a safer and lower-cost chemistry compared to other lithium-ion cells (A123 Systems Inc., n.d.). However, the cells also have lower specific energy and energy density compared to competing cells. These cells were selected because their characteristics make them particularly suited to a two-battery powertrain. The primary power source for the vehicle is expected to be small relative to a conventional BEV, making it more likely to experience deep discharging; the battery will also require high power density to compensate for its small size. A123 cells not only have high power density, they have also demonstrated high cycle life at deep discharge. The top-line cell performance metrics are given in Table 4 (A123 Energy Solutions, 2014):

Table 4: A123 lithium-ion cell characteristics. (A123 Energy Solutions, 2014)

Parameter	Unit	Value
Cell Weight	g	496
Cell Capacity	Ah	19.5
Nominal Voltage	V	3.3
Nominal Energy	Wh	65
Specific Energy	Wh kg^{-1}	131
Energy Density	Wh L^{-1}	247
Cycle Life (1C, 100% DOD)		7000

In order to model the cell's real-time polarization curve, an equivalent circuit model was used. An equivalent circuit model represents the cell as an electrical circuit comprised of resistors and capacitors. This sort of model is less computationally intensive than electrochemical models, which attempt to model the true internal dynamics of the cell. The A123 cell is modelled using a modified Rint model (shown in Figure 9), treating the cell as a two-resistor circuit in which all the current passes through one resistor during discharge and all the current passes through the other resistor during charging. A123 provided UWAFT with detailed resistance values for both charging

and discharging, indexed by temperature and state of charge (SOC). Resistance increases with decreasing temperature and with decreasing SOC. The charge-discharge curves of the cell are shown in Figures 10 and 11.

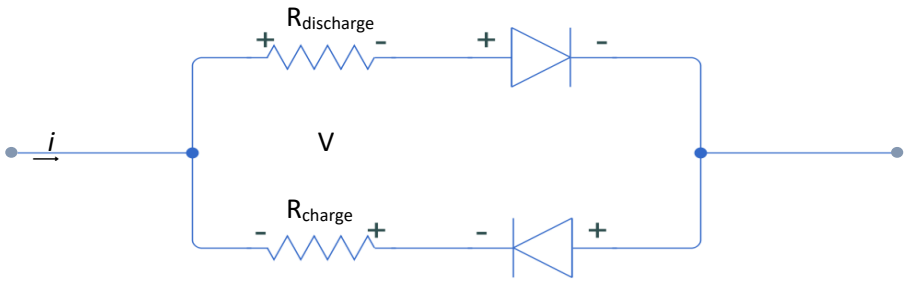

Figure 9: The modified Rint model.

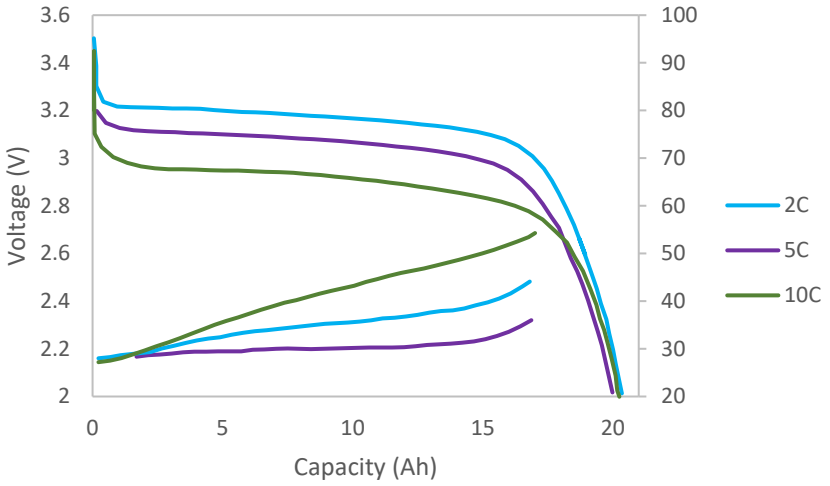

Figure 10: A123 20 Ah cell charge-discharge curves by C-rate (A123 Energy Solutions, 2014).

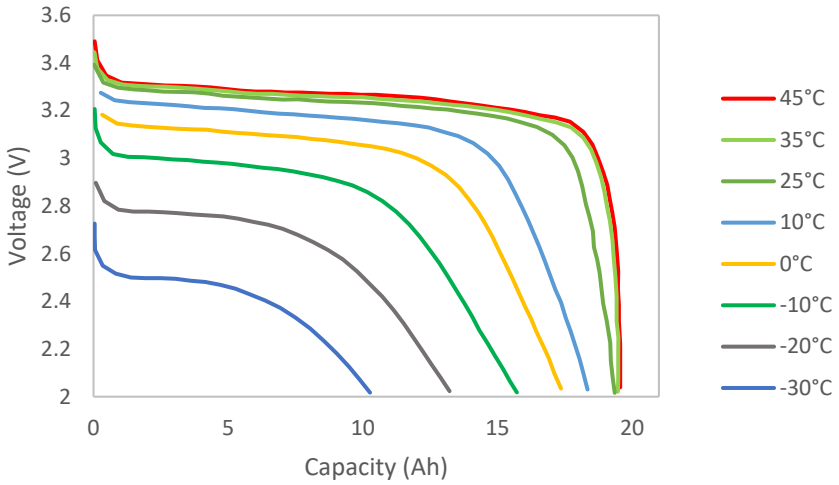

Figure 11: A123 20 Ah cell discharge curves at 1C by temperature (A123 Energy Solutions, 2014).

For both the 2BEV model and the cBEV model, the lithium-ion battery pack is comprised of modules, each of which contain 15 cells connected in series. These modules are connected in series to form arrays, and several arrays are connected in parallel to form the battery pack. Increasing the number of modules in series increases the voltage of the pack, while increasing the number of arrays increases battery pack capacity. In the UWAFT EcoCAR 3 vehicle the lithium-ion battery pack, which is based on the same A123 cells in a similar configuration, the battery pack is 25% heavier than the combined weight of the individual cells due to additional components such as packaging, vehicle mounts, the pack cooling system, etc. This 25% weight factor is used in both vehicle models. The pack is set to cycle between 100% and 5% SOC – A123 cells can maintain deep discharge cycling and still achieve extremely good cycle life. Nykvist and Nilsson (2015) estimated in 2014 that market-leading lithium-ion battery packs cost \$300 kWh^{-1} (\$399 kWh^{-1} CAD) and were declining in cost at 8% per year, which would put them at \$200 kWh^{-1} (\$266 kWh^{-1} CAD) in 2019. The cost of the lithium-ion battery packs used in the modelled vehicles will be based on this price point. The effect of capacity fade on vehicle range is ignored for simplicity, but this effect should be incorporated into future work. The pack-level characteristics are shown in Table 5:

Table 5: Lithium-ion battery pack characteristics.

Parameter	Unit	Value
Cells per module[1]		15
Modules per array[2]		7
Nominal array[2] voltage	V	346.5
Nominal array[2] energy	kWh	6.8
Packaging factor		1.25
Mass per array[2]	kg	65.1
Cost	CAD kWh^{-1}	266
Cost per array	CAD	1807

[1]Cells are connected in series within the module
[2]An array is a set of modules connected in series

3.1.4. Zinc-air battery model

There are very few commercialized secondary zinc-air batteries in existence, all of them designed for stationary storage and relatively unproven compared to lithium-ion batteries. Furthermore, the electrochemical characteristics of these batteries are not public. Therefore, in order to incorporate this technology into the vehicle model, the zinc-air battery performance characteristics are generated using results from literature. This has the advantage of testing the cutting edge of zinc-air cell electrochemical performance; however, generating cell performance characteristics from papers describing the performance of individual components of a zinc-air cell, must be done carefully. The subcomponents must perform under similar conditions, and at conditions that are practical for a commercial cell. It would not be appropriate to use an anode tested in an alkaline environment but a cathode tested in a neutral environment, for example; neither would it make sense to use an anode that was extremely thin or highly porous or otherwise had low loading mass per unit area, as this would make the resulting cell insufficiently energy dense.

The anode was based on the work of Jing Li and coworkers (2017). They produced zinc oxide microspheres that were doped with and coated with carbon. Doping the zinc oxide particles with carbon improves the structure of the particles as well as internal conductivity, and coating the particles in carbon improves conductivity substantially. By coating and doping the zinc oxide particles with carbon dendrite formation was repressed and the anode achieved 200 charge-discharge cycles at 1C with 94.7% capacity retention. The anode demonstrated a specific capacity of 502 mAh g^{-1} with a mass loading of 0.06 g cm^{-2}. Although the anode was tested against a nickel

cathode rather than an air cathode, the anodic reaction is the same as in a zinc-air cell and zinc anodes tested against nickel cathodes are generally considered viable alongside an air cathode. The full specifications and properties of the anode are detailed in Table 6:

Table 6: Zinc anode properties (J. Li et al., 2017).

Parameter	Unit	Value
Mass loading	g cm^{-2}	0.06
Tap density	g cm^{-3}	3.03
Thickness (calculated)	cm	0.0198
Area	cm^2	4.0
Specific capacity @ 1C	mAh g^{-1}	502.2
Volumetric capacity @ 1C	mAh cm^{-3}	1521.7
Cycles @ 1C		200
Capacity retention		94.7%

The cathode performance was based on the work of Jing Fu and coworkers (2017). They developed a new bifunctional catalyst: cobalt oxide with partial sulphur substitution on nitrogen-doped graphene nanomeshes ($CoO_{0.87}S_{0.13}$/GN). The partial substitution of sulphur creates distorted structures which optimizes the oxygen reduction reaction (ORR) and oxygen evolution reaction (OER) performance while maintaining overall crystal stability. The graphene nanomeshes improves the electrical contact of the catalyst and improves transport of reactants and reaction intermediates. The catalyst demonstrated improved stability compared to platinum and iridium, and reduced voltage polarization compared to a control catalyst without sulphur doping. The cathode of the test cell demonstrated 320 cycles at 20 mA cm^{-2} at 1 h per cycle, and an energy efficiency of 60.6%. The cathode properties are listed in Table 7; Figure 12 shows the polarization curve of the cathode, which is based on an interelectrode distance of 100 μm.

Table 7: Air cathode properties (Fu, Hassan, et al., 2017).

Parameter	Unit	Value
Mass	g	0.100
Thickness	cm	0.0250
Area	cm^2	2
Catalyst mass	mg	2.0
Discharge voltage @ 20 mA cm^{-2}	V	1.17
Charge voltage @ 20 mA cm^{-2}	V	1.93
Voltage efficiency @ 20 mA cm^{-2}		60.6%
Cycles (1h @ 20 mA cm^{-2})		320

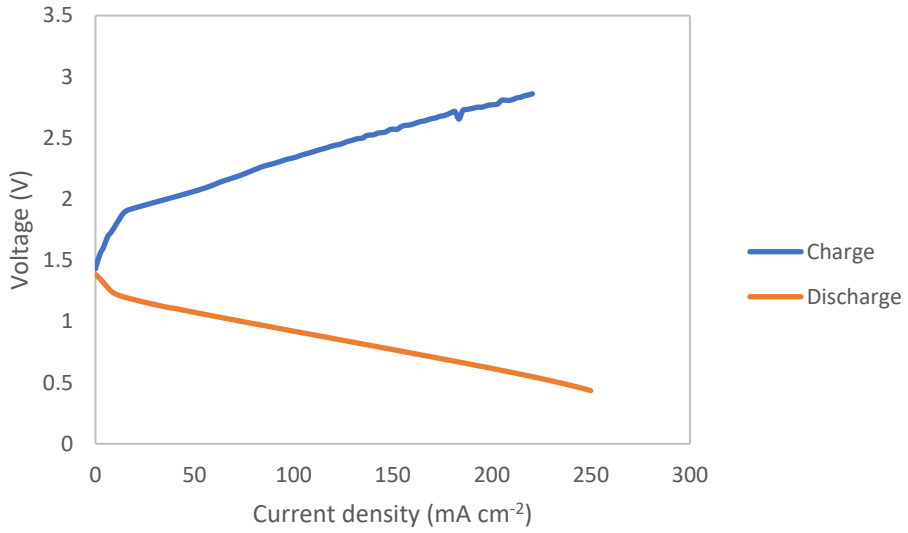

Figure 12: Cathode polarization curves (Fu, Hassan, et al., 2017).

The two electrodes were tested using different electrolytes – for the anode, a solution of 4 M KOH, 1.6 M K_2BO_3, 0.9 M KF and 0.1 M LiOH, saturated with ZnO; for the cathode, a 6 M KOH solution saturated with ZnO – but they are similar enough that comparable results can be expected with either electrolyte. They are both highly alkaline solutions with similar ionic conductivities. In this work the 6 M KOH electrolyte is used, being the more common of the two electrolytes in literature. The separator is the same as that used by Jing Fu and coworkers in characterizing the cathode – a binder-free cellulose membrane assembly (CMA), 100 μm thick and weighing 50 mg. 200 mg of electrolyte was used. By combining the electrochemical performance and physical characteristics of the anode, cathode, electrolyte and separator a model of a zinc-air cell is created.

The cell takes on the polarization curve of the cathode; the other main characteristics of this model are shown in Table 8:

Table 8: Zinc-air cell properties, based on (J. Li et al., 2017) and (Fu, Hassan, et al., 2017).

Parameter	Unit	Value
Area	cm^2	100
Cell casing thickness	cm	0.05
Overall thickness	cm	0.2138
Volume	cm^3	21.38
Mass	g	55.6
Capacity	Ah	6.7
Nominal Voltage	V	1.2
Nominal Energy	Wh	8.0
Specific Energy	Wh kg^{-1}	144
Energy Density	Wh L^{-1}	375
Cycles		200
Voltage efficiency @ 20 mA cm^{-2}		60.6%

It is important to be clear about the structure of the zinc-air cell. The cell consists of a single anode with a cathode on either side, as shown in Figure 13. Both cathodes are bifunctional, and the anode is double the thickness reported by Jing Li and coworkers. The cell is effectively two layers of anode and cathode squashed together in a single envelope; this configuration reduces the amount of weight from the cell casing for the individual cell, and having cathodes on either side of the cell increases the area for air intake. This configuration is still somewhat limited compared to lithium-ion cells, which can have many layers of anode and cathode repeated within a single cell (Schröder et al., 2017). With more development accounting for the need for air intake to the cell, future zinc-air cells may employ this tactic to reduce cell weight and increase specific energy. The dimensions of the cell are shown in Table 9.

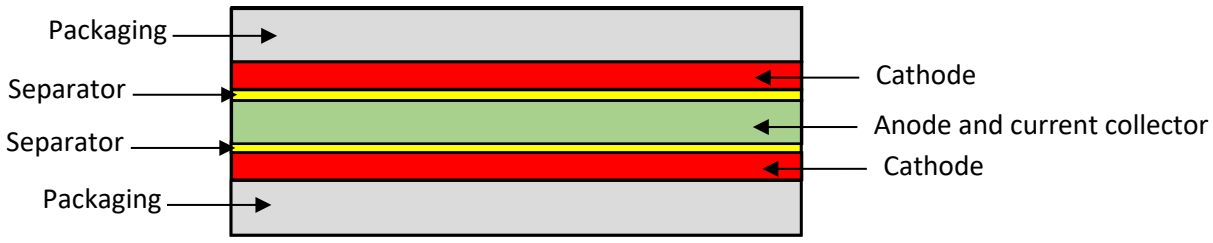

Figure 13: Zinc-air battery cell configuration.

Table 9: Component-level description of a single zinc-air cell

Component	Total mass	Area density	Thickness	Number of layers
Units	g	g cm^{-2}	mm	
Zinc anode	12.7	0.127	0.396	1
Separator	5	0.025	0.1	2
Electrolyte	20	0.100	N/a	N/a
Cathode	10	0.050	0.250	2
Cell casing	7.9	0.035	0.500	2
Total	55.6	0.556	2.096	1

An important consideration is which of the anode and cathode limits the cycle life of the battery. The anode demonstrated 200 cycles at 502 mAh g^{-1}; at 0.06 g cm^{-2} anode loading (J. Li et al., 2017), this implies a lifetime capacity of 6024 mAh cm^{-2}. The cathode achieved 320 cycles at 20 mA cm^{-2} and 1 hour per cycle (Fu, Hassan, et al., 2017), implying a lifetime capacity of 6400 mAh cm^{-2}. Therefore, the anode is the limiting electrode in terms of cycle life.

There are currently few reliable estimates of what a commercial rechargeable zinc-air battery might cost. The materials cost is likely far lower due to the absence or near-absence of cobalt from zinc-air batteries, and due to zinc being much cheaper than lithium; however, manufacturing costs are difficult to predict. EOS Energy Storage has commercialized a zinc-air battery and is selling it for \$160 kWh^{-1} while taking orders for \$95 kWh^{-1} for orders fulfilled in 2022 (\$212 kWh^{-1} and \$126 kWh^{-1} respectively in 2019 CAD) ("Eos Energy Storage Now Taking Orders at \$95/kWh for the Eos Aurora® DC Battery System," 2017). Electric Fuels Ltd estimated the cost of their mechanically rechargeable zinc-air battery at \$80 kWh^{-1} for a high-power pack (Goldstein, Brown, & Koretz, 1999), which is equivalent to \$173 kWh^{-1} (CAD) accounting for inflation and the different nominal voltage (1.15 V in their paper, 1.2 V in this work). NantEnergy claims their zinc-air battery will sell for \$100 kWh^{-1} (\$133 kWh^{-1} CAD) once they begin manufacturing at scale, but this claim is thus far unproven (Spector, 2018). Given the considerable uncertainty on what a non-flow electrically rechargeable zinc-air battery would cost, the middle price of \$173 kWh^{-1} is taken. The zinc-air battery pack characteristics are shown in Table 10:

Table 10: Zinc-air battery pack characteristics.

Parameter	Unit	Value
Cells per module[1]		75
Modules per array[2]		4
Nominal array[2] voltage	V	360
Nominal array[2] energy	kWh	2.4
Packaging factor		1.25
Mass per array[2]	kg	20.8
Cost	CAD kWh^{-1}	173
Cost per array	$	416

[1]Cells are connected in series within the module
[2]An array is a set of modules connected in series

3.1.5. Battery control system

Figure 14 illustrates the decision logic regarding battery operation for the 2BEV. When both batteries are fully charged the range extender is inactive; the vehicle is powered by the primary ESS. When the primary ESS reaches 15% SOC, the range extender activates and charges the primary ESS as the primary ESS continues powering the motor. If the primary ESS SOC increases to 25% the range extender is deactivated until the primary ESS SOC falls to 15% again. Once the range extender runs out of charge the primary ESS powers the vehicle independently until it reaches its minimum SOC of 5%, at which point the vehicle is completely out of charge. By only activating the range extender once the lithium-ion SOC gets below 15%, usage of the range extender is minimized while also ensuring there will be sufficient energy for a sudden increase in power demand. The zinc-air deactivation setpoint was set at 25% because there was sufficient separation between 15% and 25% lithium-ion SOC that the range extender would not switch on and off with great frequency.

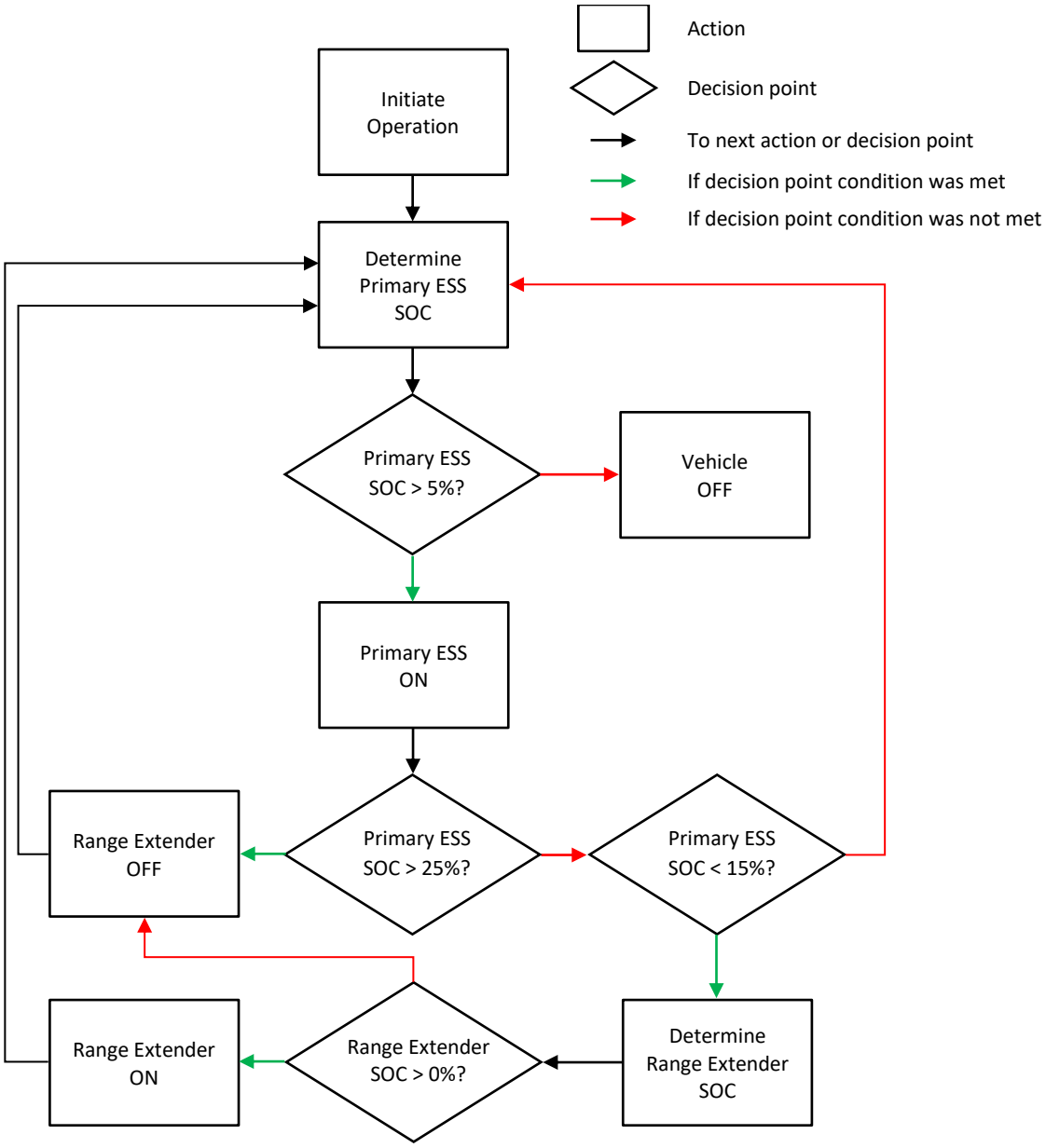

Figure 14: 2BEV battery pack control logic.

3.2. Analysis of Vehicle Model

The purpose of modelling the 2BEV and cBEV is to determine the relative advantage of the 2BEV on key performance metrics. In particular, comparing the vehicles on range, cost and fuel efficiency is critical, as these parameters are among the most important metrics prospective EV buyers consider. Battery longevity is another important consideration, especially for the zinc-air battery with its short cycle life. In this section some important analysis considerations are detailed.

3.2.1. Drive cycles

In order to demonstrate vehicle performance under standard conditions, the US Environmental Protection Agency's (EPA) drive cycles are used as inputs to the model. Drive cycles represents the driver's target speed, and with modification can also incorporate elements such as road grade and wind speed. In this work, the two main EPA drive cycles are used. The Urban Dynamometer Driving Schedule (UDDS) represents typical city driving patterns, while the Highway Fuel Economy Test (HWFET) is used to represent highway driving (EPA, n.d.-c). In order to determine vehicle performance under city or highway driving conditions, the vehicle model is set to run the appropriate drive cycle on repeat until the vehicle runs out of charge. This is done so that performance over the entire range of the lithium-ion battery's SOC and the zinc-air battery's SOC is captured. Then the range and fuel economy for the two drive cycles are averaged, assuming that 55% of all driving can be approximated with the UDDS and the remaining 45% of all driving can be approximated using the HWFET, in line with EPA compliance testing (EPA, n.d.-a). The drive cycles are shown in Figure 15.

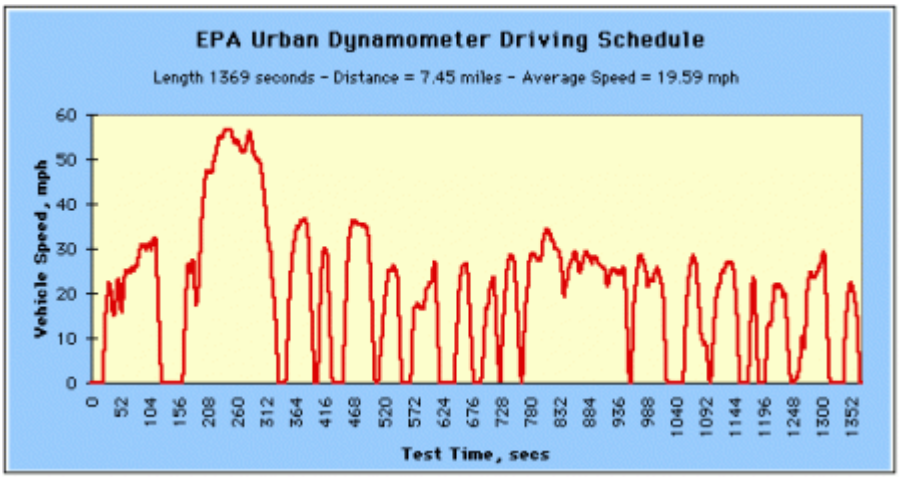

Figure 15(a): City drive cycle UDDS (EPA, n.d.-c).

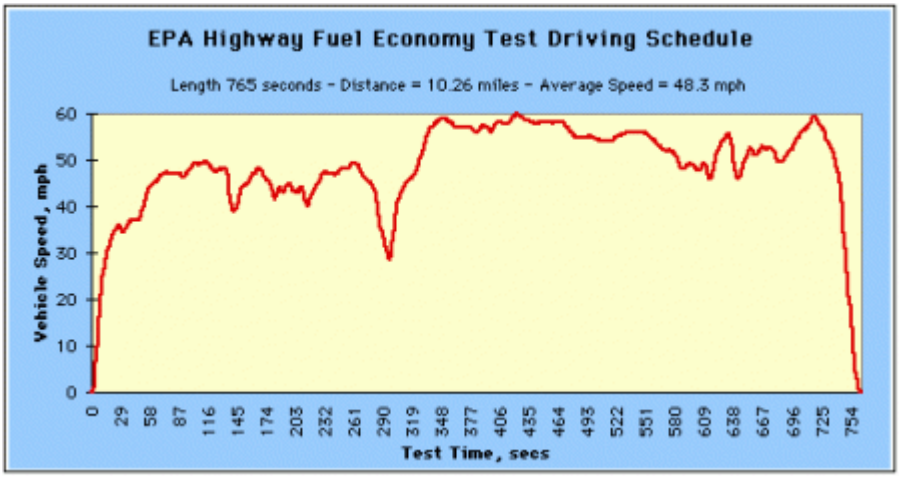

Figure 15(b): Highway drive cycle HWFET (EPA, n.d.-c).

3.2.2. Zinc-air battery life cycle analysis

The longevity of the zinc-air battery pack is an important consideration. The zinc-air battery is assumed to have a cycle life of only 200 cycles in line with the demonstrated performance of the anode of Jing Li and coworkers (2017). In order to extend the battery life, the two-battery system should be configured so as to minimize use of the zinc-air battery, effectively stretching the 200 charge-discharge cycles over a long period of time. In order to evaluate lifetime zinc-air battery usage data from the 2017 US National Household Transportation Survey is used to characterize the daily driven distance of US drivers. Figure 16 shows the frequency at which US drivers (in aggregate) travel a certain distance in a day; for example, the data shows that US drivers travel roughly 15 km throughout the day 8.77% of the year (corresponding to 32 days per year). The figure shows that US drivers usually travel only short or medium distances in a single day; 50% of the time drivers travel 35 or fewer kilometers in a single day, and only 12% of the time do drivers travel over 100 km in a day ("National Household Travel Survey," n.d.). The methodology for creating Figure 16 is outlined in Appendix A. A well designed two-battery powertrain will have a lithium-ion battery large enough to independently power the vehicle most days of the year, reserving the zinc-air battery for the relatively few days of the year when drivers travel long distances.

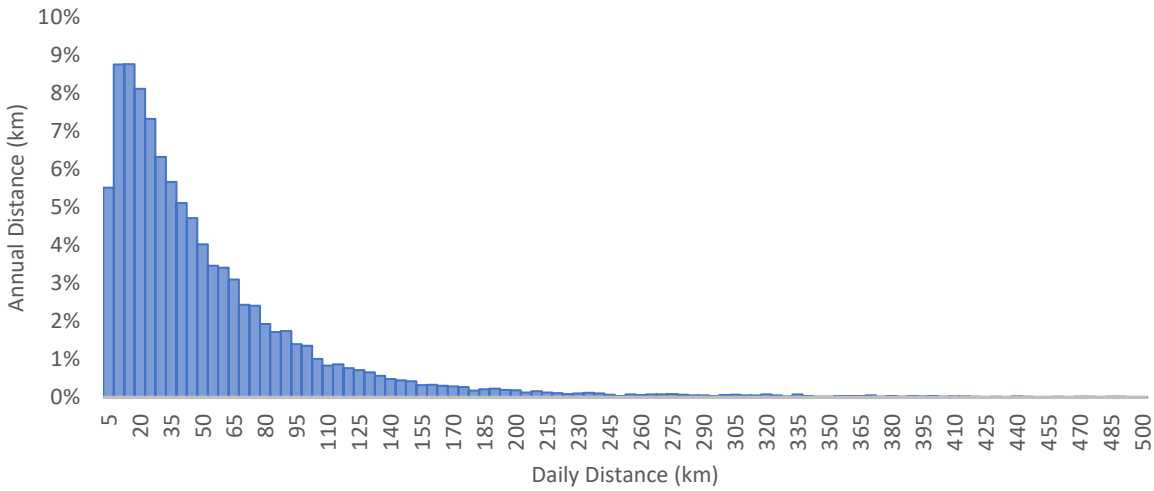

Figure 16: US Daily Driven Distance ("National Household Travel Survey," n.d.).

3.2.3. Battery size optimization

In order to achieve the optimal combination of range, fuel economy, cost and battery life, the batteries of the 2BEV have to optimally sized. The batteries have to be large enough for the vehicle to achieve a respectable range, but having larger batteries makes the vehicle more expensive. Increasing zinc-air battery size at the expense of lithium-ion battery size may reduce costs, but having a smaller lithium-ion battery will result in more frequent use of the zinc-air battery and may reduce its longevity. The respective specific energies and efficiencies of the batteries will also impact the optimal battery configuration. In order to optimize the powertrain, the vehicle model is run at different battery sizes and the performance metrics are recorded. Based on the results the optimal lithium-ion and zinc-air battery sizes will be determined.

In optimizing the battery packs of the 2BEV it is helpful to establish targets for key metrics such as vehicle range, battery pack costs and zinc-air battery lifetime. The ARPA-E RANGE Program run by the US Department of Energy (DOE) has established vehicle-level targets which electric vehicles need to achieve in order to be viable. This includes a 240 mile (384 km) vehicle range target, a 10-year battery lifetime target and a $30,000 ($39,900 CAD) vehicle cost target – which assumes a 60 kWh battery pack with a $100 kWh^{-1} ($133 kWh^{-1} CAD) battery price (ARPA-E, 2012). These targets are adapted for this work: a 400 km range target, a 10-year zinc-air battery lifetime target and a $8,000 CAD battery pack cost target. In this work the cost target is secondary

to the range and battery life targets. Although achieving these targets is the primary goal of the battery pack optimization process there is still benefit to surpassing these targets. For example, in the US the average age of cars on the road is over 11 years and with care cars can be made to last up to 15 years, so improved battery life beyond 10 years is valuable (Consumer Reports, 2018). In this work increased battery life is considered valuable up to 15 years, increased range is considered valuable up to 500 km, and lower battery cost is always valuable.

The power output of the zinc-air battery is an important consideration when optimizing the battery sizes. Ideally, the vehicle model would feature a controller which would match the zinc-air battery power output with the average energy demand of the vehicle over the course of the drive cycle. This would enable more efficient operation of the zinc-air battery while maintaining sufficient lithium-ion battery capacity to handle power demand spikes. Unfortunately incorporating such a controller into the model proved impractical, creating algebraic loops and slowing down the model significantly. To approximate the impact of the controller the zinc-air battery's power output is set to a constant power output, which maintains the lithium-ion battery SOC for the duration of the drive cycle. The constant power output is set individually for each battery configuration and for each drive cycle to slightly above the average power required of the vehicle for that battery configuration and drive cycle. Setting the power this way keeps the lithium-ion battery SOC from falling significantly below the 15% setpoint but also minimizes the instances when the lithium-ion battery SOC reaches 25%, causing the zinc-air battery to shut off. This allows the zinc-air battery to minimize its power output and increases its operating efficiency.

3.3. Air pollution model

An important aspect of this work is to quantify the air pollution benefits of EVs. This could be achieved different ways. One way would be to take estimates for the amount of air pollution emitted per passenger vehicle and the costs per ton of the relevant pollutants, and multiply that by the number of passenger vehicles in the province, to estimate the societal benefits from reducing air pollution from vehicles. This method has the advantage of simplicity, but does not take into account pollutant distribution, traffic patterns or population characteristics. A better way would be to model an entire traffic network, taking into account traffic patterns, population characteristics and air flow patterns; this method would generate a detailed and systemic economic impact assessment. However, this would be a massive undertaking, requiring traffic data for all of the

city's major roads and highways, detailed population data and weather data. In this work, an air pollution model is created which incorporates traffic data, but not population data or weather patterns. It does not cover the entire city of Toronto, only its busiest highway – Highway 401 – and its immediate vicinity. This method takes advantage of the data which is available to demonstrate the difference EVs could make in a highly polluted corridor, is not reliant on massive amounts of difficult-to-obtain data, and has a reasonable scope. However, it does rely on published cost per unit of pollutant values and does not take into account the characteristics of the population immediately proximate to the highway.

3.3.1. Modelling software and model overview

The main modelling software is an air pollution modelling software, called the Transportation Air Quality System (TRAQS). TRAQS has been generously supplied for this project by Lakes Environmental, a Waterloo, Ontario based company which models air pollution for companies or governments involved in large projects which may affect air pollution. TRAQS itself is built on top of two publicly available air pollution modelling software: Motor Emissions Vehicle Simulator (MOVES) and American Meteorological Society/Environmental Protection Agency Regulatory Model (AERMOD). MOVES models traffic patterns and determines the emission rates, while AERMOD transforms those emissions rates into pollutant distributions using air dispersion modelling. TRAQS improves on MOVES and AERMOD by packaging both programs into one interface, improving user-friendliness and making it easier to run large simulations covering long time periods and varying conditions. Although AERMOD is incorporated into TRAQS, technical limitations prevented this component of TRAQS from being used for the full suite of pollutants analyzed. The TRAQS interface is shown in Figure 17:

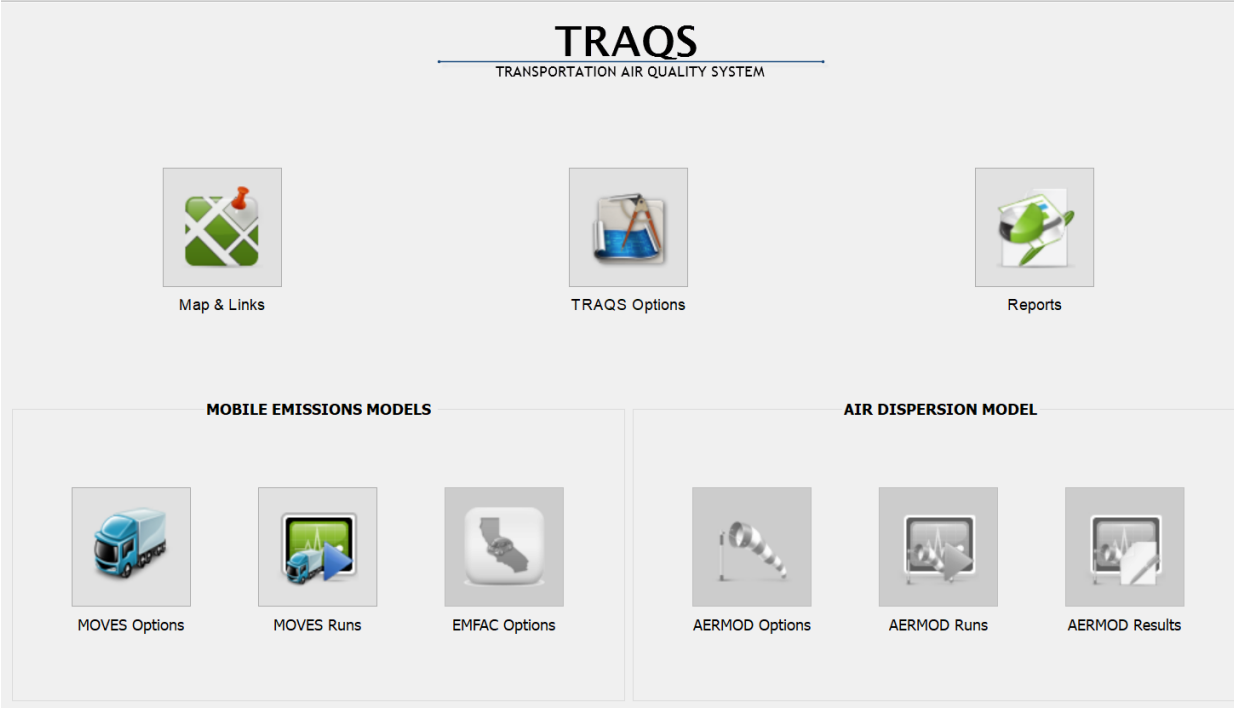

Figure 17: TRAQS interface (Thé, Thé, Chamberlin, & Johnson, n.d.).

The TRAQS model defines the pollution source (Highway 401) as a series of connected roads (or "links") defined so that each individual section approximates a section of the highway between main ramps. This is because traffic flows along stretches of highway between ramps should not change drastically, as vehicles are incapable of entering or exiting the highway for most of that section. There are a few instances where this is not true due to the large number of on or off ramps across a section of highway, for example near Allen Road, but most sections represent a constant traffic flow. For each section of highway, the traffic volume and average speed is specified for each season and for different times of the day – morning peak (6 A.M. to 9 A.M.), mid-day (9 A.M. to 4 P.M.), afternoon peak (4 P.M. to 7 P.M.), and overnight (7 P.M. to 6 A.M.). The width of the highway is specified and average pollution release height is calculated. The entire project area is specified as the highway plus the 500 m on either side of the highway, from Kingston road in the east to Renforth drive in the west. Figure 18 shows the route in the TRAQS interface. The green line represents the highway's segments, and the non-shaded area extends 500 m on either side of the green line.

Figure 18: TRAQS study area: Highway 401 from Kingston Road to Renforth Drive.

There are several more steps after defining the highway and the traffic flow patterns in the model. The vehicle-fuel combinations (e.g. gasoline-powered passenger car, diesel-powered truck, etc.), as well as the pollutants to be modelled have to be selected. Then, for each season and each portion of the day (morning peak, mid-day, afternoon peak and overnight), several additional traffic characteristics have to be specified: the vehicle age distribution, fuel supply and formulation, the climactic conditions, and the fraction of vehicles corresponding to particular vehicle-fuel combinations (e.g. 59% gasoline-powered passenger cars, 8% diesel-powered trucks). Note that here the climactic condition refers to the average temperature and humidity by time of day and year, not the detailed meteorological data required for air dispersion modelling. Once the model is fully specified, it can be run to generate an emissions report, which includes emissions estimate by tons/year.

3.3.2. Data overview

TRAQS comes with built-in default values for several model inputs; for this model the vehicle age distribution, fuel supply and formulation and climactic conditions are all generated from TRAQS default values (which are really MOVES default values generated by the US EPA). The remaining data comes mainly from the Ontario Ministry of Transportation (MTO). MTO publishes annual average daily traffic (AADT) volumes on Ontario's major highways, including Highway

401 (Ontario Ministry of Transportation, 2016). These traffic volumes are broken down by highway segment but not by season or by hour. To calculate the seasonal traffic volume from the annual traffic volume, MTO provided for this work data and a formula (Equation 8) to determine the average daily traffic during a given period of the year *i* (ADT_i) from the AADT:

$$AADT = f_i \cdot ADT_i \tag{8}$$

f_i is a conversion factor which depends on the period *i* (which may refer, for example, to the second half of July) and on the highway subsection. Different sections of highway have different seasonal variation patterns and may have different values of f_i even for the same time of year. Using the given formula and the values of f_i provided by MTO, seasonal average daily traffic volumes were calculated. Additionally, MTO provided sample hourly traffic data along most of Highway 401 for the first week of March 2016. From this data an estimate of the hourly distribution was created. There was variation across the subsections of highway, but this error was not substantial (standard deviation less than 6%), so the same hourly distribution was used for all sections of the highway. Using the hourly distribution and the seasonal ADT values hourly traffic volumes were estimated for each of morning peak, mid-day, afternoon peak and overnight, for each season and for each section of highway.

Apart from the traffic volumes, the MTO also provided average hourly speed data for each hour of the day in for each section of highway. This data was used to characterize the average speeds on the highway in the model. The relative amount of each vehicle-fuel type combination was calculated using data from MTO and from the Bureau of Transportation Statistics (BTS). According to the BTS 95% of the US vehicle fleet is comprised of gasoline cars and light trucks – 56% cars, 39% light trucks. Of the remaining 5% of the vehicle fleet, medium and heavy diesel trucks comprise 3% of the total; gasoline trucks and diesel cars each comprise 1% of the total fleet (Chambers & Schmitt, 2015). Due to their negligible portion of the vehicle fleet, gasoline trucks and diesel cars are excluded from the analysis. The MTO provided estimates for the percent of vehicles on each section of Highway 401 which were trucks. The share of traffic attributable to each vehicle-fuel type combination was therefore calculated for each section as follows: first, the percentage of traffic which was trucks (as specified by MTO) was split evenly between short-haul and long-haul single-unit trucks running on diesel; then, the remaining traffic was split proportionally between gasoline-powered cars and light trucks based on the BTS data.

3.3.3. Estimation of economic cost methodology

The best method to determine the economic cost due to pollution from Highway 401 would be to take the emissions output from TRAQS and use air dispersion modelling to generate a concentration profile in the immediate vicinity of the highway, and then determine the health costs based on that concentration profile and the characteristics of the population around the highway. Health costs can be related to concentration levels much more reliably than to generic emission rates. However, the part of TRAQS which performs air dispersion modelling only works with PM and not with other pollutants. Therefore, an alternate method is used based on guidance by Transport Canada (Transport Canada, 2008). Transport Canada has calculated costs per ton of pollutant which represent the economic impact of that pollutant including personal health impacts, the burden on the health care system and missed work due to illness. Based on these cost numbers (shown in Table 11) and the annual emissions calculated by TRAQS, the overall cost to the Canadian economy from pollution on Highway 401 is estimated. This calculation likely underestimates the true cost, since the published cost values represent an average across the Canadian economy and the pollution from the highway is both in high concentrations and in a high population density area.

Table 11: Pollution cost values (Transport Canada, 2008).

Pollutant	**Cost**
Units	CAD $tonne^{-1}$
NO_x	$5,155
$PM_{2.5}$	$20,016
SO_2	$5,702
VOCs	$628

In order to quantify the potential air pollution reduction and the resulting economic benefits the traffic and resulting pollution coming from Highway 401 is modelled in TRAQS and the annual emissions of the relevant pollutants is determined. Using the per unit costs of these pollutants an annual cost to the Canadian economy is estimated. Then model variations are created in which a percentage of the light passenger vehicles are replaced with electric vehicles, from which new pollution and cost estimates are generated. The overall methodology is illustrated schematically in Figure 19:

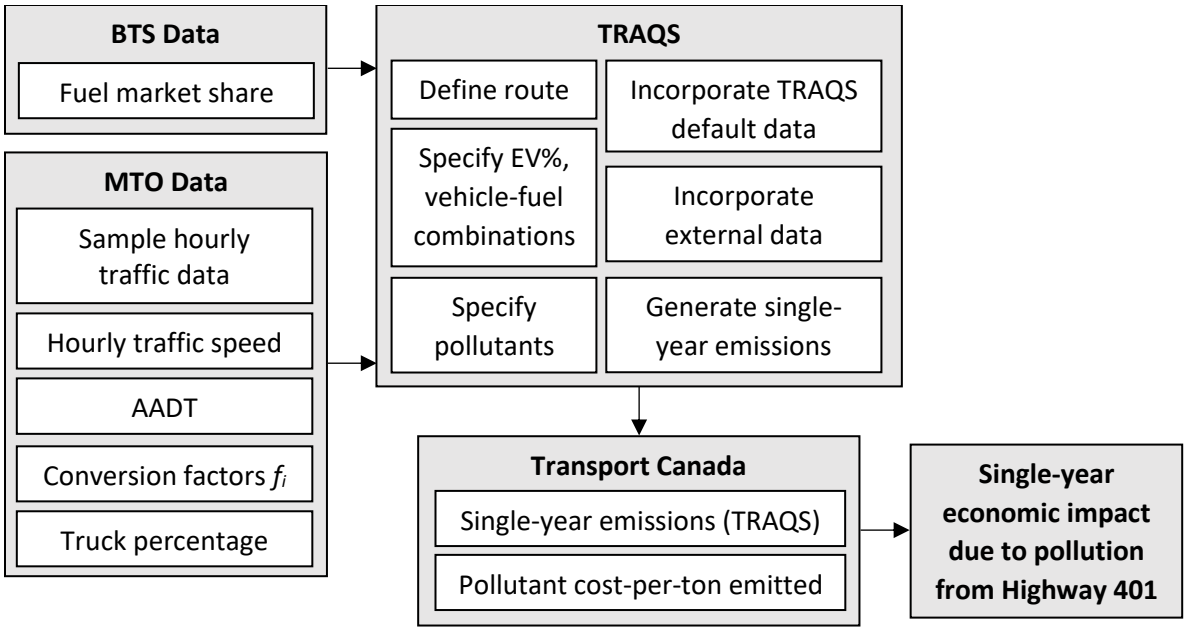

Figure 19: Air pollution cost estimation methodology.

4. Results and Discussion

4.1. Battery pack optimization

Initially the 2BEV was tested with different combinations of lithium-ion battery size and zinc-air battery size. The lithium-ion battery was tested with 1, 2, and 3 arrays while the zinc-air battery was tested with 12, 20 and 28 arrays. These combinations were tested on both the UDDS and HWFET drive cycles and the results averaged with a 55/45% weighting for UDDS/HWFET, respectively. Table 12 shows the results:

Table 12: First optimization of 2BEV battery pack sizes.

ID[1]	Li-ion energy[2]	Zn-air energy[2]	Total energy	Range	Battery cost	Zn-air battery life	Fuel economy[3]	Battery weight
Units	kWh	kWh	kWh	km	CAD	years	kWh (100 km)$^{-1}$	kg
Li1-Zn12	6.5	28.8	35.3	239	$6,800	4.4	14.8	315
Li2-Zn12	12.9	28.8	41.7	278	$8,600	8.9	15.0	380
Li3-Zn12	19.4	28.8	48.2	315	$10,410	15.0	15.3	445
Li1-Zn20	6.5	48.1	54.5	353	$10,120	6.6	15.4	482
Li2-Zn20	12.9	48.1	61.0	388	$11,930	12.5	15.7	547
Li3-Zn20	19.4	48.1	67.5	420	$13,740	20.3	16.0	612
Li1-Zn28	6.5	67.3	73.7	451	$13,450	8.3	16.3	649
Li2-Zn28	12.9	67.3	80.2	483	$15,260	15.0	16.6	714
Li3-Zn28	19.4	67.3	86.7	512	$17,060	24.3	16.9	779

[1]ID refers to the battery size combinations; for example, Li2-Zn28 refers to the battery pack combination with 2 lithium-ion battery arrays and 28 zinc-air battery arrays; [2]Usable energy accounts for the SOC limits for each battery; [3]Does not factor in charging inefficiency – this will be factored in later

The preliminary results show that several of the battery combinations are easily identified as being impractical; four of the combinations achieve a zinc-air battery life of less than 10 years, and five of the combinations achieve a range of less than 400 km. Increasing the size of the lithium-ion battery and the zinc-air battery both increase the zinc-air battery life, though for different reasons. Increasing the lithium-ion battery size increases the distance the vehicle can travel on the lithium-ion battery alone, avoiding activation of the zinc-air battery. This effect is particularly pronounced because a disproportionate share of annual driving distance is accounted for by short- and medium-distance driving. Increasing the size of the zinc-air battery also improves zinc-air cycle life, though more moderately. This is because with a larger zinc-air battery each kilometer powered using the zinc-air battery uses a smaller fraction of zinc-air battery capacity, which means for the same driven distance fewer zinc-air battery cycles are required. Of course, having a larger

battery also improves the range of the vehicle at the expense of increased weight and cost. There is a clear fuel efficiency penalty with the larger battery pack sizes as well.

Excluding the low-range and low-battery life configurations leaves three viable battery configurations – four if the Li2-Zn20 configuration, which nearly meets the range target, is included. Across those five configurations the vehicle range falls between 388 km and 512 km, while the battery cost ranges from $11,930 to $17,060 and the zinc-air battery lasts a projected 12.5-24.3 years. The minimum established range is 400 km, although increased range up to 500 km is valuable, and the minimum established battery life is 10 years, though increased longevity up to 15 years is valuable. Low cost is another important consideration. To determine more exactly the best battery pack configuration, the 2BEV was retested with 2 and 3 lithium-ion arrays and 22, 24 and 26 zinc-air arrays. Table 13 shows the key results:

Table 13: Second optimization of 2BEV battery pack sizes.

ID[1]	**Li-ion energy**[2]	**Zn-air energy**[2]	**Total energy**	**Range**	**Battery cost**	**Zn-air battery life**	**Fuel economy**[3]	**Battery weight**
Units	kWh	kWh	kWh	km	CAD	years	kWh (100 km)$^{-1}$	kg
Li2-Zn22	12.9	52.9	65.8	413	$12,760	13.2	15.9	589
Li3-Zn22	19.4	52.9	72.2	443	$14,570	21.3	16.3	654
Li2-Zn24	12.9	57.7	70.6	438	$13,590	13.8	16.1	631
Li3-Zn24	19.4	57.7	77.0	466	$15,400	22.2	16.5	696
Li2-Zn26	12.9	62.5	75.4	463	$14,420	14.5	16.3	672
Li3-Zn26	19.4	62.5	81.8	489	$16,230	23.3	16.7	737

[1]ID refers to the battery size combinations; for example, Li2-Zn26 refers to the battery pack combination with 2 lithium-ion battery arrays and 26 zinc-air battery arrays; [2]Usable energy accounts for the SOC limits for each battery; [3]Does not factor in charging inefficiency – this will be factored in later

Considering the results shown in Tables 12 and 13, several battery pack configurations demonstrate good performance. In particular, a configuration with two lithium-ion battery arrays makes the most sense. Adding a third lithium-ion battery array increases the zinc-air battery life significantly but to little benefit, given the target battery life of up to 15 years. Vehicle range is also increased but only marginally, and at great cost. Ultimately the Li2-Zn22 battery pack configuration was selected for the 2BEV because it is the cheapest configuration that meets the minimum range target of 400 km and is comfortably in excess of the minimum battery life target of 10 years. For this configuration the zinc-air battery was set to provide, when activated, a constant 6.5 kW of power during the UDDS cycle and a constant 12 kW of power during the HWFET cycle. This results in a zinc-air battery current density of 3.94 mA cm^{-2} during the UDDS

cycle and 7.59 mA cm^{-2} during the HWFET cycle, well below the current density demonstrated in the literature by the anode (J. Li et al., 2017) and cathode (Fu, Hassan, et al., 2017).

To illustrate the discharge patterns of both battery packs Figure 20 below shows the energy of both the lithium-ion battery pack and zinc-air battery pack as the vehicle experiences repeated UDDS cycles. The lithium-ion battery pack energy decreases steadily until it reaches 2.04 kWh (15% SOC,) at which point the zinc-air battery pack activates. Then the zinc-air battery pack energy decreases steadily, but the lithium-ion battery pack energy rises unsteadily because it is matching the power demand from the driver. This continues until the lithium-ion battery pack energy reaches 3.4 kWh (25% SOC), at which point the zinc-air battery pack switches off. The zinc-air battery pack energy level remains constant until the lithium-ion battery pack energy reaches 2.04 kWh (15% SOC) again, at which point the zinc-air battery pack reactivates. This pattern continues until the zinc-air battery pack runs out of energy, at which point the lithium-ion battery pack energy decreases to 0.68 kWh (5% SOC).

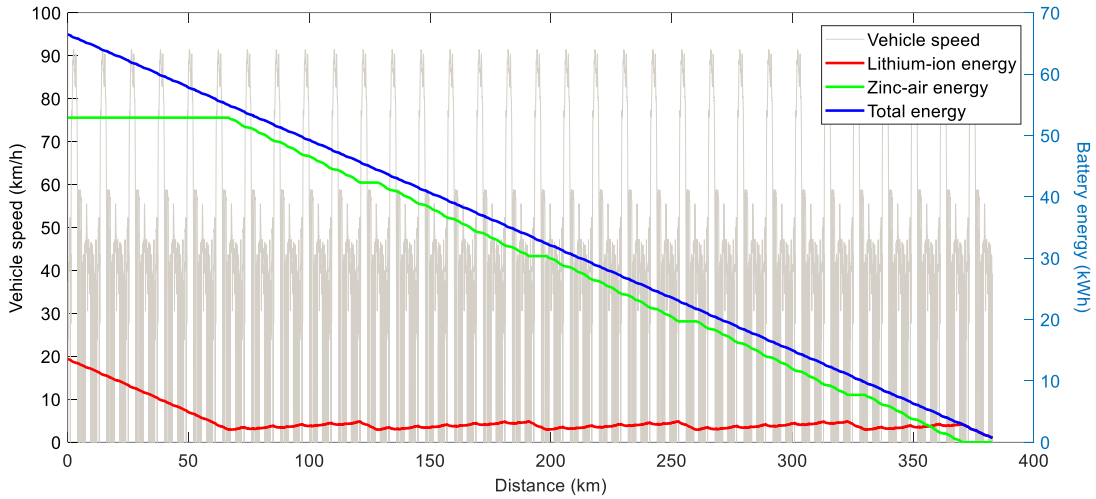

Figure 20: Battery energy and vehicle speed of the 2BEV during repeated UDDS cycling.

An important facet of 2BEV operation which affects fuel economy and zinc-air battery longevity is the utilization factor (UF) of the zinc-air battery. Figure 21 shows the total annual distance travelled by the 2BEV in categories based on the daily driven distance. For example, the first bar on the chart shows that the 2BEV travels 101 km per year counting only the days in which it travels 5 km or less. The chart also shows the distance travelled before the zinc-air battery is

activated. Overall 70% of the annual distance travelled by the 2BEV is powered by the lithium-ion battery with no assistance from the zinc-air battery. Based on this the true fuel economy of the vehicle can be calculated according to equation 9 to be 21.0 kWh (100 km)$^{-1}$.

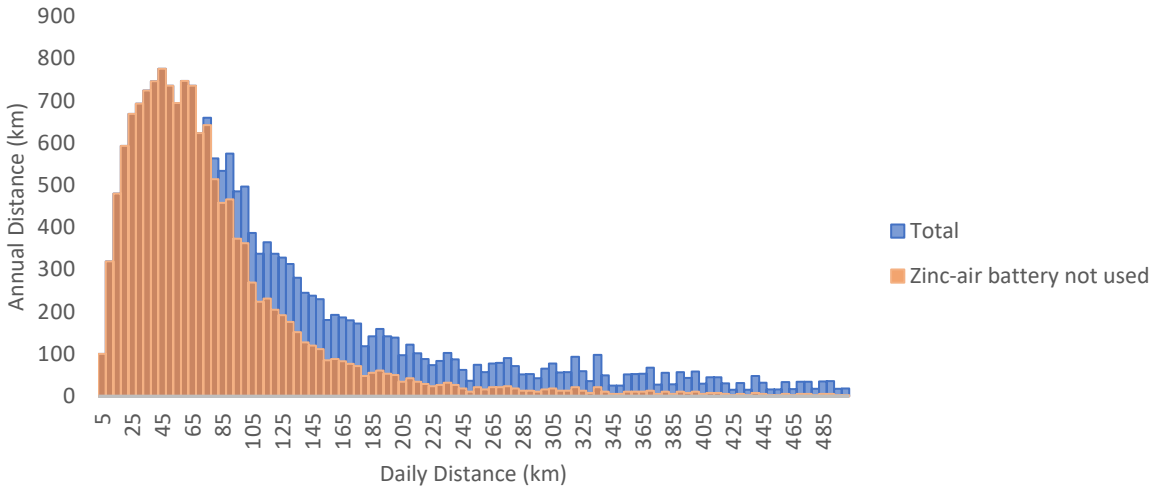

Figure 21: Annual driven distance sorted by daily driven distance.

$$FE_{final} = FE_{initial} \times \left(\frac{1 - UF}{0.85} + \frac{UF}{0.606}\right) \quad (9)$$

$FE_{initial}$ and FE_{final} are the vehicle fuel economies respectively not including and including charging efficiency, and UF is the utilization factor; The zinc-air battery has a charging efficiency of 60.6%, while the lithium-ion battery has a charging efficiency of 85%.

Figure 22 shows the number of zinc-air cycles required for ten years of operation based on the battery configuration. The figure shows a drastic drop in the required zinc-air battery cycles with an increase in the size of the lithium-ion battery, while increasing the size of the zinc-air battery results in modest lifetime gains. Going from one lithium-ion battery array (6.5 kWh) to two arrays (12.9 kWh) reduces the number of battery cycles per year by 45-50%, and going from two arrays to three arrays (19.4 kWh) reduces the number of battery cycles by 38-41%. The figure also shows that if the zinc-air battery cycle life increased from 200 cycles to 300 a smaller lithium-ion battery would suffice to extend the zinc-air battery life over ten years; a configuration such as the Li1-Zn28 configuration, which costs $980 more than the Li2-Zn22 configuration but which travels 38 km further, may become a preferable battery pack configuration.

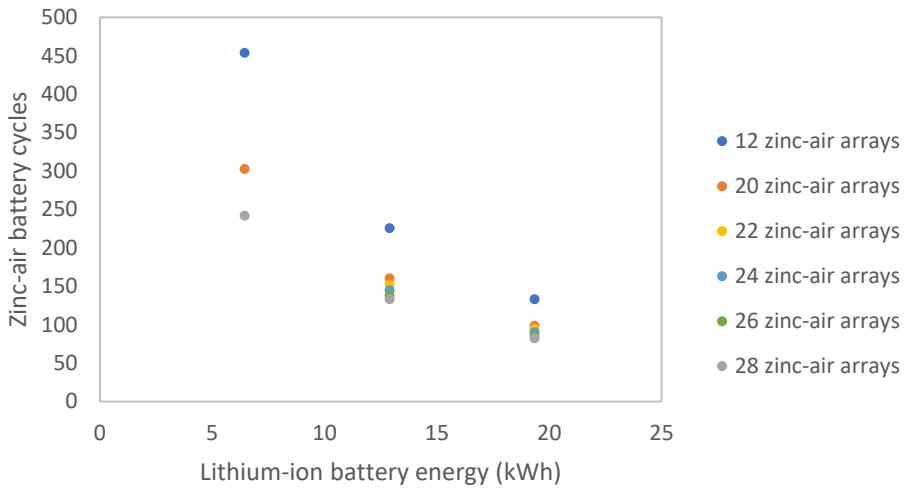

Figure 22: Zinc-air battery cycles required to last 10 years.

4.2. Accounting for CO_2 filter in zinc-air feed clean-up

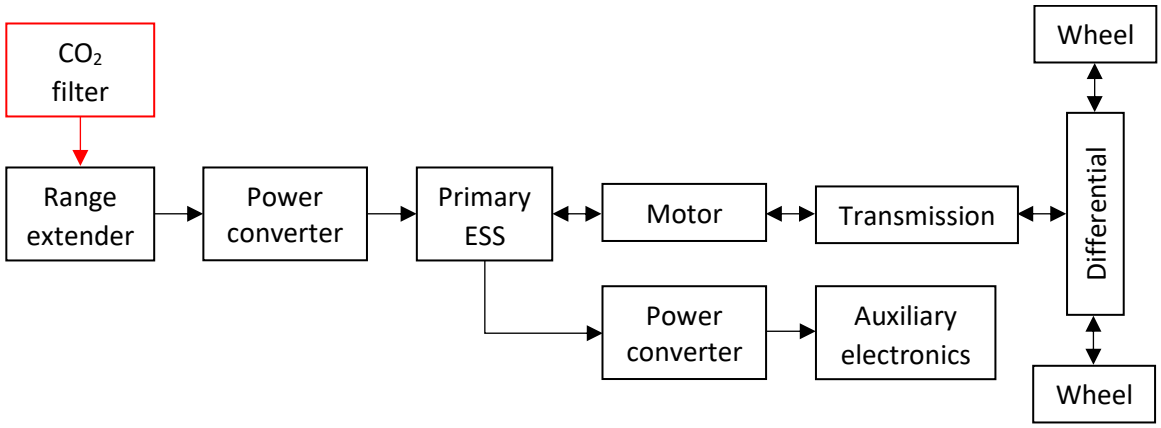

Figure 23: Schematic depiction of the 2BEV model, including a CO_2 filter.

A CO_2 filter for the air intake is necessary to prevent degradation of the zinc-air cells, and accounting for the mass of the filter may marginally affect vehicle performance. The filter was sized using equation 10, and the amount of water necessary for humidification determined using equation 11. Table 14 details the values of the parameters. Humidification is necessary because the absorbent, LiOH-$Ca(OH)_2$, performs significantly better with high humidification (Drillet, Holzer, Kallis, Muller, & Schmidt, 2001). The value of K_{100} is an average of the results of Table 2 of Drillet and coworkers (2001). Based on an estimated 15.2 cycles per year and a 30% buffer, the filter needs 3.4 kg of absorbent and 45.5 kg of water. Accounting for this additional weight reduces the vehicle range to 405 km, increases energy consumption to 21.4 kWh per 100 km and

reduces zinc-air battery life to 12.6 years. However, in practice the vehicle would not use a 45 L tank – firstly because such a tank would be too large to be practical, and secondly because the water usage is calculated assuming the incoming air is completely dry, whereas in practice the air is usually partially humidified already.

$$m_{ads} = \left[\left(\frac{m_{Zn} \times (SOC_{max} - SOC_{min})}{mm_{Zn}} \times \frac{n_{O_2}}{n_{zn}} \times \frac{n_{air}}{n_{O_2}} \times C_{CO_2} \times mm_{CO_2}\right) \div K_{100}\right] \times N \times (1 + B) \quad (10)$$

$$m_{H_2O} = \left(\frac{m_{Zn} \times (SOC_{max} - SOC_{min})}{mm_{Zn}} \times \frac{n_{O_2}}{n_{zn}} \times \frac{P_{vap}}{0.21 P_{atm}} \times mm_{H_2O}\right) \times N \times (1 + B) \quad (11)$$

Table 14: Parameters for calculating size of CO_2 filter and humidification tank.

Parameter	Symbol	Unit	Value
Mass of absorbent	m_{ads}	kg	3.4
Mass of water	m_{H2O}	kg	45.5
Mass of zinc in battery pack	m_{Zn}	kg	83.8
Maximum SOC of zinc-air battery	SOC_{max}		1
Minimum SOC of zinc-air battery	SOC_{min}		0
Molar mass of zinc	mm_{Zn}	kg kmol^{-1}	65.4
Ratio of reacting oxygen to reacting zinc	(n_{O2}/n_{zn})		0.5
Ratio of moles of air to moles of oxygen in the air	(n_{air}/n_{O2})		4.76
Concentration of CO_2 in the air	C_{CO2}	ppm	400
Vapour pressure of water (@ 30°C)	P_{vap}	kPa	4.25
Atmospheric pressure	P_{atm}	kPa	101.325
Molar mass of CO_2	mm_{CO2}	kg kmol^{-1}	44
Molar mass of water	mm_{H2O}	kg kmol^{-1}	18
Adsorption capacity of absorbent	K_{100}	kg_{CO2} kg_{ads}^{-1}	0.3135
Number of zinc-air cycles per year	N		15.2
Buffer	B		30%

4.3. Performance comparison between 2BEV and cBEV

The cBEV had no zinc-air battery, only a large lithium-ion battery of 10 arrays and a nominal energy of 68 kWh. This is similar to the combined energy of the 2BEV with the Li2-Zn22 configuration (67 kWh). Table 15 compares the battery packs for each vehicle, and Table 16 compares the two vehicles on certain performance metrics. The most interesting result of this comparison is how similar the vehicles are. The 2BEV is slightly less fuel efficient, has slightly better range, has slightly better acceleration and weighs slightly less, but the differences are

negligible. The only significant difference is the battery pack cost – the 2BEV battery pack is over $5300 cheaper than the cBEV battery pack, a difference of 28%.

Table 15: Comparison of battery packs between cBEV and 2BEV.

Parameter	Units	2BEV lithium-ion pack	2BEV zinc-air pack	cBEV lithium-ion pack
Cells per module		15	4	15
Modules in series		7	75	7
Arrays in parallel		2	22	10
Total cell weight	kg	104	367	521
Packaging factor		1.25	1.25	1.25
Pack weight	kg	130	459	651
Nominal pack voltage	V	347	360	347
Pack capacity	Ah	39	147	196
Pack energy	kWh	13.6	52.9	67.9
Maximum SOC		1	1	1
Minimum SOC		0.05	0	0.05
Pack cost	CAD	$3,610	$9,150	$18,070

Table 16: Performance comparison between cBEV and 2BEV.

Parameter	Units	2BEV[2]	cBEV
Vehicle weight	kg	2005	2014
City range	km	383	375
Highway range	km	432	437
Combined average range	km	405	403
City fuel economy[1]	kWh (100 km)$^{-1}$	21.7	20.2
Highway fuel economy[1]	kWh (100 km)$^{-1}$	20.1	17.4
Combined average fuel economy[1]	kWh (100 km)$^{-1}$	21.4	18.8
Battery pack cost	CAD	$12,760	$18,070
Time from 0 to 100 km h^{-1}	s	15.06	15.23

[1]Includes charging efficiency
[2]for 2BEV includes weight of filter and water

4.4. Zinc-air battery sensitivity analysis

4.4.1. Analysis of zinc-air specific energy

The fact that, cost aside, the 2BEV and cBEV achieve similar range and fuel efficiency for similarly-sized combined battery packs is curious given that one of the supposed advantages of zinc-air batteries is their superior energy density and specific energy. The performance similarity

can be explained by noting that given the specifics of the zinc-air cell model, the zinc-air cell is actually not that much more energy dense than the lithium-ion cell. The zinc-air cell achieves a specific energy of 144 Wh kg^{-1}, while the lithium-ion cell has a specific energy of 131 Wh kg^{-1}, a mere 10% improvement. Given that 8% of the energy from the zinc-air battery pack is lost to the power converter, this difference shrinks to almost nothing. This begs the question: why is the zinc-air cell specific energy so low?

As shown in Figure 13 and described in Table 9, the zinc-air cell consists of a single zinc anode sandwiched between two air cathodes, with two separators and cell casing on the edge. The key to understanding the zinc-air cell's low specific energy is to note that the anode comprises only 23% of the cell by mass and 19% by thickness. This can be partially explained by the need for a cell casing. If the weight of the cell casing can be reduced by 50% using a lighter material, the proportion of the cell weight and thickness accounted for by the anode would rise to 25%, and the cell specific energy would increase to 156 Wh kg^{-1}. This could also be achieved by stacking multiple anode/cathode layers inside a single cell, thus reducing the cell casing weight as a proportion of the overall cell weight.

Increasing the anode thickness is another way for zinc-air cells to improve their energy density, but increasing anode thickness also increases the internal resistance of the anode. The anode is not as thick as some of the anodes described by Jing Fu and coworkers (2017), so perhaps increasing the thickness is viable, but detailed studies of the effect of zinc anode thickness on internal resistance will need to be conducted before this solution can be implemented. Anode porosity must also be maintained, or else the total amount of active material in the cell will remain unchanged. A 50% increase in anode thickness would increase the weight and thickness of the anode to 37% and 32% of the total cell, respectively, and the specific energy would rise to 194 Wh kg^{-1}.

Finally, the single largest contributor to the mass of the cell is the electrolyte, at 36% of the total mass. Because of the immature nature of zinc-air battery technology there has been little to no study on the necessary amount of electrolyte for good electrochemical and cycling performance, but reducing the weight of the electrolyte is another potential avenue for reducing the weight of the cell. Cutting the weight of the electrolyte by half would increase the weight of the anode to account for 28% of the total mass of the cell and increase the specific energy of the cell to 176 Wh kg^{-1}. These findings are summarized in Table 17. The values in Table 17 are calculated as follows:

begin with the modelled cell described in Table 9, apply the specified modification and account for the differences in mass and energy content due to those modifications.

Table 17: Zinc-air cell performance with different modifications to cell.

	Anode mass %	**Anode thickness %**	**Specific energy**	**Energy density**
Units			Wh kg^{-1}	Wh L^{-1}
Zinc-air cell model (base case)	23%	19%	144	375
Reduce cell casing weight 50%	25%	25%	156	497
Increase anode thickness by 50%	31%	26%	194	514
Reduce electrolyte weight by 50%	28%	19%	176	375

Beyond finding ways to increase the ratio of active material to non-active material in the cell, the true potential improvement in specific energy from a lithium-ion cell to a zinc-air cell merits further scrutiny. An LFP cathode such as that used in the A123 cell has a practical specific capacity of 165 mAh g^{-1} and a 3.2 V nominal voltage (Nitta et al., 2015), implying a specific energy of 528 Wh kg^{-1}. The zinc anode used in this work has a specific capacity of 500 mAh g^{-1} and a nominal voltage of 1.2, implying a specific energy of 600 Wh kg^{-1}. So, looking exclusively at the specific energy of the limiting electrode, zinc-air offers an improvement of only 13.6%. Of course, part of the appeal of a zinc-air battery is that the cathode should be light given the reactant is oxygen and only an inert cathode is needed, but in the modelled zinc-air cell the cathode is almost as heavy as the anode. Therefore, further work – either lightening the cathode or adding to the anode – is necessary to achieve the hoped-for specific energy gains.

One final reason why the modelled zinc-air battery is not significantly more energy dense than the modelled lithium-ion battery may have to do with reasons not related to the cell itself. The packaging factor for the lithium-ion battery represents the battery pack weight additional to the cells itself, and which was determined by UWAFT to be 1.25 for the vehicle they designed. Absent a comparable zinc-air battery pack, the same packaging factor was used for the modelled zinc-air battery. However, there is reason to believe that the packaging factor for a zinc-air battery could be less than that of a lithium-ion battery pack, for several reasons. First, zinc-air batteries are inherently safer than lithium-ion batteries, lacking reactive lithium and explosive electrolytes; thus, a robust battery cooling system might not be necessary. Furthermore, the battery requires significant air intake in order to facilitate the reaction; in a practical zinc-air battery pack, the air

flow might be made to cool the battery as well as fuel it. Finally, because of the way the zinc-air battery is used in the 2BEV all power spikes due to sudden accelerations are dealt with by the lithium-ion battery – the zinc-air battery need only maintain a power output equal to the average power demands of the vehicle (with suitable margin) and never the peak demand. The absence of high current densities which would be caused by high power demand may reduce the risk of the zinc-air battery overheating in the first place. Bockstette and coworkers (2013) propose a packaging factor of 1.10 for their "energy pack" – a high energy density, low power density lithium-ion battery which is utilized in a similar fashion to the zinc-air battery pack in this work. Reducing the packaging factor from 1.25 to 1.10 would reduce the weight of the zinc-air battery pack by 12%.

4.4.2. 2BEV analysis using an improved zinc-air cell

To demonstrate the potential performance of the improved zinc-air cell the 2BEV is retested with a new zinc-air cell model. The new cell model has a 50% thicker anode and 80% thinner cell casing thickness. This improved cell is then substituted into the 2BEV model, so that the range extender uses the same number and configuration of cells but with the improved cell instead of the original cell. The component breakdown of the new cell is shown in Table 18 and the properties of the new cell are shown in Table 19. The polarization curves remain unchanged. Some of he values in Table 19 such as efficiency are taken directly from literature, while other parameters such as capacity use literature values as well as the cell construction specifics outlined in Table 18.

Table 18: Component-level description of improved zinc-air cell.

Component	Total mass	Area density	Thickness	Number of layers
Units	g	g cm^{-2}	mm	
Zinc anode	19.1	0.191	0.594	1
Separator	5	0.025	0.100	2
Electrolyte	20	0.100	N/a	N/a
Cathode	10	0.050	0.250	2
Cell casing	1.5	0.015	0.100	2
Total	55.6	0.556	1.494	1

Table 19: Properties of improved zinc-air cell.

Parameter	Units	Value
Area	cm^2	100
Cell casing thickness	cm	0.01
Overall thickness	cm	0.149
Volume	cm^3	15
Mass	g	55.6
Capacity	Ah	10.0
Nominal Voltage	V	1.2
Nominal Energy	Wh	12.0
Specific Energy	Wh kg^{-1}	216
Energy Density	Wh L^{-1}	801
Cycles*		141
Voltage efficiency @ 20 mA cm^{-2}		60.6%

*Cathode-limited

In the previous model the battery pack packaging weight was represented by a packaging factor applied to the weight of the cells. However, just because the weight of the cells has changed does not mean the packaging weight should change proportionally. The weight of the components external to the cells in the zinc-air battery pack model was 91.7 kg (based on the 1.25 packaging factor), so in the new simulation that weight is fixed at 91.7 kg rather than calculated from a packaging factor. Similarly, the cost of the battery pack is fixed at $12,760, as the addition of zinc and the reduction of the cell casing weight should not drastically affect the overall pack cost.

Finally, it should be noted that since the cell capacity of zinc-air cells has increased the cycle life of the cell is now limited by the cathode rather than the anode. The air cathode tested by J. Fu and coworkers (2017) demonstrated 320 cycles at 20 mA cm^{-2} and 1 h/cycle, which corresponds to a lifetime capacity of 6400 mAh cm^{-2}; at the new anode mass loading of 0.09 g cm^{-2} and anode capacity of 500 mAh g^{-1} this corresponds to a cell cycle life of 141 cycles. In other words, even though the new thicker anode can still achieve 200 cycles the cathode has only demonstrated enough durability to last 141 cycles in the new cell with the thicker anode.

The 2BEV model was run with the new zinc-air cell model; the results are shown in Tables 20 and 21:

Table 20: Comparison of battery packs between cBEV and 2BEV with new zinc-air cell model.

Parameter	Units	2BEV lithium-ion pack	2BEV zinc-air pack	cBEV lithium-ion pack
Cells per module		15	4	15
Modules in series		7	75	7
Arrays in parallel		2	22	10
Total cell weight	kg	104	367	521
Packaging factor		1.25	N/a	1.25
Pack weight	kg	130	458	651
Nominal pack voltage	V	347	360	347
Pack capacity	Ah	39	220	196
Pack energy	kWh	13.6	79.3	67.9
Maximum SOC		1	1	1
Minimum SOC		0.05	0	0.05
Pack cost	CAD	$3,610	$9,150	$18,070

Table 21: Performance comparison between cBEV and 2BEV with new zinc-air cell model.

Parameter	Units	2BEV	cBEV
Vehicle weight	kg	1957	2014
City range	km	530	375
Highway range	km	593	437
Combined average range	km	558	403
City fuel economy[1]	kWh (100 km)$^{-1}$	22.3	20.2
Highway fuel economy[1]	kWh (100 km)$^{-1}$	20.0	17.4
Combined average fuel economy[1]	kWh (100 km)$^{-1}$	21.2	18.8
Battery pack cost	CAD	$12,760	$18,070
Zinc-air battery pack lifetime	years	13.2	N/a
Time from 0 to 100 km h^{-1}	s	15.06	15.23

[1]Includes charging efficiency, with new UF 0.22 for the 2BEV

These results show how sensitive vehicle performance can be to small changes in cell construction. The 2BEV range is significantly improved with the new zinc-air cell compared to the 2BEV with the original zinc-air cell, so that a clear difference between the 2BEV and cBEV now exists. Other performance parameters remain nearly unchanged, but the 2BEV already had a cost advantage on the cBEV. Further benefits are undoubtedly obtainable with improvements at the pack level.

4.5. Economic and environmental analysis

In order to analyze the economics and the environmental impact of the cBEV and 2BEV, these vehicles are compared to a commercial ICEV. This comparison is imperfect due to the inevitable discrepancies between the simulated vehicle performance of the EVs and the real-world performance of the ICEV, but the simulated EV performance was broadly in line with real-world EV performance. The commercial vehicle used for comparison is the 2019 Honda Civic, which is similar in size to the Nissan Leaf body upon which the model vehicles are based. Table 22 shows the measures on which the vehicles were compared:

Table 22: Economic and Environmental comparison between the cBEV, 2BEV and ICEV.

	Units	**2BEV**	**cBEV**	**ICEV**
Estimated MSRP	CAD	$26,321	$31,625	$17,890[1]
Harmonized Sales Tax (13%)	CAD	$3,422	$4,111	$2,326
Fuel costs	CAD yr^{-1}	$416	$373	$1,686[2]
Maintenance costs	CAD yr^{-1}	$584	$584	$720
Combined Costs	CAD	$36,680	$42,380	$36,930
CO_2 emissions scenario 1	kg yr^{-1}	75	56	3354
CO_2 emissions scenario 2	kg yr^{-1}	2283	2044	3354

[1](Honda Canada, n.d.); [2]Based on 7.1 L (100 km)$^{-1}$ (Honda Canada, n.d.)

The manufacturer's suggested retail price (MSRP) is calculated by adding the cost of the battery packs and the electric powertrain components to the Civic MSRP and subtracting the costs of the Civic powertrain components (Fries et al., 2017). Maintenance costs for the Civic are based on the CAA estimate (CAA, 2013), and the electric vehicle maintenance costs are set to be 19% cheaper (Propfe, Redelbach, Santini, & Friedrich, 2012). Fuel costs are based on gasoline prices of \$1.20 L^{-1} and electricity prices of \$0.10 kWh^{-1}, and do not factor in a federal price on carbon. The combined costs combine the upfront price, fuel costs and maintenance costs are calculated using equation 12 with an interest rate of 7.25% (CAA, 2013) to transform the fuel costs and maintenance costs of the vehicles into a 2019 single-year equivalent value. A ten-year vehicle lifespan is assumed for all vehicles. The annual CO_2 emissions per vehicle are estimated under two scenarios for electricity generation. In the first scenario, the electricity is assumed to come from the Ontario electricity grid, which has an emissions intensity of 0.0296 kg_{CO2} kWh^{-1} (National Energy Board, n.d.-b). In the second scenario, the electricity is assumed to come from the Alberta

electricity grid, which has an emissions intensity of 0.5485 kg_{CO2} kWh^{-1} (National Energy Board, n.d.-a).

$$CC = MSRP + HST + (FC + MC) \sum_{n=1}^{10} 1.0725^{-n} \quad (12)$$

In equation 12 CC is the combined costs, MSRP is the manufacturer's suggested retail price, HST is the harmonized sales tax, FC is the fuel costs and MC is the maintenance costs.

There are several notable findings from this analysis. That the 2BEV has higher fuel costs and higher emissions than the cBEV is due to the low efficiency of the zinc-air battery. This is somewhat but not entirely mitigated by the fact that the lithium-ion battery in the 2BEV is responsible for powering the vehicle most of the time. However, this higher fuel cost is not enough to mitigate the 2BEV's advantage on the combined costs of the up-front vehicle price and fuel and maintenance costs. Comparing the three vehicles, the cBEV is 14.8% more expensive than the Civic and the 2BEV is 0.68% less expensive, a difference attributable to the low cost of the zinc-air battery.

The emissions scenarios are interesting as well. Ontario's electricity is generated mostly from renewable energy and nuclear power, with only a small amount generated from natural gas. The environmental benefits of electric vehicles in Ontario are clear and dramatic – direct emissions are reduced by 98% compared to the Civic, a relatively fuel-efficient small car. In Alberta the benefits are still large but less substantial than in Ontario. Alberta relies heavily on coal-fired and natural gas power plants to generate electricity, with only a small amount of zero-emissions electricity generation. Nevertheless, using electric vehicles can reduce emissions by 32-39% on a per-vehicle basis.

4.6. Air pollution results

Highway 401 was modelled in TRAQS based on the average speed and traffic flow data provided by MTO, and based on the vehicle distribution information from the BTS and MTO. Table 23 shows the annual emissions from the highway of relevant pollutants, and their associated economic costs due to impacts on human health, missed time at work, etc.:

Table 23: Baseline (0% EVs) emissions and costs of pollution from Highway 401 over one year.

Pollutant	**tons year^{-1}**	**CAD tonne^{-1}**	**CAD year^{-1}**
NO_x	2366	$5,155	$13,436,000
$PM_{2.5}$	198	$20,016	$4,356,000
SO_2	9.4	$5,702	$59,000
VOCs	959	$628	$663,000
Total			**$18,514,000**

Then the model was modified so that the passenger gasoline vehicles were partially replaced with electric vehicles. The annual pollution and economic costs at different levels of EV penetration are shown in Figures 24 and 25:

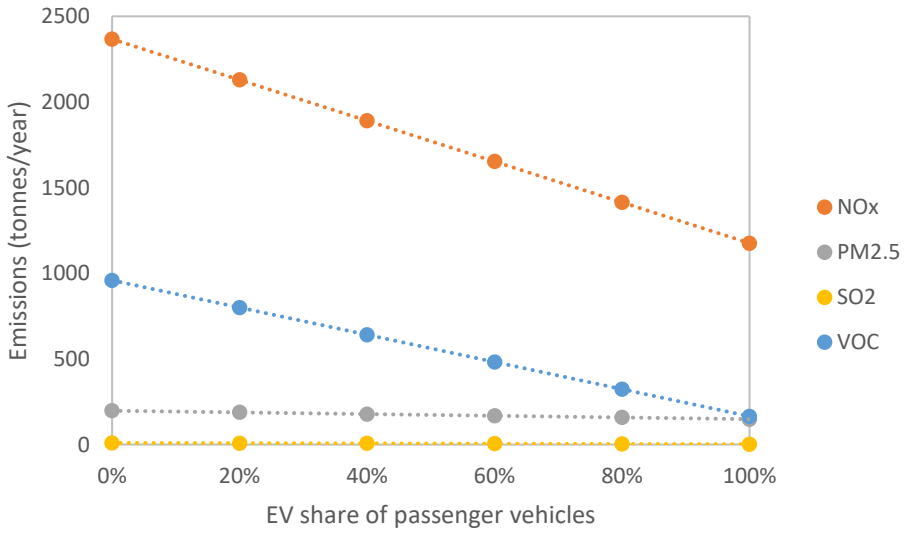

Figure 24: Annual emissions from Highway 401 at different BEV penetrations.

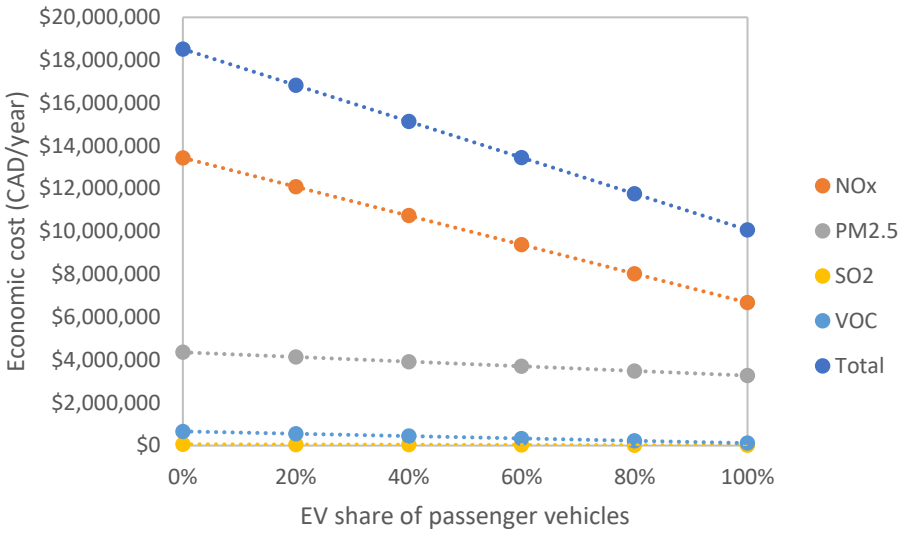

Figure 25: Cost of emissions from Highway 401 at different BEV penetrations.

Overall emissions costs dropped by 45% at full EV penetration, indicating that a substantial portion of overall pollution costs can be traced back to trucks, not passenger cars. NO_x emissions dominate both by volume and by cost, as indicated by Sawyer and coworkers (2007), while SO_2 emissions were negligible and barely impacted the total cost, in line with work by N. Li and coworkers (2016). VOCs were a large portion of the emissions by mass, but due to their relatively low impact comprised a low share of the overall cost. $PM_{2.5}$ emissions comprised the second largest portion of the total economic costs and saw the least impact from increasing EV penetration. While NO_x emissions decreased by 10% for every additional 20% EV penetration, and SO_2 and VOC emissions decreased by roughly 16% for every additional 20% EV penetration, $PM_{2.5}$ emissions decreased by only 5% for every additional 20% EV penetration. Contrary to some of the research which suggested most of the $PM_{2.5}$ emissions from vehicles is attributable to road dust, brakewear and tirewear (Timmers & Achten, 2016), TRAQS ascribes most of the $PM_{2.5}$ emissions to engine exhaust. Futhermore, the simulation results show that brakewear and tirewear decrease at a faster rate than the exhaust emissions, perhaps due to the reduction in brake usage in electric vehicles due to regenerative braking. The $PM_{2.5}$ emissions at different EV penetrations and from different sources are shown in Figure 26:

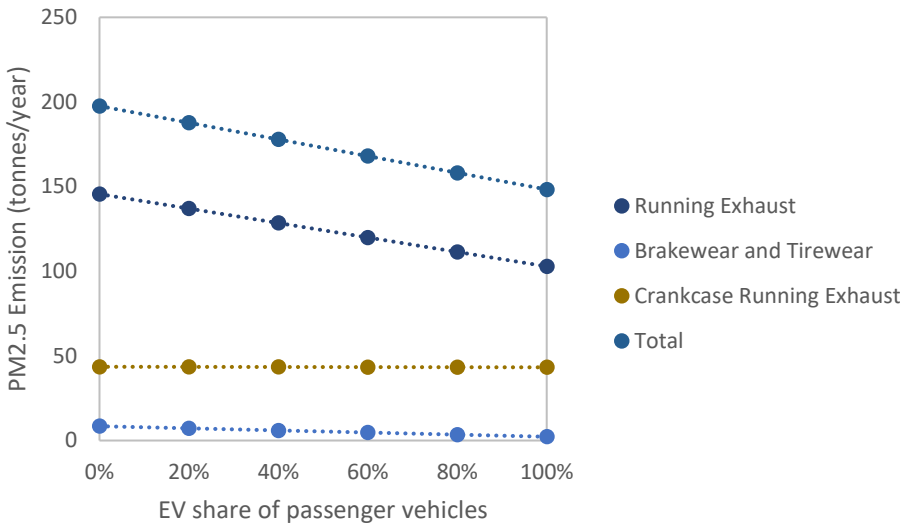

Figure 26: $PM_{2.5}$ emissions from Highway 401.

An interesting finding from this analysis is the extent to which trucks are responsible for air pollution in spite of their small traffic volume (8-10% on Highway 401, according to the MTO data). At 100% EV penetration of passenger vehicles the overall cost of pollution from Highway 401 was reduced by less than 50%, and almost all the remaining pollution is attributable to the presence of trucks – all of the NO_x, SO_2 and VOC pollution, and all of the $PM_{2.5}$ pollution except the brakewear and tirewear $PM_{2.5}$ pollution, which amounts to only $49,000 per year.

5. Conclusions

This work had several aims with the overarching goals of improving upon existing EV technology and quantifying the benefits of EVs. A new EV powertrain was proposed which would incorporate a zinc-air battery range extender alongside a lithium-ion battery as the primary ESS, with a simple control strategy for maximizing range extender life. In order to accomplish this, appropriate zinc-air cell articles were selected from the literature to form the basis of the zinc-air cell model. Once this model was fully specified it was incorporated into an existing vehicle model based on the work of UWAFT and which was modified to suit this work by changing the vehicle weight, air resistance and vehicle motor. A second version of the model which had a large primary ESS but no range extender was created to serve as a control. The configuration of the range extender and the primary ESS in the 2BEV was optimized and the performance of the vehicle was characterized. The battery pack of the cBEV was sized to match that of the 2BEV and the vehicle performance was characterized. Based on these results, the vehicles were characterized economically and environmentally. Additionally, the 2BEV was retested with a modified zinc-air cell model with improved performance in order to demonstrate the potential of an improved zinc-air cell. Finally, in order to characterize the broader benefits of EVs, the traffic flow and pollution from Highway 401 in Toronto was modelled based on data provided by the MTO, and the economic cost of the pollution was quantified. Then the model was rerun at different EV penetration levels in order to quantify the benefits of EVs.

There were several key findings that resulted from this work, including:

- The optimized 2BEV achieved a range of 405 km and a fuel economy of 21.4 kWh per 100 km, with a battery pack cost of $12,760. The cBEV achieved a similar range and a slightly better fuel economy but cost over $5,000 more.
- In spite of the range extender's low cycle life, it was quite feasible to size the battery packs of the 2BEV so that the range extender lasted over ten years. Several configurations achieved this target, and in the chosen configuration the range extender lasted 12.6 years. This was achieved by sizing the batteries so that the primary ESS powered the vehicle independently for 70% of the vehicle's annual driven distance.
- The range extender had a specific energy only 10% greater than the primary ESS. This is primarily due to the high proportion of mass in the zinc-air cell which is not anode and which

therefore does not contribute directly to specific energy. Reducing cell casing weight and increasing anode thickness increases the specific energy of the cell by 50% – from 144 mAh g^{-1} to 216 mAh g^{-1} – and the range of the 2BEV improves to 558 km.

- Comparing the 2BEV and cBEV to a commercial ICEV – the 2019 Honda Civic – on certain economic and environmental metrics demonstrated the benefits of EV technology and of the two-battery powertrain in particular. The cBEV was 15% more expensive than the ICEV when considering fuel costs, maintenance costs and upfront cost, but the 2BEV was slightly cheaper than the ICEV. Both vehicles were shown to result in significantly less greenhouse gas emissions, even in a highly carbon intensive electricity grid such as Alberta's electricity grid. When charged with electricity from Ontario's grid, emissions were reduced by over 97%.
- The pollution resulting from the traffic on Highway 401 was found to be substantial - $18.5M per year. Consequently, increasing the percentage of passenger vehicles which are electric has substantial benefits – but even at 100% EV penetration, the costs from the air pollution are only reduced by 45.6%. This demonstrates the substantial contribution of trucks to air pollution, and the necessity of reducing pollution from trucks to realize the maximum air pollution reduction benefits.
- NO_x was the costliest air pollutant at $13.4M per year, but also saw substantial reductions with increased EV penetration. $PM_{2.5}$ was the next most costly air pollutant at $4.4M per year and the least affected by increased EV penetration.

6. Recommendations

This work demonstrated the potential of the zinc-air battery in an electric vehicle and expounded on the benefits of electric vehicles generally. However, there are several aspects of this work which would be improved with more analysis; there are also several avenues of investigation not directly addressed in this work.

This work demonstrated the limitations of current zinc-air battery technology but also revealed possible avenues for improvement. The zinc-air cell model had a specific energy only 10% greater than that of the lithium-ion cell, and this difference was reduced further after accounting for the additional powertrain losses for power from the zinc-air battery. This in spite of the fact that the zinc-air cell was based on among the most recent and high-performing zinc-air anode and cathode in the literature. Several possibilities for improving the specific energy of future zinc-air cells were suggested in this work, including increasing anode thickness, decreasing electrolyte weight and reducing cell container weight. These and other investigations must be done rigorously so that the potential downsides of these modifications, such as increased internal resistance or poorer electrochemical performance, are addressed.

In addition to suggesting avenues for future research into zinc-air battery technology, greater certainty of zinc-air cell performance would be highly beneficial to future work attempting to model zinc-air battery performance. For example, testing experimental anodes and cathodes together would provide greater certainty that the electrodes can work as described in a practical cell. The temperature dependence of zinc-air cell performance is another important subject for future research. The wide span of temperatures vehicles face makes all-weather performance important for all vehicle batteries, but zinc-air cells have not yet been tested at a wide range of temperatures. This work demonstrated the importance of the lower expected cost of zinc-air cells; estimating the cost of mass-produced zinc-air cells using a manufacturing model is a worthy exercise onto itself and would clarify the true potential of this technology.

This work adds to a body of existing work which attempts to quantify the air pollution benefits of electric vehicles. The air pollution modelling in this work provides a good estimate of local pollution from a particular source, but there are improvements that could make the work more impactful. In particular, complementing the existing work with air dispersion modelling would

generate a more detailed estimate of local pollution effects. This work is of particular importance for convincing policy makers to invest in EV infrastructure.

Finally, one EV barrier which was not analyzed in detail in this work is the extent of the charging network and how having EVs such as the 2BEV changes how the charging infrastructure is planned compared to having regular BEVs. Most BEVs today have smaller battery packs and lower ranges than the vehicles modelled in this work, which means there may be a greater need for charging stations compared to the longer-range 2BEV. On the other hand, the zinc-air battery of the 2BEV cannot be charged as quickly as regular BEVs, which may increase charging times and wait times. Charging infrastructure is crucial to supporting EVs, so exploring how BEVs with zinc-air batteries affects charging infrastructure planning and use is an important area of study.

References

A123 Energy Solutions. (2014). *Battery Pack Design, Validation, and Assembly Guide using A123 Systems AMP20M1HD-A Nanophosphate ® Cells*. Retrieved from http://www.formula-hybrid.org/wp-content/uploads/A123_AMP20_battery_Design_guide.pdf

A123 Systems Inc. (n.d.). *Nanophosphate® Basics: An Overview of the Structure, Properties and Benefits of A123 Systems' Proprietary Lithium Ion Battery Technology*. Retrieved from https://www.neces.com/assets/A123-Systems_Nanophosphate-overview-whitepaper_FINAL1.pdf

Ahmadi, S., Bathaee, S. M. T., & Hosseinpour, A. H. (2018). Improving fuel economy and performance of a fuel-cell hybrid electric vehicle (fuel-cell, battery, and ultra-capacitor) using optimized energy management strategy. *Energy Conversion and Management*, *160*, 74–84. https://doi.org/10.1016/J.ENCONMAN.2018.01.020

ARPA-E. (2012). *RANGE Program Overview*. Retrieved from https://arpa-e.energy.gov/sites/default/files/documents/files/RANGE_ProgramOverview.pdf

Berkeley, N., Jarvis, D., & Jones, A. (2018). Analysing the take up of battery electric vehicles: An investigation of barriers amongst drivers in the UK. *Transportation Research Part D: Transport and Environment*, *63*, 466–481. https://doi.org/10.1016/j.trd.2018.06.016

Bockstette, J., Habermann, K., Ogrzewalla, J., Pischinger, M., & Seibert, D. (2013). Performance Plus Range: Combined Battery Concept for Plug-In Hybrid Vehicles. *SAE International Journal of Alternative Powertrains*, *2*, 156–171. https://doi.org/10.4271/2013-01-1525

Brewer, K., Egyed, M., Huang, L., Ling, B., Matz, C., & Rouleau, M. (2016). *Human Health Risk Assessment for Diesel Exhaust*. *Health Canada*. Ottawa, Canada. Retrieved from http://publications.gc.ca/collections/collection_2016/sc-hc/H129-60-2016-eng.pdf

Brinkman, G. L., Denholm, P., Hannigan, M. P., & Milford, J. B. (2010). Effects of Plug-In Hybrid Electric Vehicles on Ozone Concentrations in Colorado. *Environmental Science & Technology*, *44*(16), 6256–6262. https://doi.org/10.1021/es101076c

Bullard, N. (2019). Bullard: Electric Car Price Tag Shrinks Along With Battery Cost. Retrieved July 24, 2019, from https://about.bnef.com/blog/bullard-electric-car-price-tag-shrinks-along-battery-cost/

CAA. (2013). *Driving Costs*. Retrieved from https://www.caa.ca/wp-content/uploads/2016/09/CAA_Driving_Cost_English_2013_web.pdf

Catton, J., Wang, C., Sherman, S., Fowler, M., & Fraser, R. (2017). Extended Range Electric Vehicle Powertrain Simulation, and Comparison with Consideration of Fuel Cell and Metal-Air Battery. In *SAE Technical Paper*. https://doi.org/10.4271/2017-01-1258

Chambers, M., & Schmitt, R. (2015). *Fact Sheet Diesel-powered Passenger Cars and Light Trucks*. Retrieved from https://www.bts.gov/sites/bts.dot.gov/files/legacy/DieselFactSheet.pdf#targetText=Light Trucks&targetText=Only 1.5 percent of all,Year 2014 were diesel-powered.

Chamoun, M., Hertzberg, B. J., Gupta, T., Davies, D., Bhadra, S., Van Tassell, B., … Steingart, D. A. (2015). Hyper-dendritic nanoporous zinc foam anodes. *NPG Asia Materials*, *7*(4), e178. https://doi.org/10.1038/am.2015.32

Charman, N., Edmonds, N., Egyed, M., Eng, L., Ling, B., Matz, C., & Rouleau, M. (2017). *Human Health Risk Assessment for Gasoline Exhaust*. Ottawa, Canada. Retrieved from http://publications.gc.ca/collections/collection_2017/sc-hc/H144-52-2017-eng.pdf

Chen, C. H., Liu, J., Stoll, M. E., Henriksen, G., Vissers, D. R., & Amine, K. (2004). Aluminum-doped lithium nickel cobalt oxide electrodes for high-power lithium-ion batteries. *Journal of Power Sources*, *128*(2), 278–285. https://doi.org/10.1016/J.JPOWSOUR.2003.10.009

Consumer Reports. (2018). Make Your Car Last 200,000 Miles. Retrieved August 26, 2019, from https://www.consumerreports.org/car-repair-maintenance/make-your-car-last-200-000-miles/

Dahn, J. R., Fuller, E. W., Obrovac, M., & von Sacken, U. (1994). Thermal stability of LixCoO2, LixNiO2 and λ-MnO2 and consequences for the safety of Li-ion cells. *Solid State Ionics*, *69*(3–4), 265–270. https://doi.org/10.1016/0167-2738(94)90415-4

Deign, J. (2019). Battery Storage Markets to See Growth Across the Globe. Retrieved May 21, 2019, from https://www.greentechmedia.com/articles/read/battery-storage-markets-to-see-growth-across-the-globe#gs.ctrx5o

Doughty, D. H., & Roth, E. P. (2012). A General Discussion of Li Ion Battery Safety. *The Electrochemical Society Interface*, *21*(2), 37–44. https://doi.org/10.1149/2.F03122if

Drillet, J.-F., Holzer, F., Kallis, T., Muller, S., & Schmidt, V. M. (2001). Influence of CO2 on the stability of bifunctional oxygen electrodes for rechargeable zinc/air batteries and study of different CO2 filter materials. *Physical Chemistry Chemical Physics*, *3*, 368–371. https://doi.org/10.1039/b005523i

Du Pasquier, A., Plitz, I., Menocal, S., & Amatucci, G. (2003). A comparative study of Li-ion battery, supercapacitor and nonaqueous asymmetric hybrid devices for automotive applications. *Journal of Power Sources*, *115*(1), 171–178. https://doi.org/10.1016/S0378-7753(02)00718-8

Eckl, R., Burda, P., Foerg, A., Finke, H., & Lienkamp, M. (2013). Alternative Range Extender for Electric Cars – Zinc Air Batteries. In M. Lienkamp (Ed.), *Conference on Future Automotive Technology* (pp. 3–18). Springer Vieweg, Wiesbaden. https://doi.org/10.1007/978-3-658-01141-3_1

Edwards, O. (2006). The Death of the EV-1. Retrieved July 23, 2019, from https://www.smithsonianmag.com/science-nature/the-death-of-the-ev-1-118595941/

Electric car with massive range in demo by Phinergy, Alcoa. (2014). Retrieved July 24, 2019, from https://www.cbc.ca/news/technology/electric-car-with-massive-range-in-demo-by-phinergy-alcoa-1.2664653

Environment and Climate Change Canada. (2019). *Canadian Environmental Sustainability Indicators - Greenhouse gas emissions*. Ottawa, Canada. Retrieved from https://www.canada.ca/content/dam/eccc/documents/pdf/cesindicators/ghg-emissions/2019/national-GHG-emissions-en.pdf

Eos Energy Storage LCC. (2013). *US20150244031A1*. Retrieved from https://patents.google.com/patent/US20150244031A1/en

Eos Energy Storage Now Taking Orders at $95/kWh for the Eos Aurora® DC Battery System. (2017). Retrieved August 5, 2019, from https://www.businesswire.com/news/home/20170418005284/en/Eos-Energy-Storage-Orders-95kWh-Eos-Aurora®

EPA. (n.d.-a). About the Automotive Trends Data. Retrieved August 5, 2019, from https://www.epa.gov/automotive-trends/about-automotive-trends-data

EPA. (n.d.-b). Air Pollution: Current and Future Challenges. Retrieved July 2, 2019, from https://www.epa.gov/clean-air-act-overview/air-pollution-current-and-future-challenges

EPA. (n.d.-c). Dynamometer Drive Schedules. Retrieved August 5, 2019, from https://www.epa.gov/vehicle-and-fuel-emissions-testing/dynamometer-drive-schedules

EPA. (2019). *The 2018 EPA Automotive Trends Report: Greenhouse Gas Emissions, Fuel Economy, and Technology since 1975*. Retrieved from https://nepis.epa.gov/Exe/ZyPDF.cgi/P100W5C2.PDF?Dockey=P100W5C2.PDF

Fernández, R. Á., Cilleruelo, F. B., & Martínez, I. V. (2016). A new approach to battery powered electric vehicles: A hydrogen fuel-cell-based range extender system. *International Journal of Hydrogen Energy*, *41*(8), 4808–4819. https://doi.org/10.1016/J.IJHYDENE.2016.01.035

Fries, M., Kerler, M., Rohr, S., Schickram, S., Sinning, M., Lienkamp, M., … Matz, S. (2017). *An Overview of Costs for Vehicle Components, Fuels, Greenhouse Gas Emissions and Total Cost of Ownership Update 2017*. https://doi.org/10.13140/RG.2.2.11685.40164

Fu, J., Cano, Z. P., Park, M. G., Yu, A., Fowler, M., & Chen, Z. (2017). Electrically Rechargeable Zinc-Air Batteries: Progress, Challenges, and Perspectives. *Advanced Materials*, *29*(7), 1604685. https://doi.org/10.1002/adma.201604685

Fu, J., Hassan, F. M., Zhong, C., Lu, J., Liu, H., Yu, A., & Chen, Z. (2017). Defect Engineering of Chalcogen-Tailored Oxygen Electrocatalysts for Rechargeable Quasi-Solid-State Zinc-Air Batteries. *Advanced Materials*, *29*(35), 1702526. https://doi.org/10.1002/adma.201702526

GKN Land Systems. (n.d.). *GKN Electric Motor and Generator Technology Technical Datasheet*.

Goldstein, J., Brown, I., & Koretz, B. (1999). New developments in the Electric Fuel Ltd. zinc/air system. *Journal of Power Sources*, *80*(1–2), 171–179. https://doi.org/10.1016/S0378-7753(98)00260-2

Haustein, S., & Jensen, A. F. (2018). Factors of electric vehicle adoption: A comparison of conventional and electric car users based on an extended theory of planned behavior. *International Journal of Sustainable Transportation*, *12*(7), 484–496. https://doi.org/10.1080/15568318.2017.1398790

Health Canada. (2017). *Health Impacts of Air Pollution in Canada*. Ottawa, Canada. Retrieved from http://publications.gc.ca/collections/collection_2018/sc-hc/H144-51-2017-eng.pdf

Honda Canada. (n.d.). Specifications | The 2019 Civic | Honda Canada. Retrieved September 4, 2019, from https://www.honda.ca/civic_sedan/specs

Huang, J., Yang, Z., Wang, R., Zhang, Z., Feng, Z., & Xie, X. (2015). Zn–Al layered double oxides as high-performance anode materials for zinc-based secondary battery. *Journal of Materials Chemistry A*, *3*(14), 7429–7436. https://doi.org/10.1039/C5TA00279F

Husain, I. (2011). *Electric and Hybrid Vehicles Design Fundamentals* (2nd ed.). Boca Raton, Florida: CRC Press Taylor & Francis Group.

IPCC. (2014). *Climate Change 2014: Synthesis Report. Contribution of Working Groups I, II and III to the Fifth Assessment Report of the Intergovernmental Panel on Climate Change*. (Core Writing Team R.K. Pachauri and L.A. Meyer, Ed.), *IPCC*. Geneva, Switzerland. Retrieved from https://www.ipcc.ch/site/assets/uploads/2018/05/SYR_AR5_FINAL_full_wcover.pdf

IPCC. (2018). *Global warming of 1.5°C. An IPCC Special Report on the impacts of global warming of 1.5°C above pre-industrial levels and related global greenhouse gas emission pathways, in the context of strengthening the global response to the threat of climate change,*. (V. Masson-Delmotte, P. Zhai, H.-O. Pörtner, D. Roberts, J. Skea, P. R. Shukla, … T. Waterfield, Eds.), *IPCC*. Geneva, Switzerland: IPCC. Retrieved from https://www.ipcc.ch/site/assets/uploads/sites/2/2018/07/SR15_SPM_version_stand_alone_LR.pdf

Itou, Y., & Ukyo, Y. (2005). Performance of LiNiCoO2 materials for advanced lithium-ion batteries. *Journal of Power Sources*, *146*(1–2), 39–44. https://doi.org/10.1016/J.JPOWSOUR.2005.03.091

Jain, S. (2017). Emerging trends in battery technology. *Auto Tech Review*, *6*(1), 52–55. https://doi.org/10.1365/s40112-017-1278-0

Ji, S., Cherry, C. R., Zhou, W., Sawhney, R., Wu, Y., Cai, S., … Marshall, J. D. (2015). Environmental Justice Aspects of Exposure to PM2.5 Emissions from Electric Vehicle Use in China. *Environmental Science & Technology*, *49*(24), 13912–13920. https://doi.org/10.1021/acs.est.5b04927

Jiji. (2018, October 27). Hybrids account for nearly 20 percent of cars in Japan, automobile association says. *The Japan Times*. Retrieved from https://www.japantimes.co.jp/news/2018/10/27/business/hybrids-account-nearly-20-percent-cars-japan-automobile-association-says/#.XRt6OuhKg2x

Lee, D. U., Choi, J.-Y., Feng, K., Park, H. W., & Chen, Z. (2014). Advanced Extremely Durable 3D Bifunctional Air Electrodes for Rechargeable Zinc-Air Batteries. *Advanced Energy Materials*, *4*, 1301389. https://doi.org/10.1002/aenm.201301389

Li, B., Ge, X., Goh, F. W. T., Hor, T. S. A., Geng, D., Du, G., … Zong, Y. (2015). Co_3O_4 nanoparticles decorated carbon nanofiber mat as binder-free air-cathode for high performance rechargeable zinc-air batteries. *Nanoscale*, *7*(5), 1830–1838. https://doi.org/10.1039/C4NR05988C

Li, J., Zhao, T., Shangguan, E., Li, Y., Li, L., Wang, D., … Li, Q. (2017). Enhancing the rate and cycling performance of spherical ZnO anode material for advanced zinc-nickel secondary batteries by combined in-situ doping and coating with carbon. *Electrochimica Acta*, *236*, 180–189. https://doi.org/10.1016/J.ELECTACTA.2017.03.164

Li, M., Lu, J., Chen, Z., & Amine, K. (2018). 30 Years of Lithium-Ion Batteries. *Advanced Materials*, *30*(33), 1800561. https://doi.org/10.1002/adma.201800561

Li, N., Chen, J.-P., Tsai, I.-C., He, Q., Chi, S.-Y., Lin, Y.-C., & Fu, T.-M. (2016). Potential impacts of electric vehicles on air quality in Taiwan. *Science of The Total Environment*, *566–567*, 919–928. https://doi.org/10.1016/J.SCITOTENV.2016.05.105

Lithium Ion Battery Market To Reach USD 109.72 Billion By 2026. (2019). Retrieved May 21, 2019, from https://www.globenewswire.com/news-release/2019/03/18/1756530/0/en/Lithium-Ion-Battery-Market-To-Reach-USD-109-72-Billion-By-2026.html

Martel, F., Dubé, Y., Kelouwani, S., Jaguemont, J., & Agbossou, K. (2016). Long-term assessment of economic plug-in hybrid electric vehicle battery lifetime degradation management through near optimal fuel cell load sharing. *Journal of Power Sources*, *318*, 270–282. https://doi.org/10.1016/J.JPOWSOUR.2016.04.029

McInnis, P. (2017). *Intelligent Vehicle Development through Scalable Data Collection Processes and Simulation*. UWSpace. Retrieved from https://uwspace.uwaterloo.ca/handle/10012/12230

Mohamad, A. A. (2006). Zn/gelled 6 M KOH/O2 zinc–air battery. *Journal of Power Sources*, *159*(1), 752–757. https://doi.org/10.1016/J.JPOWSOUR.2005.10.110

Mokhtar, M., Talib, M. Z. M., Majlan, E. H., Tasirin, S. M., Ramli, W. M. F. W., Daud, W. R. W., & Sahari, J. (2015). Recent developments in materials for aluminum-air batteries: A review. *Journal of Industrial and Engineering Chemistry*, *32*, 1–20. https://doi.org/10.1016/j.jiec.2015.08.004

National Energy Board. (n.d.-a). Provincial and Territorial Energy Profiles - Alberta. Retrieved September 1, 2019, from https://www.cer-rec.gc.ca/nrg/ntgrtd/mrkt/nrgsstmprfls/ab-eng.html

National Energy Board. (n.d.-b). Provincial and Territorial Energy Profiles - Ontario. Retrieved September 1, 2019, from https://www.cer-rec.gc.ca/nrg/ntgrtd/mrkt/nrgsstmprfls/on-eng.html

National Household Travel Survey. (n.d.). Retrieved August 5, 2019, from https://nhts.ornl.gov/

Nealer, R., Reichmuth, D., & Anair, D. (2015). *Cleaner Cars from Cradle to Grave: How Electric Cars Beat Gasoline Cars on Lifetime Global Warming Emissions*. UCS. Retrieved from https://www.ucsusa.org/sites/default/files/attach/2015/11/Cleaner-Cars-from-Cradle-to-Grave-full-report.pdf

Nitta, N., Wu, F., Lee, J. T., & Yushin, G. (2015). Li-ion battery materials: present and future. *Materials Today*, *18*(5), 252–264. https://doi.org/10.1016/j.mattod.2014.10.040

Nixon, D. B. (1994). *United States Patent No. US 5542488*. Retrieved from http://patft.uspto.gov/netacgi/nph-Parser?Sect1=PTO1&Sect2=HITOFF&d=PALL&p=1&u=%2Fnetahtml%2FPTO%2Fsrchnum.htm&r=1&f=G&l=50&s1=5542488.PN.&OS=PN/5542488&RS=PN/5542488

Nykvist, B., & Nilsson, M. (2015). Rapidly falling costs of battery packs for electric vehicles. *Nature Climate Change*, *5*(4), 329–332. https://doi.org/10.1038/nclimate2564

Ontario Ministry of Transportation. (2016). *Provincial Highways Traffic Volumes*. Retrieved from http://www.raqsa.mto.gov.on.ca/techpubs/TrafficVolumes.nsf/fa027808647879788525708a004b5df8/f51986ea499a13b08525745f006dd30b/$FILE/Provincial Highways Traffic Volumes 2016 AADT Only.pdf

Parker, J. F., Chervin, C. N., Nelson, E. S., Rolison, D. R., & Long, J. W. (2014). Wiring zinc in three dimensions re-writes battery performance—dendrite-free cycling. *Energy Environ. Sci.*, *7*(3), 1117–1124. https://doi.org/10.1039/C3EE43754J

Propfe, B., Redelbach, M., Santini, D., & Friedrich, H. (2012). Cost analysis of Plug-in Hybrid Electric Vehicles including Maintenance & Repair Costs and Resale Values. *World Electric Vehicle Journal*, *5*(4), 886–895. https://doi.org/10.3390/wevj5040886

Reimers, J. N., & Dahn, J. R. (1992). Electrochemical and In Situ X-Ray Diffraction Studies of Lithium Intercalation in LixCoO2. *Journal of The Electrochemical Society*, *139*(8), 2091–2097. https://doi.org/10.1149/1.2221184

Requia, W. J., Mohamed, M., Higgins, C. D., Arain, A., & Ferguson, M. (2018). How clean are electric vehicles? Evidence-based review of the effects of electric mobility on air pollutants, greenhouse gas emissions and human health. *Atmospheric Environment*, *185*, 64–77. https://doi.org/10.1016/j.atmosenv.2018.04.040

Riczu, C., Habibi, S., & Bauman, J. (2018). Design and Optimization of An Electric Vehicle with Two Battery Cell Chemistries. In *2018 IEEE Transportation Electrification Conference and Expo (ITEC)* (pp. 506–512). Long Beach, USA: IEEE. https://doi.org/10.1109/ITEC.2018.8450156

Sawyer, D., Seton, S., & Welburn, C. (2007). *Evaluation of Total Cost of Air Pollution Due to Transportation in Canada*. Retrieved from http://publications.gc.ca/collections/collection_2008/tc/T22-148-2007E.pdf

Schmuch, R., Wagner, R., Hörpel, G., Placke, T., & Winter, M. (2018). Performance and cost of materials for lithium-based rechargeable automotive batteries. *Nature Energy*, *3*(4), 267–278. https://doi.org/10.1038/s41560-018-0107-2

Schröder, R., Aydemir, M., & Seliger, G. (2017). Comparatively Assessing different Shapes of Lithium-ion Battery Cells. *Procedia Manufacturing*, *8*, 104–111. https://doi.org/10.1016/J.PROMFG.2017.02.013

Sherman, D. (2014). Drag Queens: Aerodynamics Compared. Retrieved June 5, 2019, from https://www.caranddriver.com/features/a15108689/drag-queens-aerodynamics-compared-comparison-test/

Sherman, S. B., Cano, Z. P., Fowler, M., & Chen, Z. (2018). Range-extending Zinc-air battery for electric vehicle. *AIMS Energy*, *6*(1), 121–145. https://doi.org/10.3934/energy.2018.1.121

Smith, R., & McDougal, K. (2017). *Costs of pollution in Canada*. Winnipeg, Canada. Retrieved from https://www.iisd.org/sites/default/files/publications/costs-of-pollution-in-canada.pdf

Spector, J. (2018). With 3,000 Systems and Money to Scale, Will NantEnergy Make Long-Duration Storage Profitable? Retrieved August 5, 2019, from https://www.greentechmedia.com/articles/read/with-3000-systems-and-money-to-scale-will-nantenergy-make-long-duration-sto#gs.ucgjkr

Statistics Canada. (2018a). Table 20-10-0001-01 New motor vehicle sales. Retrieved June 28, 2019, from https://www150.statcan.gc.ca/t1/tbl1/en/cv.action?pid=2010000101#timeframe

Statistics Canada. (2018b). Table 23-10-0067-01 Vehicle registrations, by type of vehicle. Retrieved June 28, 2019, from https://www150.statcan.gc.ca/t1/tbl1/en/tv.action?pid=2310006701

Tessum, C. W., Hill, J. D., & Marshall, J. D. (2014). Life cycle air quality impacts of conventional and alternative light-duty transportation in the United States. *Proceedings of the National Academy of Sciences of the United States of America*, *111*(52), 18490–18495. https://doi.org/10.1073/pnas.1406853111

Thé, J. L., Thé, C. L., Chamberlin, R., & Johnson, M. (n.d.). Transportation Air Quality System. Lakes Environmental Software & RSG Inc.

Thomas Goh, F. W., Liu, Z., Andy Hor, T. S., Zhang, J., Ge, X., Zong, Y., … Khoo, W. (2014). A Near-Neutral Chloride Electrolyte for Electrically Rechargeable Zinc-Air Batteries. *Journal of The Electrochemical Society*, *161*(14), A2080–A2086. https://doi.org/10.1149/2.0311414jes

Timmers, V. R. J. H., & Achten, P. A. J. (2016). Non-exhaust PM emissions from electric vehicles. *Atmospheric Environment*, *134*, 10–17. https://doi.org/10.1016/J.ATMOSENV.2016.03.017

Toronto Public Health. (2014). *Path To Healthier Air: Toronto Air Pollution Burden of Illness Update*. *Toronto Public Health*. Toronto, Canada. Retrieved from https://www.toronto.ca/wp-content/uploads/2017/11/9190-tph-Air-Pollution-Burden-of-Illness-2014.pdf

Transport Canada. (2008). *Estimates of the Full Cost of Transportation in Canada*. Retrieved from http://publications.gc.ca/collections/collection_2009/tc/T22-165-2008E.pdf

Union of Concerned Scientists. (n.d.-a). Cars, Trucks, Buses and Air Pollution. Retrieved July 23, 2019, from https://www.ucsusa.org/clean-vehicles/vehicles-air-pollution-and-human-health/cars-trucks-air-pollution

Union of Concerned Scientists. (n.d.-b). Series vs Parallel vs Series/Parallel Drivetrains. Retrieved July 3, 2019, from https://www.ucsusa.org/clean-vehicles/electric-vehicles/series-vs-parallel-drivetrains

Wang, C., Xie, Z., & Zhou, Z. (2019). Lithium-air batteries: Challenges coexist with opportunities. *APL Materials*, *7*, 40701. https://doi.org/10.1063/1.5091444

Wang, R., Yang, Z., Yang, B., Fan, X., & Wang, T. (2014). A novel alcohol-thermal synthesis method of calcium zincates negative electrode materials for NieZn secondary batteries. *Journal of Power Sources*, *246*, 313–321. https://doi.org/10.1016/j.jpowsour.2013.07.097

Wu, Y., & Zhang, L. (2017). Can the development of electric vehicles reduce the emission of air pollutants and greenhouse gases in developing countries? *Transportation Research Part D: Transport and Environment*, *51*, 129–145. https://doi.org/10.1016/j.trd.2016.12.007

Yamauchi, S., Inoue, T., Chandra, R., Makino, S., & Komatsu, D. (2018). Development of a Combined Battery System for Electric Vehicles with Battery Lifespan Enhancements. In *SAE International*. https://doi.org/10.4271/2018-01-0448

Yan, Z., Wang, E., Jiang, L., & Sun, G. (2015). Superior cycling stability and high rate capability of three-dimensional Zn/Cu foam electrodes for zinc-based alkaline batteries. *RSC Advances*, *5*(102), 83781–83787. https://doi.org/10.1039/C5RA16264E

Appendix A – Procedure for creating Figure 16 from NHTS data

In order to create Figure 16 from the NHTS data available online, the raw data has to be manipulated. Of the files available online, the trippub and vehpub documents contain the required data. The trippub document contains the detailed trip data of every person surveyed including start time, end time, trip distance, which vehicle was driven and whether the person surveyed was the driver of the vehicle for the trip; the data was organized by household. The vehpub document contains the list of vehicles by household. The data from these documents was imported into MATLAB and the following script was run:

```
for i = 1:256115
    hID = HOUSEID1(i);
    vID = VEHID1(i);
    vTy = VEHTYPE(i);

    if (vTy == 1 || vTy == 3) && vID > 0 && vID < 13
        hIndex = find(HOUSEID == hID);
        vIndex = hIndex.*(VEHID(hIndex)==vID);
        vIndex(vIndex==0) = [];
        dIndex = vIndex.*(DRVR_FLG(vIndex)==1);
        dIndex(dIndex==0) = [];

        if isempty(dIndex)
            DDD(i) = 0;
        elseif sum(TRVLCMIN(dIndex) < 0) > 0 || ...
           sum(TRPMILES(dIndex)./TRVLCMIN(dIndex) > 100/60) > 0
            DDD(i) = -1;
        elseif prod(sum(STRTTIME(dIndex)==STRTTIME(dIndex)')) ~= 1 && ...
                prod(sum(ENDTIME(dIndex)==ENDTIME(dIndex)')) ~= 1
            DDD(i) = -2;
        else
            DDD(i) = sum(TRPMILES(dIndex));
        end
    end
end
clear ans dIndex hID hIndex i vID vIndex vTy vWt
```

The script matches the trip data in trippub to the vehicle data in vehpub. For each vehicle in vehpub (denoted by a combination of household ID and vehicle ID) the script first checks that the vehicle is a car or SUV. If it is, the script then finds within the trippub data all instances in which the trip has the matching household ID and vehicle ID and in which the person surveyed was the driver of the trip (this is done to ensure trips are not double counted by the driver and passengers). The script then checks for certain errors – such as negative travel times, or trips where either the recorded distance or recorded time did not make sense based on the average speed implied. Finally,

if there are no errors the distances from all the trips recorded by the vehicle that day are summed to obtain the total distance travelled by that vehicle that day. After the execution of the script all the vehicles in vehpub which are cars or SUVs and which do not have misrecorded data have an associated distance travelled that day. This data is contained in the variable DDD.

Following the execution of the above script the daily driven distances are sorted into bins corresponding to a distance range; for example, if the daily driven distance is 8 km that corresponds to the 5-10 km bin (which is the 2nd bin, after the 0-5 km bin). Each data entry in vehpub which has a daily driven distance associated with it is assigned a bin number (DDDbins) based on the DDD value. Then a new script is executed in order to calculate the weights for each bin. The weights are necessary for accurate representation of the population from the NHTS sample data.

```
weights = zeros(100,1);
weightSum = 0;

for i = 1:256115
    if DDD(i) > 0.01/1.60934 && DDD(i) <= 500/1.60934
        n = DDDbins(i);
        weights(n) = weights(n) + WTHHFIN(i);
        weightSum = weightSum + WTHHFIN(i);
    elseif DDD(i) > 500/1.60934
        weightSum = weightSum + WTHHFIN(i);
    end
end
```

The script loops through each vehicle entry in vehpub, checks that it has a valid daily driven distance associated with it and reads the vehicle weighting. That weight is then added to the weight total for the associated daily driven distance bin and to the overall weight total. Following the execution of this script, the NHTS graph is created by dividing the summed bin weights by the total weight sum, giving the frequency of each bin.

Appendix B: Tabulated data for select figures

Table B1: Data for Figure 16

Daily Driven Distance (km)	Frequency	Daily Driven Distance (km)	Frequency	Daily Driven Distance (km)	Frequency
5	5.52%	185	0.21%	365	0.04%
10	8.76%	190	0.23%	370	0.05%
15	8.77%	195	0.20%	375	0.02%
20	8.12%	200	0.19%	380	0.04%
25	7.33%	205	0.13%	385	0.02%
30	6.33%	210	0.16%	390	0.04%
35	5.67%	215	0.13%	395	0.03%
40	5.11%	220	0.11%	400	0.04%
45	4.72%	225	0.09%	405	0.02%
50	4.03%	230	0.10%	410	0.03%
55	3.46%	235	0.12%	415	0.03%
60	3.41%	240	0.10%	420	0.02%
65	3.10%	245	0.07%	425	0.01%
70	2.44%	250	0.04%	430	0.02%
75	2.41%	255	0.08%	435	0.01%
80	1.93%	260	0.06%	440	0.03%
85	1.72%	265	0.08%	445	0.02%
90	1.75%	270	0.08%	450	0.01%
95	1.40%	275	0.09%	455	0.01%
100	1.36%	280	0.07%	460	0.02%
105	1.01%	285	0.05%	465	0.01%
110	0.84%	290	0.05%	470	0.02%
115	0.87%	295	0.04%	475	0.02%
120	0.77%	300	0.06%	480	0.01%
125	0.72%	305	0.07%	485	0.02%
130	0.66%	310	0.05%	490	0.02%
135	0.57%	315	0.05%	495	0.01%
140	0.48%	320	0.08%	500	0.01%
145	0.45%	325	0.05%		
150	0.42%	330	0.03%		
155	0.32%	335	0.08%		
160	0.33%	340	0.04%		
165	0.31%	345	0.02%		
170	0.29%	350	0.02%		
175	0.27%	355	0.04%		
180	0.18%	360	0.04%		

Table B2: Data for Figure 21

Daily Driven Distance (km)	Total Annual Driven Distance (km)	Annual Distance without zinc-air battery (km)
5	100.7	0.0
10	319.7	0.0
15	480.2	0.0
20	592.8	0.0
25	668.9	0.0
30	693.1	0.0
35	724.3	0.0
40	746.1	0.0
45	775.3	0.0
50	735.5	0.0
55	694.6	0.0
60	746.8	0.0
65	735.5	0.0
70	623.4	0.0
75	659.7	17.6
80	563.6	49.3
85	533.6	75.3
90	574.9	108.6
95	485.5	112.4
100	496.4	134.0
105	387.1	118.0
110	337.3	113.4
115	365.2	133.4
120	337.3	132.1
125	328.5	136.7
130	313.2	137.3
135	280.9	129.0
140	245.3	117.4
145	238.2	118.3
150	230.0	118.0
155	181.0	95.8
160	192.7	104.8
165	186.7	104.1
170	179.9	102.7
175	172.5	100.5
180	118.3	70.3
185	141.8	85.8
190	159.5	98.2

195	142.4	89.1
200	138.7	88.1
205	97.3	62.6
210	122.6	80.0
215	102.0	67.4
220	88.3	59.0
225	73.9	49.9
230	84.0	57.3
235	102.9	71.0
240	87.6	61.0
245	62.6	43.9
250	36.5	25.8
255	74.5	53.1
260	56.9	41.0
265	77.4	56.1
270	78.8	57.5
275	90.3	66.4
280	71.5	52.9
285	52.0	38.7
290	52.9	39.6
295	43.1	32.4
300	65.7	49.7
305	77.9	59.3
310	56.6	43.3
315	57.5	44.2
320	93.4	72.1
325	59.3	46.0
330	36.1	28.1
335	97.8	76.5
340	49.6	39.0
345	25.2	19.9
350	25.6	20.2
355	51.8	41.2
360	52.6	41.9
365	53.3	42.6
370	67.5	54.2
375	27.4	22.0
380	55.5	44.8
385	28.1	22.8
390	56.9	46.3
395	43.3	35.3
400	58.4	47.7
405	29.6	24.2
410	44.9	36.9

415	45.4	37.4
420	30.7	25.3
425	15.5	12.8
430	31.4	26.1
435	15.9	13.2
440	48.2	40.2
445	32.5	27.2
450	16.4	13.8
455	16.6	13.9
460	33.6	28.3
465	17.0	14.3
470	34.3	29.0
475	34.7	29.3
480	17.5	14.9
485	35.4	30.1
490	35.8	30.4
495	18.1	15.4
500	18.3	15.6

Table B3: Data for Figure 24 (tonnes year^{-1})

EV%	NO_x	$PM_{2.5}$	SO_2	VOCs
0%	2366	198	9	959
20%	2129	188	8	800
40%	1891	178	6	641
60%	1652	168	5	482
80%	1414	158	3	323
100%	1175	148	2	165

Table B4: Data for Figure 25 (CAD year^{-1})

EV%	NO_x	$PM_{2.5}$	SO_2	VOCs	Total
0%	$13,436,270	$4,356,103	$59,112	$662,953	$18,514,438
20%	$12,088,444	$4,138,956	$49,766	$553,143	$16,830,309
40%	$10,737,222	$3,921,831	$40,432	$443,329	$15,142,814
60%	$9,382,598	$3,704,376	$31,079	$333,492	$13,451,545
80%	$8,027,975	$3,486,920	$21,727	$223,655	$11,760,277
100%	$6,673,352	$3,269,464	$12,374	$113,818	$10,069,008

Table B5: Data for Figure 26 (tonnes year^{-1})

EV%	Running Exhaust	Brakewear	Tirewear	Crankcase Running Exhaust	Total
0%	146	8.4	4.5	44	198
20%	137	7.2	3.7	44	188
40%	128	6.0	3.0	43	178
60%	120	4.7	2.2	43	168
80%	111	3.5	1.5	43	158
100%	103	2.2	0.7	43	148

Appendix C – Code for the zinc-air cell model

```
%% VPA - ESS2
% Model - polarization curve lookup
% Technology - Zinc-air

% Pack level
ess2.plant.init.element_per_module      = 75;
ess2.plant.init.num_module              = 4;      % the number of series connected
modules;
ess2.plant.init.num_module_parallel     = 22;
ess2.plant.init.num_cell_series         =
ess2.plant.init.num_module*ess2.plant.init.element_per_module;
ess2.plant.init.num_cell                =
ess2.plant.init.num_module*ess2.plant.init.element_per_module*ess2.plant.init.num_modu
le_parallel;

ess2.plant.init.packaging_factor        = 1.25;  % >=1
ess2.plant.init.mass.cell               = 0.0562;
ess2.plant.init.mass.module             =
ess2.plant.init.mass.cell*ess2.plant.init.element_per_module;
ess2.plant.init.mass.pack               = round(ess2.plant.init.mass.cell *
ess2.plant.init.num_cell);% calculate the mass of the pack
ess2.plant.init.mass.packaging          = (ess2.plant.init.packaging_factor -
1).*ess2.plant.init.mass.pack;% calculate the mass of the pack
ess2.plant.init.mass.total              = ess2.plant.init.mass.pack +
ess2.plant.init.mass.packaging;

ess2.plant.init.pwr_constant             = 12500;

% Cell level
ess2.plant.init.soc_init                = 1;
ess2.plant.init.soc_min                 = 0;
ess2.plant.init.soc_max                 = 1;

ess2.plant.init.volt_nom                = 1.20;
ess2.plant.init.volt_min                = 0.1;
ess2.plant.init.volt_max                = 2.00;

ess2.plant.init.surface_area            = 100;      %cm^2
ess2.plant.init.surface_area_ref        = 2;        %cm^2
ess2.plant.init.surface_area_ratio      =
ess2.plant.init.surface_area/ess2.plant.init.surface_area_ref;

% LOSS AND EFFICIENCY parameters
ess2.plant.init.soc_index               = [0:.1:1];         % SOC RANGE over which
data is defined
ess2.plant.init.temp_index              = [20 25 30];       % Temperature range over
which data is defined(C)
ess2.plant.init.current_index           = ...
    [0.06192 2.60049 5.13905 7.67762 10.18523 12.7238 15.23141 17.73902 20.27759 ...
    22.7852 25.29281 27.83138 30.33899 32.87756 35.41613 37.92374 40.46231 42.96992
...
    45.50849 48.0161 50.55467 53.06228 55.60085 58.10846 60.64703 63.15464 65.69321
...
    68.20082 70.73939 73.247 75.78557 78.29318 80.83175 83.37032 85.87793 88.4165 ...
    90.92411 93.46268 95.97029 98.4779 101.01647 103.55504 106.06265 108.60122
111.10883 ...
    113.6474 116.18597 118.69358 121.20119 123.73976 126.24737 128.78594 131.29355 ...
    133.83212 136.37068 138.8783 141.38591 143.92448 146.46304 148.97065 151.47827 ...
    154.01683 156.5554 159.06301 161.60158 164.10919 166.64776 169.15537 171.69394 ...
    174.20155 176.74012 179.27869 181.7863 184.32487 186.83248 189.37105 191.87866 ...
```

```
    194.41723 196.92484 199.46341 202.00198 204.50959 207.04816 209.55577 212.09434
...
    214.60195 217.10956 219.64813 222.1867 224.69431 227.23288 229.74049 232.27906 ...
    234.81763 237.32524 239.83285 242.37142 244.90999 247.4176 249.92521]' ...
    * ess2.plant.init.surface_area/1000;

%= [0:1:200]*ess2.plant.init.surface_area/1000; % Current range (A)

ess2.plant.init.cap_max.idx1_temp       = ess2.plant.init.temp_index;
ess2.plant.init.cap_max.map             = [6.68 6.68 6.68];         % (A*h), at C/5,
indexed by ess2.plant.init.temp_index

ess2.plant.init.eff_coulomb.idx1_temp   = ess2.plant.init.temp_index;
ess2.plant.init.eff_coulomb.map         = [1 1 1];                  % not supplied
data. Average coulombic (a.k.a. amp-hour) efficiency below, indexed by
ess2.plant.init.temp_index

% cell's open-circuit (a.k.a. no-load) voltage, indexed by ess2.plant.init.soc_index
ess2.plant.init.voc.idx1_temp   = ess2.plant.init.temp_index;
ess2.plant.init.voc.idx2_soc    = ess2.plant.init.soc_index;
ess2.plant.init.voc.map         = [...
    1.4 1.4 1.4 1.4 1.4 1.4 1.4 1.4 1.4 1.4 1.4;
    1.4 1.4 1.4 1.4 1.4 1.4 1.4 1.4 1.4 1.4 1.4;
    1.4 1.4 1.4 1.4 1.4 1.4 1.4 1.4 1.4 1.4 1.4];

% cell's R1, indexed by ess2.plant.init.soc_index
ess2.plant.init.r1.idx1_temp    = ess2.plant.init.temp_index;
ess2.plant.init.r1.idx2_soc     = ess2.plant.init.soc_index;
ess2.plant.init.r1.map          = [...
    1.6  1.6   1.6   1.6   1.6   1.6   1.6   1.6   1.6   1.6   1.6;
    1.6  1.6   1.6   1.6   1.6   1.6   1.6   1.6   1.6   1.6   1.6;
    1.6  1.6   1.6   1.6   1.6   1.6   1.6   1.6   1.6   1.6
1.6]/ess2.plant.init.surface_area_ratio; % (ohm)
ess2.plant.init.voltage.idx1_current = ess2.plant.init.current_index;
ess2.plant.init.voltage.map = [1.38367  1.34288 1.29626 1.25056 1.22388 1.20854 ...
    1.19628 1.18523 1.17481 1.16468 1.15518 1.14567 1.13647 1.12757 1.11868 1.1107
...
    1.10488 1.0969  1.08862 1.08065 1.07237 1.0647  1.05672 1.04875 1.04078 1.03311
...
    1.02513 1.01747 1.0098  1.00182 0.99416 0.98649 0.97882 0.97115 0.96379 0.95551
...
    0.94815 0.94048 0.93281 0.92515 0.91748 0.91012 0.90245 0.89478 0.88712 0.87975
...
    0.87209 0.86442 0.85675 0.84939 0.84172 0.83406 0.82639 0.81903 0.81136 0.80369
...
    0.79602 0.78836 0.781   0.77333 0.76566 0.75799 0.75032 0.74266 0.73499 0.72732
...
    0.71965 0.71199 0.70432 0.69634 0.68868 0.68101 0.67334 0.66567 0.6577  0.64972
...
    0.64175 0.63378 0.62611 0.61783 0.60985 0.60157 0.5936  0.58532 0.57704 0.56845
...
    0.55986 0.55127 0.54268 0.53379 0.5249  0.51569 0.50649 0.49698 0.48748 0.47766
...
    0.46754 0.45681 0.44607 0.43442]';

% Battery density
ess2.plant.init.pwr_dis_nom         = max((ess2.plant.init.volt_nom-
ess2.plant.init.volt_min).*ess2.plant.init.volt_min./ess2.plant.init.r1.map);%per cell
ess2.plant.init.pwr_density         =
ess2.plant.init.pwr_dis_nom/ess2.plant.init.mass.cell;
ess2.plant.init.energy_density      =
(ess2.plant.init.volt_nom*ess2.plant.init.cap_max.map)/ess2.plant.init.mass.cell;
ess2.plant.init.energy = max(ess2.plant.init.cap_max.map).*ess2.plant.init.volt_nom;
```

Appendix D – Some sections of the 2BEV Simulink model

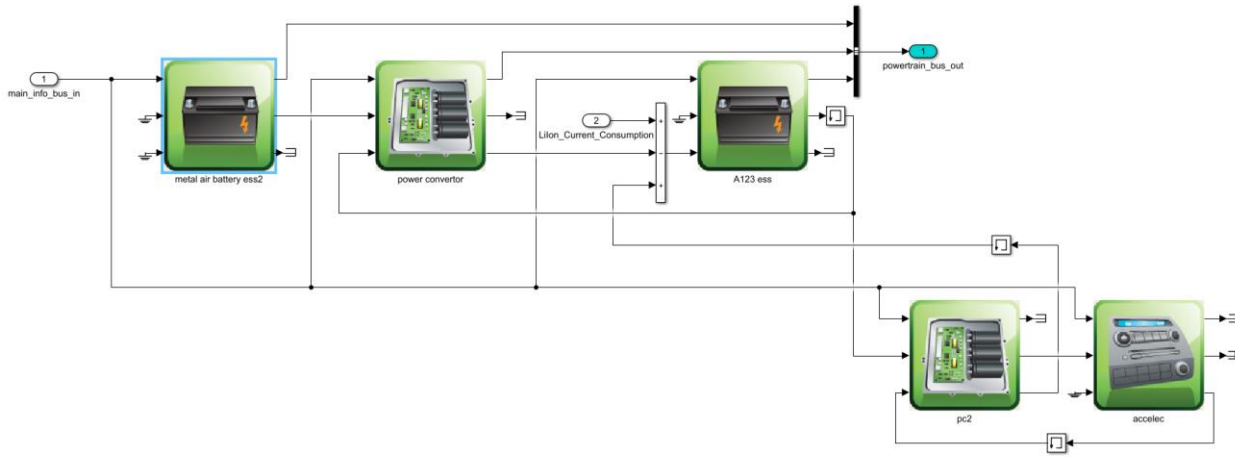

Figure D1: 2BEV powertrain (motor not depicted)

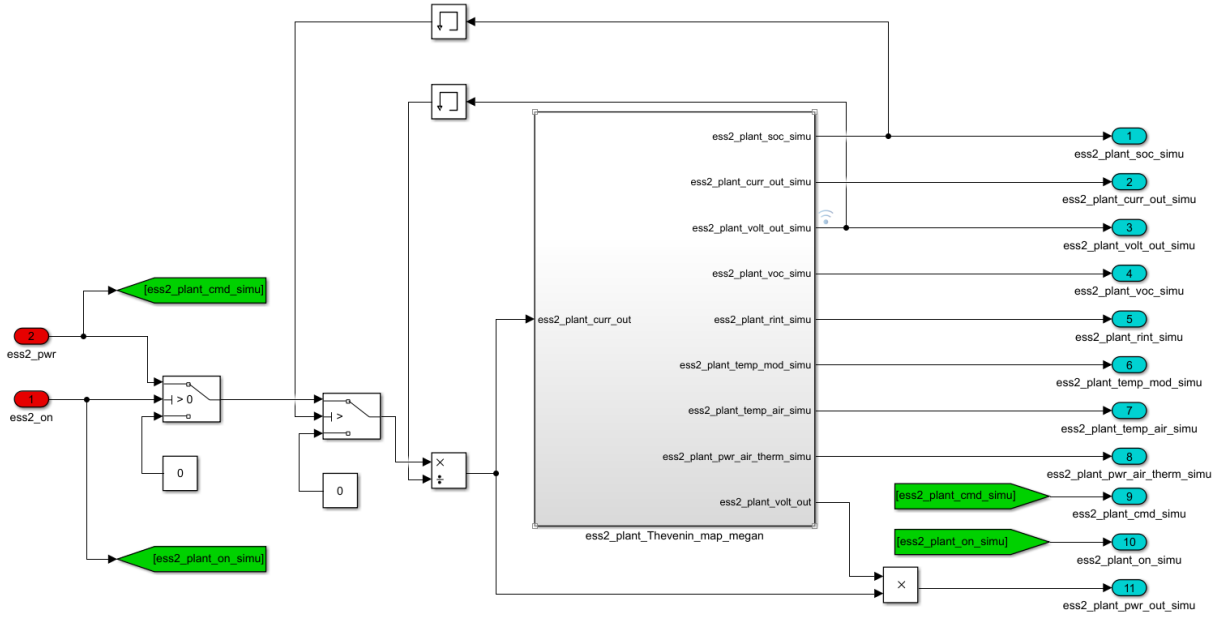

Figure D2: Zinc-air battery model (highest subsystem)

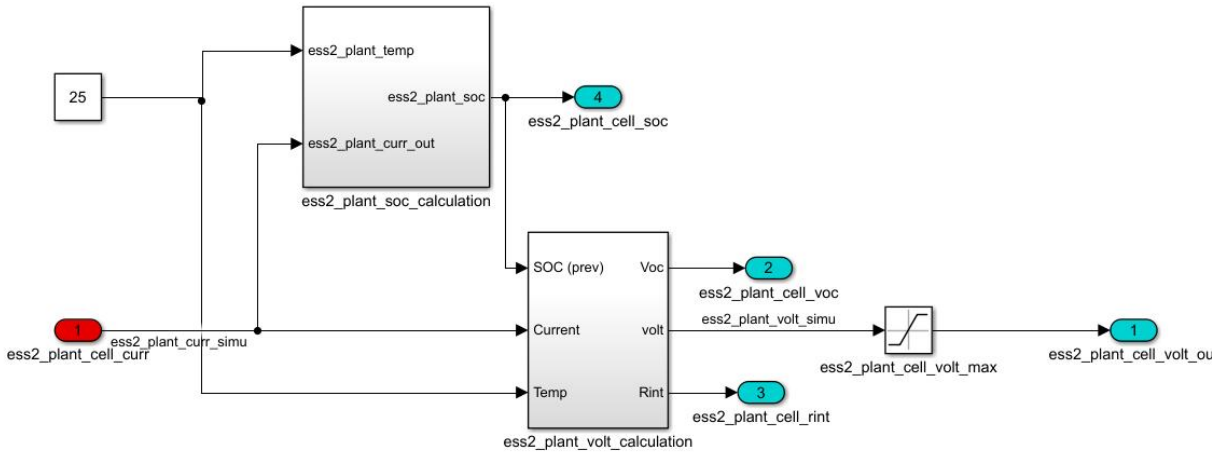

Figure D3: Zinc-air cell model

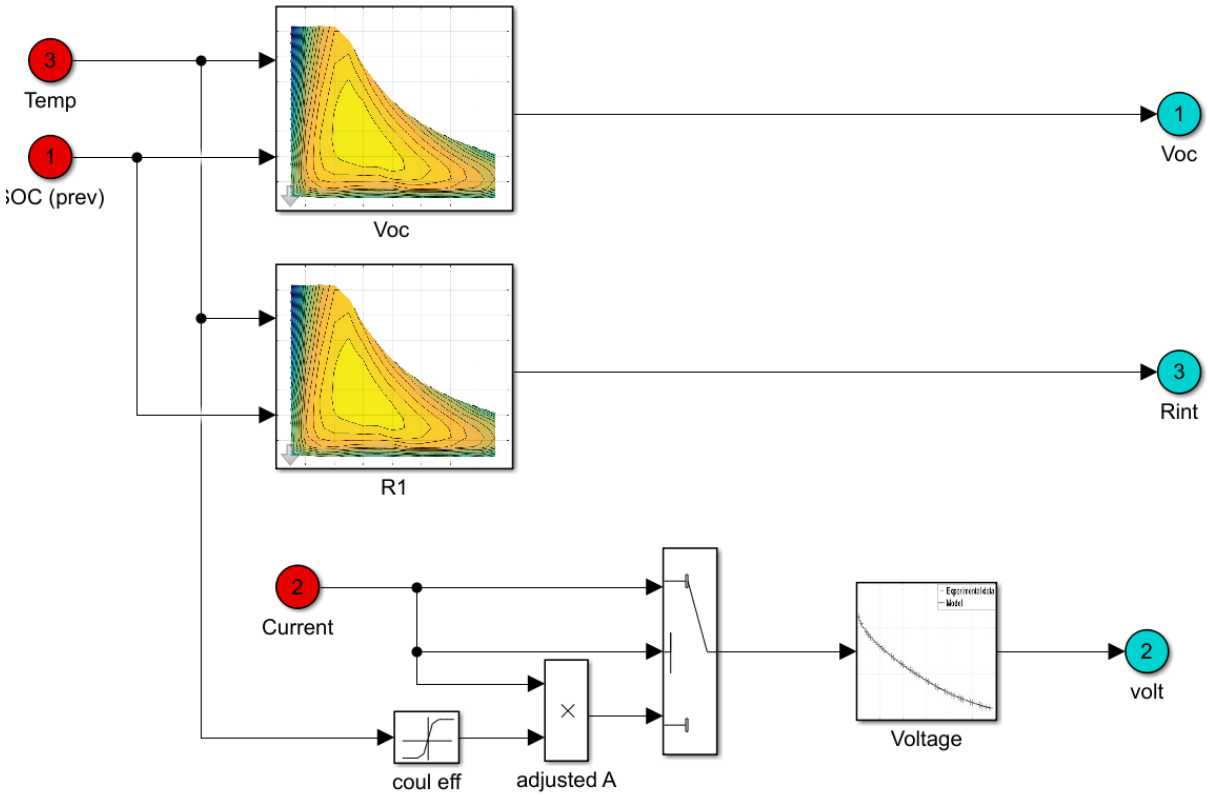

Figure D4: Zinc-air cell calculation of voltage